Master's thesis

NTNU
Norwegian University of Science and Technology
Faculty of Natural Sciences
Department of Chemical Engineering

Nora Birgitte Vikse

Reservoir-on-a-chip: Two-phase flow in porous media studied by advanced microfluidic methods

Master's thesis in Chemical Engineering
Supervisor: Gisle Øye, Marzieh Saadat
July 2020

NTNU
Norwegian University of
Science and Technology

Nora Birgitte Vikse

Reservoir-on-a-chip: Two-phase flow in porous media studied by advanced microfluidic methods

Master's thesis in Chemical Engineering
Supervisor: Gisle Øye, Marzieh Saadat
July 2020

Norwegian University of Science and Technology
Faculty of Natural Sciences
Department of Chemical Engineering

NTNU
Norwegian University of
Science and Technology

Preface

This thesis was written during the spring semester of 2020 as the final part of my master's degree at the Department of Chemical Engineering at the Norwegian University of Science and Technology.

I would like to express my greatest gratitude to my supervisor, Professor Gisle Øye, and my co-supervisor, Marzieh Saadat, for all the guidance, support and valuable feedback throughout the semester. I would also like to give a great thanks to Marcin Dudek for help during the lab work, and feedback regarding the thesis.

I want to thank all the employees at Ugelstad Laboratory for great support, motivation and useful discussions this last year of my education.

Last but not least, I want to thank all my friends for a great time during these five years of education.

Trondheim, 01.07.2020

Nora Birgitte Vikse

Abstract

Crude oil is the most crucial source of energy in the world. With an increasing demand for energy, it has become essential to enhance oil recovery. Several methods are applied to produce crude oil. However, a large amount of crude oil remains trapped in the pores. An established technique to enhance the oil recovery is surfactant flooding, where the aim is to reduce the capillary forces, which are the main reason for trapped oil. Recently, low salinity water (LSW) flooding has shown to improve the oil recovery by altering surface wettability towards water wetness. Besides, the loss of surfactant has shown to decrease under low salinity conditions. Thus, a combination of low salinity water flooding and surfactant flooding, also called low salinity surfactant (LSS) flooding, has demonstrated the potential to enhance oil recovery.

This master's thesis aimed to investigate how a varying amount of calcium ions affect the displacement of crude oils by low salinity solutions, with and without surfactant, with constant ionic strength. The molar calcium/sodium ranged from 0 to 0.040, and the surfactant used was AOT. Besides, the use of two crude oils studied the effect of oil composition. The interfacial tension between the crude oils and low salinity solutions, with and without AOT, was measured to find the molar calcium/sodium ratio giving minimum IFT. One-step and two-step displacement experiments were performed under both hydrophilic and hydrophobic conditions. Two constant injection rates were used to vary the capillary numbers. The capillary numbers in these experiments ranged from $1.4{\cdot}10^{-7}$ to $6.2{\cdot}10^{-4}$.

The IFT measurements showed a minimum IFT between the crude oils and the LS-AOT solutions with the molar calcium/sodium ratio equal to 0.017. Hence, the ratio expected as the optimum point for oil recovery. However, the recovery trends obtained with an increasing amount of calcium in the one-step displacement experiments did not seem to be consistent with the IFT results. When the LS-AOT solutions with molar calcium/sodium ratio equal to 0 and 0.017 were flooded at the EOR stage, the recovery of oil A increased by approximately 5 and 6%, respectively. For oil C, the recovery increased by approximately 1 and 4% after injection of the LS-AOT solutions with molar calcium/sodium ratio equal to 0 and 0.017, respectively. Hence, the presence of calcium led to an increase in oil recovery. However, further investigations need to be performed to know if this is the optimal ratio for oil recovery.

Sammendrag

Råolje er den viktigste energikilden i verden. Med en økende etterspørsel etter energi har det blitt viktig å forbedre oljeutvinningen. Flere metoder brukes for å produsere råolje. Imidlertid forblir en stor mengde råolje fanget i porene. En etablert teknikk for å forbedre oljeutvinningen er surfaktant fløming, der målet er å redusere kapillærkreftene, som er hovedårsaken til fanget olje. Vann med lavt saltinnhold har nylig vist seg å forbedre oljeutvinningen ved å endre fuktegenskapene i overflaten til vannfuktighet. Dessuten har tapet av surfaktant vist å avta under forhold med lavt saltinnhold. Dermed har en kombinasjon av lav salinitet vann fløming og surfaktant fløming vist potensial til å forbedre utvinningen av olje.

Denne masteroppgaven tok sikte på å undersøke hvordan en varierende mengde kalsiumioner påvirker fortrengningen av råoljer med løsninger med lavt saltinnhold, med og uten surfaktant, med konstant ionestyrke. Det molare kalsium/natrium forholdet varierte fra 0 til 0.040, og surfaktanten som ble brukt var AOT. Dessuten, studerte bruken av to råoljer effekten av oljesammensetning. Grenseflatespenningen mellom råoljene og løsningene med lavt saltinnhold, med og uten AOT, ble målt for å finne det molare kalsium/natrium forholdet som ga minimum grenseflatespenning. Ett-trinns og to-trinns fortrengningsforsøk ble utført under både hydrofile og hydrofobe forhold. To konstante injeksjonshastigheter ble brukt for å variere kapillærnumrene. Kapillærnumrene i disse eksperimentene varierte fra $1.4{\cdot}10^{-7}$ til $6.2{\cdot}10^{-4}$.

Målingene av grenseflatespenningene viste en minimum grenseflatespenning mellom råoljene og lav salinitet vann løsningene med surfaktant med det molare kalsium/natrium forholdet lik 0.017. Derfor forventes dette forholdet til å være det optimale punktet for oljeutvinning. Utvinningstrendene oppnådd med en økende mengde kalsium i ett-trinns forskyvningsforsøk så derimot ikke ut til å stemme overens med grenseflatespenning målingene. Når lav salinitet vann løsningene med surfaktant med det molare kalsium/natrium forholdet lik 0 og 0.017 ble injisert på EOR-trinnet, økte utvinningen av olje A med henholdsvis 5 og 6%. For olje C økte utvinningen med omtrent 1 og 4% etter injeksjonen av lav salinitet vann løsningene med surfaktant med det molare kalsium/natrium forholdet på henholdsvis 0 og 0.017. Derfor førte tilstedeværelsen av kalsium til en økning i oljeutvinning. Imidlertid må ytterligere undersøkelser utføres for å vite om dette er det optimale forholdet for oljeutvinning.

Contents

List of Figures

List of Tables

List of Symbols

List of Symbols.

Symbol	Description	Unit
A	Specific constant of the density meter	-
A_o	Percentage of area with crude oil	%
$A_{o,start}$	Percentage of area with crude oil before water invades the network area	%
B	Specific constant of the density meter	-
c	Concentration	g/L
c_i	Concentration of ion, i	g/L
C_{el}	Molar ion concentration in bulk phase	mol/L
CMC	Critical micelle concentration	mol/L
Ca	Capillary number	-
e	Elementary charge	C
ϵ	Dielectric permeability	$C^2/(N{\cdot}m^2)$
f_1	Correction factor for viscosity, temperature and nonlinearity	-
f_2	Correction factor for viscosity, temperature and nonlinearity	-
h_c	Height of channel	μm
I	Ionic strength	mol/L
k_B	Boltzmann constant	J/K
κ	Debye-length	m
l	Length	μm
n	Amount of moles	mol
N_A	Avogadro number	-
m	Mass	g
M_m	Molecular weight	g/mol
M	Viscosity ratio	-
ΔP	Pressure difference	mN/m^2
ρ	Density	kg/m^3
$\Delta\rho$	Difference in density	kg/m^3
q	Volumetric flow rate	μL/min
Q	Ratio between the oscillation period of the U-tube and the reference oscillator	-
r_t	Radius of the tube	m
R	Recovery	-
R_d	Radius of the cylindrical drop at its center	m

R_1	Radii of curvature in one direction	m
R_2	Radii of curvature in perpendicular direction	m
T	Temperature	K
u_i	Velocity of the invading aqueous solution	m/s
V	Volume	μL
V_p	Rock pore volume	μL
w	Width	μm
w_c	Width of channel	μm
ω	Rotational speed	rpm
$X_{ca^{2+}/Na^{+}}$	Molar ratio between calcium and sodium ions	-
z	Ion valence	-
Z_i	Valency of ion, i	-
θ	Contact angle	Degree
μ_i	Viscosity of invading aqueous solution	cP
μ_d	Viscosity of defending oil	cP
γ	Interfacial tension	mN/m
γ_{id}	Interfacial tension between invading aqueous solution and defending oil	mN/m
γ_{lg}	Interfacial tension between liquid and gas phase	mN/m
γ_{sg}	Interfacial tension between solid and gas phase	mN/m
γ_{sl}	Interfacial tension between solid and liquid phase	mN/m
λ	Potential movement of the drop from the rotation axis	

List of Abbrevations

List of Abbrevations.

Acronym	Description
CMC	Critical micelle concentration
CPP	Critical packing parameter
DI	Deionized
EOR	Enhanced oil recovery
HSW	High salinity water
IFT	Interfacial tension
IOR	Improved oil recovery
LSS	Low salinity surfactant
LSW	Low salinity water
MIE	Multicomponent ion exchange
OOIP	Original oil in place
OTS	Trichloro(octadecyl)silane
O/W	Oil in water
PTFE	Polytetrafluoroethylene
RF	Recovery factor
ROI	Region of interest
SAM	Self-assembled monolayers
TAN	Total acid number
TBN	Total base number
UMP	Universal Microfluidic Platform

1 Introduction

Today, the world's most supplied source of energy is oil. For each day, the demand for oil is rising, and it becomes more important to develop new advanced enhanced oil recovery (EOR) methods to meet the energy demands and to ensure optimal use of resources [1]. Oil production can be separated into three stages: primary, secondary and tertiary. After primary and secondary recovery methods, normally, two-thirds of the original oil in place (OOIP) is still trapped in the reservoir. This is mainly due to capillary forces [2]. Further increase in recovery can be achieved by different EOR techniques in the tertiary stage. One of the well-known methods used in EOR is surfactant flooding, which can lead to about 60% recovery of the OOIP [3]. By using surfactants, the interfacial tension (IFT) between oil and water is reduced. In addition, the rock wettability is altered towards water wetness. Both interactions lead to an increase in oil recovery [2].

During the past decade, the injection of low salinity water (LSW) has shown potential as a new EOR technique. Compared to high salinity water (HSW), the injection of LSW has increased the oil recovery [4–9]. However, the mechanism dominating the improved recovery is yet not known [10]. For sandstone reservoirs, many mechanisms have been suggested where interactions between active ions, such as calcium, and the surface can lead to wettability alteration toward water wetness [11–13]. The amount of non-active ions such as NaCl has also shown to be an important factor for oil recovery in carbonates [14].

One major problem with surfactant flooding is the loss of surfactant due to precipitation, adsorption, or phase trapping in the porous media [15]. However, it is shown that surfactant adsorption is reduced and that surfactant solubility is improved under low salinity conditions [15, 16]. Thus, a combination of surfactant flooding and LSW flooding, also called low salinity surfactant (LSS) flooding, has recently been studied [15, 17–19]. The idea is to obtain the benefits from both of the flooding techniques.

The aim of this master thesis is to study the displacement of crude oils by low salinity solutions, with and without surfactant, when the molar calcium/sodium ratio is varied at constant ionic strength. This will be studied by one-step and two-step displacement experiments with the use of microfluidic methods.

The experiments were carried out at Ugelstad Laboratory at the Department of Chemical Engineering.

2 Background

2.1 Crude oil

Petroleum, also called crude oil, is a thick, dark-coloured, oily, flammable liquid. It is used for the production of fuel oil and petrochemical products such as plastics, solvents and fertilizers [20].

2.1.1 Origin

For many years, researchers have discussed the origin of oil, leading to two major theories: the abiogenic and the biogenic origin.

The theory of abiogenic origin describes the formation of crude oil from carbonates. Alkali metals react with carbonates and form carbides that further react with water and form acetylene. At elevated pressure and temperature, acetylene converts to crude oil. Today, a minority of geologists view the theory of abiogenic origin as the origin of crude oil [20].

The more common theory of crude oil origin is the biogenic origin theory that describes the formation of crude oil from decayed remains of prehistoric marine plants and animals. Through sedimentation over many centuries, a mixture of mud and organic matter is buried by mineral material. High temperature and pressure, then, causes the decayed remains to metamorphose into waxy materials and further into gaseous and liquid hydrocarbons by catagenesis. When these hydrocarbons get trapped in the porous rock after moving around, an oil field is formed [20].

2.1.2 Composition

Crude oil consists of a mixture of many alkanes in different phases (gas, liquid and solid), mainly hydrocarbons with fragments of nitrogen, sulfur and oxygen [20]. The composition of crude oil depends on both the location and aging of the field [21].

There are many techniques to describe the composition of crude oils, but one of the most common ways is through SARA analysis. This analysis separates the components of the crude oil into

four fractions by their polarity and polarizability: saturates, aromatics, resins and asphaltenes (SARA). The fraction of saturates contains the linear, branched and cyclic hydrocarbons that are non-polar. Aromatics are more polarizable than saturates and consist of one or more aromatic rings. Both resins and asphaltenes contain polar groups and are heavier than saturates and aromatics [22]. Asphaltenes consist of the most complex fractions in crude oil and are distinct from resins by the fact that resins are soluble in light alkanes while asphaltenes are not [21].

Crude oils can be highly acidic. Usually, it is the large molecules such as the resins and asphaltenes that consist of carboxylic groups. A measure used to express the acidity of crude oil is the total acid number (TAN). Usually, TAN is expressed by the weight of potassium hydroxide (KOH) that is needed to neutralize all the acidic components in one gram of crude oil. Crude oils are considered acidic when TAN is larger than 0.5 mg KOH/g and highly acidic when TAN is larger than 1 mg KOH/g. Thus, high values of TAN defines an inferior and heavy crude oil. The naphthenic acids are the main contributor to a high value of TAN [23]. These are a part of the fraction, resins [24]. A measure used to express the basicity of crude oil is the total base number (TBN). Usually, TBN is defined as the weight of KOH equivalent to the basicity of all the components in one gram of crude oil [25].

Polar components (asphaltenes and resins) in the crude oil are shown to be the most crucial factors in relation to the reservoir wettability, and thus, the oil recovery. This is because they are surface active components and may, therefore, adsorb to the surface altering the surface towards oil wetness [26].

2.2 Crude oil production

Today, more than 85% of the world's source of energy is supplied by fossil fuels. Around 32 billion barrels of crude oil are produced per year in the world. Oil production can be separated into three phases: primary, secondary and tertiary [27].

2.2.1 Primary recovery

Primary recovery is the initial stage of oil production. In this stage, oil production is mainly driven by the natural pressure difference between the reservoir and the bottomhole inside the wellbore. Due to this pressure difference, hydrocarbons naturally rise up to the surface. However,

the natural pressure difference will slowly decrease with the production of oil. To further increase the oil production in this stage, an artificial lift system is implemented to increase the pressure difference by decreasing the bottomhole pressure. During primary recovery, usually, around 10% of the original oil in place (OOIP) is produced [28]. At some point, it will be inefficient to continue the extraction of oil using primary recovery methods. Therefore, it is usually more economical to further increase oil production with secondary recovery techniques [20].

2.2.2 Secondary recovery

Secondary recovery describes the oil production stage where a fluid is injected into the reservoir to maintain the pressure in the reservoir and to maneuver the crude oil. The fluid is injected through injection wells and drives the oil towards the production wells. Waterflooding and gas injection are the most common techniques used in secondary recovery. After primary and secondary recovery also called the improved oil recovery (IOR), usually, around 15 to 40% of the OOIP is produced [29].

2.2.3 Tertiary recovery

Tertiary recovery also called enhanced oil recovery (EOR), is utilized to extract more residual oil after primary and secondary methods. The residual oil in the reservoir is trapped due to capillary forces [2]. Capillary forces are defined as the forces that act on the fluid meniscus contact line between the fluid and the capillary wall due to the fluids surface tension. The pressure that is exerted on the fluid meniscus due to these forces is defined as the capillary pressure. At equilibrium, the capillary pressure is equal to the pressure difference, ΔP, over the fluid meniscus defined by the Young-Laplace equation. The Young-Laplace equation is given by,

$$\Delta P = \gamma_{id}(\frac{1}{R_1} + \frac{1}{R_2}), \tag{2.1}$$

where γ_{id} is the interfacial tension between the invading aqueous solution and the defending crude oil, and R_1 and R_2 are the radii of curvature describing the curvature of the interface at a given point. For a straight tube with perfect wetting, the Young-Laplace equation can be reduced to $\Delta P = \frac{2\gamma_{id}}{r_t}$, where r_t is the radius of the tube [30].

Another important force that affects the displacement of crude oil is the viscous force. Viscous

forces describe the interactions between the molecules within the fluid and lead to the rise of a velocity profile over the flow channel. In addition, viscous forces lead to the loss of reservoir pressure [31]. Unstable displacement of two immiscible fluids can lead to capillary fingering and viscous fingering. Capillary fingering describes the flooding which may spread perpendicular or backwards to the flow direction, while viscous fingering describes the flooding which spread along the flow direction [32]. The relative importance of viscous to capillary forces is described as the capillary number, Ca, given by

$$Ca = \frac{\mu_i u_i}{\gamma_{id}}, \tag{2.2}$$

where μ_i is the viscosity and u_i is the velocity of the invading aqueous solution [33]. At capillary numbers below 10^{-4}, capillary forces dominate the flooding while for capillary numbers above 10^{-4}, viscous forces dominate the flooding [34]. The capillary number is usually in the range of 10^{-6} to 10^{-7} at the end of waterflooding. Hence, one of the purposes of EOR is to increase the capillary number and, thus, the sweep efficiency. This can be accomplished in several ways. However, the most effective way is lowering the interfacial tension between the invading aqueous solution and the defending oil. When the displacement is dominated by viscous forces, the crude oil in the reservoir can be bypassed due to an unfavorable mobility ratio between the aqueous phase and the oil phase. The mobility ratio depends on the viscosity ratio, which is the ratio between the viscosity of the invading aqueous solution and the viscosity of the defending oil, μ_d, given by $M = \frac{\mu_i}{\mu_d}$. The crude oil can, in addition, be bypassed as a result of heterogeneties in the reservoir [2].

There are three main classifications of EOR methods: miscible, thermal and chemical. These can be further subdivided into smaller categories describing the different enhanced oil displacement techniques in each classification [35]. An overview of the classification can be seen in Figure 2.1.

Miscible methods describe the injection of a solvent and depend on the miscibility of the injected solvent with the crude oil. Usually, this method utilizes a solvent that is in the form of gas. Typical gases used are enriched or lean hydrocarbon gas, carbon dioxide and nitrogen. The solvent can also be in the form of liquid but that is not necessarily economical. Good solvents are, as an example, supercritical phases such as high-pressure gas [36].

Thermal methods describe the processes that need and injection of thermal energy or in situ heat generation. Steam flooding is the most common thermal method with cyclic steam injection as the most successful technique. The main aim for both miscible and thermal processes is to lower the viscosity of the oil to increase the oil mobility [36].

Chemical methods are classified into three main categories: surfactant flooding, polymer flooding and caustic flooding, also called alkaline flooding. The key mechanism in surfactant flooding and caustic flooding is to overcome the capillary forces that trap the residual oil in the rock pores or to lower the interaction between the crude oil and the solid rock. This is done by reducing the interfacial tension between the displacing fluid and oil. The key mechanism in polymer flooding is to control and improve the relative mobility ratio of the oil-water front. A combination of the chemicals is therefore common [35]. Recently, other techniques have also been studied as new EOR methods such as low salinity flooding and low salinity surfactant flooding [8, 15, 17–19].

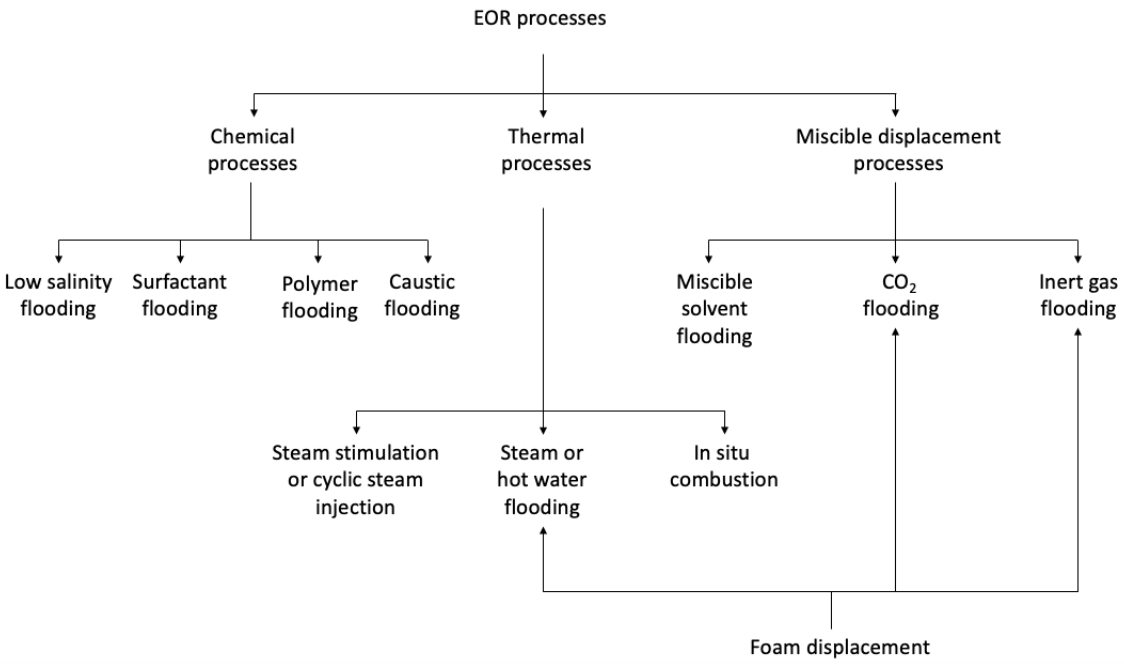

Figure 2.1: Classification of the main EOR methods.

The most attractive EOR technique for recovering the remaining entrapped oil in the reservoir is chemical flooding [3]. Although EOR methods are expensive to employ on an oil field, the total oil recovery in this stage can be increased to 30-60% [37].

2.3 Surfactant flooding

Today, surfactant flooding is a well-known technique in chemical EOR and has been utilized since the 1920s. The method has shown to be very useful and can lead to around 60% recovery [3]. The main objective of surfactant flooding is to alter the interaction between fluid/fluid and fluid/rock [2]. Before the oil displacement mechanism is described, some concepts associated with interfacial behaviour are explained.

2.3.1 Surface and interfacial tension

An uneven balance in the intermolecular forces that act on the surface between two phases leads to the rise of surface and interfacial tension. As an example, one can look at the surface between liquid and gas. The liquid molecules in the bulk phase experience attractive forces in all directions. These forces cancel out each other due to the symmetrical surrounding molecules. However, at the surface, the liquid molecules experience a net attractive force towards the bulk phase. An illustration of how the attractive intermolecular forces act on the different molecules in this system is shown in Figure 2.2.

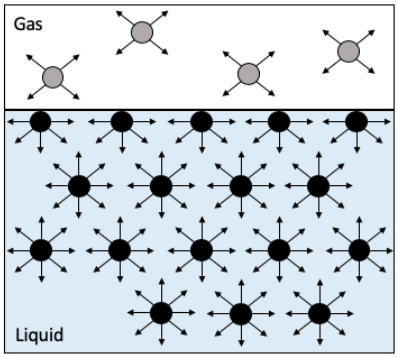

Figure 2.2: Illustration of how the intermolecular attractive forces act on the molecules in the gas phase, liquid phase and the surface between the two phases.

Surface (interfacial) tension, γ, is defined as a quantitative measure of this contracting force that exists at the surface between the two phases and tries to minimize the surface area. For a given volume, the minimum surface area is represented by a sphere. Hence, a surface will form a sphere when no external forces are present. To overcome the contracting force and expand a surface, energy is required. Thus, surface (interfacial) tension is defined as the tension force

per unit length, or the energy required to increase the surface area. Usually, surface tension is denoted as the contracting force at the interface between two different phases where one of them is gas, while interfacial tension (IFT) is denoted as the contracting force at the interface between two immiscible fluids [30].

IFT is an essential parameter in capillary forces, the main factor in trapping oil. Adhesive forces are the main forces involved in IFT. Thus, the immiscibility of oil and water leads to high IFT. Due to the high IFT during water flooding, it is difficult to extract the trapped oil properly [3]. By reducing the IFT, it is possible to increase the sweep efficiency of the trapped oil [38]. This is because a reduction in IFT leads to a reduction of work needed to deform the trapped oil droplets, also called oil ganglion. Oil ganglion that easily deforms can move through the narrow necks of pores more easily [39]. Polar components in the crude oil are surface active and may decrease the IFT between crude oil and water in the reservoir [40]. However, the IFT is not low enough to overcome the capillary forces that trap the oil in the reservoir. Thus, surfactants are added to the injected aqueous fluid.

2.3.2 Surfactant

Surface active agents, usually called surfactants, are defined as chemical compounds that have a strong tendency to adsorb to the interface between two phases and thus change its properties. For a chemical compound to be surface active, it needs to be amphiphilic. This means that the molecule has to be composed of one lyophilic (polar head) and one lyophobic (non-polar tail) part [30]. A schematic representation of one surfactant monomer is shown in Figure 2.3.

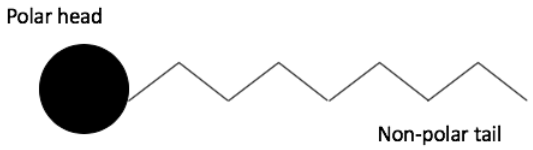

Figure 2.3: Schematic representation of a surfactant monomer.

The lyophilic part is soluble in the solvent, while the lyophobic part is rejected by the solvent. Hence, surfactants orient itself with the lyophilic part in the solvent and the lyophobic part away from the solvent. An increase in surfactant concentration, therefore, occurs at the interface between two immiscible fluids [35]. If the solvent is water, the lyophilic and the lyophobic

part are referred to as the hydrophilic and the hydrophobic part, respectively. Surfactants are classified into four main groups based on the polarity of the lyophilic part: anionics, cationics, amphoterics and non-ionics. Anionic surfactants have head groups that are negatively charged, cationic surfactants have head groups that are positively charged, amphoteric surfactants have head groups where both positive and negative charges are present and non-ionic surfactants have head groups with no formal charge [30].

The most common surfactants used in EOR for sandstone reservoirs are anionic surfactants [41]. This is because these don't have a strong tendency to adsorb to the reservoir sandstone rocks that have a negative surface charge compared to other types of surfactants. In addition, their manufacturing cost is relatively low, they are stable at high temperatures and reduce the IFT efficiently [1]. Various anionic surfactants have been used in EOR, but the most widely used are surfactant formulations that contain sulfonates. This is because they are better resisted to ions, such as calcium, Ca^{2+}, and magnesium, Mg^{2+}, in the solution [35]. Cationic surfactants can not be used in sandstone reservoirs because of their strong tendency to adsorb to the surface. However, they can be used in carbonate reservoirs for wettability alteration to more water-wet. Non-ionic surfactants are, usually, used as a co-surfactant with anionic surfactants due to their tolerance to high salinity. Amphoteric surfactants have a higher tolerance for temperature and salinity than anionic surfactants. However, their cost is high and, therefore, not common to use [1]. The major disadvantages with the use of surfactants are that the synthetic surfactants have high costs and are a concern for the environment [42]. In addition, they may lead to water quality problems if they are back produced [2].

Critical micelle concentration (CMC)

Increasing the surfactant concentration leads to increasing adsorption of surfactant at the surface or interface, and thus, decreasing surface tension or IFT. With an increasing amount of surfactant, a certain concentration will be reached where surface tension or IFT is more or less constant, and micelles start to form spontaneously. Further addition of surfactant will only lead to an increase in the number of micelles. This concentration is defined as the critical micelle concentration (CMC) [27]. An illustration of how the surfactant molecules behave at the interface between water and oil phase and how the interfacial tension varies with the logarithm of

the surfactant concentration is shown in Figure 2.4.

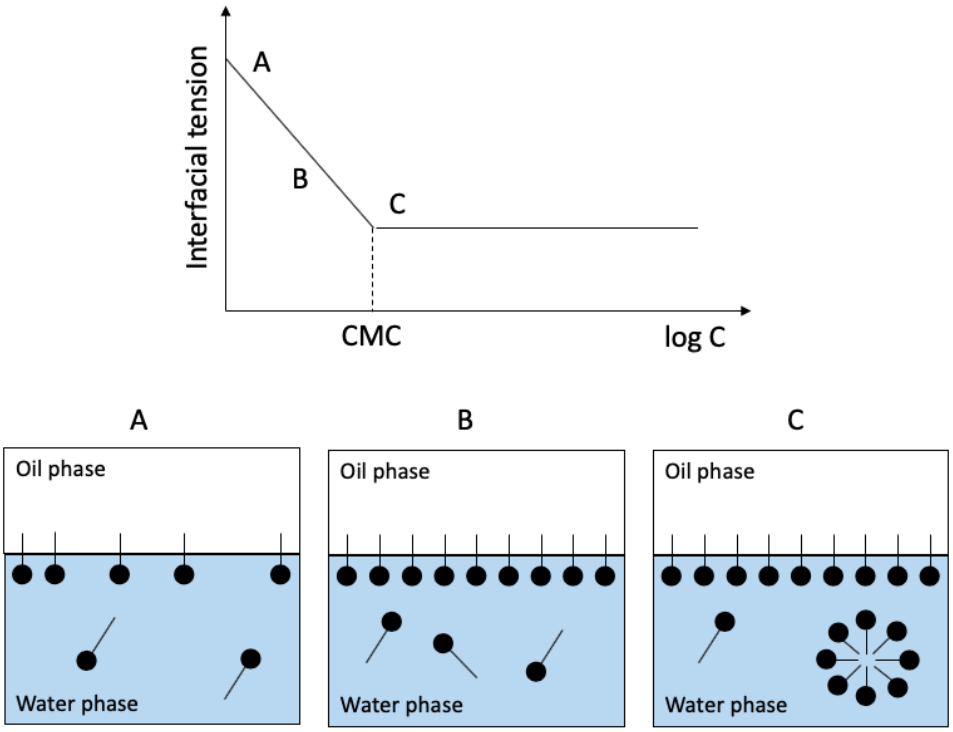

Figure 2.4: Interfacial tension vs. logarithm of surfactant concentration, C.

The IFT between crude oil and water phase decreases effectively by the addition of the surfactant. By reducing the IFT, the capillary number increases and, thus, the residual oil saturation decreases [42]. In surfactant flooding, the maximum permissible concentration of surfactant is CMC [43].

2.3.3 Wettability

Wetting is defined as the ability of a fluid to spread out on a solid plane surface. There are two types of forces that determine how well the fluid spreads out: gravitational forces and surface forces. The gravitational forces try to flat press the fluid while the surface forces act on the interfaces between the three phases. The effect of the surface forces are determined by the relative size of the surface tension between the liquid and gas phase, γ_{lg}, solid and gas phase, γ_{sg}, and solid and liquid phase, γ_{sl}.

When the cohesive forces between the molecules in the liquid are greater than the adhesive

forces between the liquid and the solid surface, the liquid will form a drop on the plane surface. On the contrary, when the adhesive forces are greater than the cohesive forces, the liquid will spread out on the plane surface. The surface forces will determine the contact angle, θ, that forms between the solid surface and the tangent of the liquid-solid surface at the three-phase point. If the contact angle is equal to zero, the liquid is completely wetting the surface. Partial wetting of the surface is obtained when the contact angle is less than 90°, and the non-wetting condition is obtained when the contact angle is between 90° and 180° [30]. An illustration of these possible wetting scenarios of a droplet placed on a plane solid surface is shown in Figure 2.5.

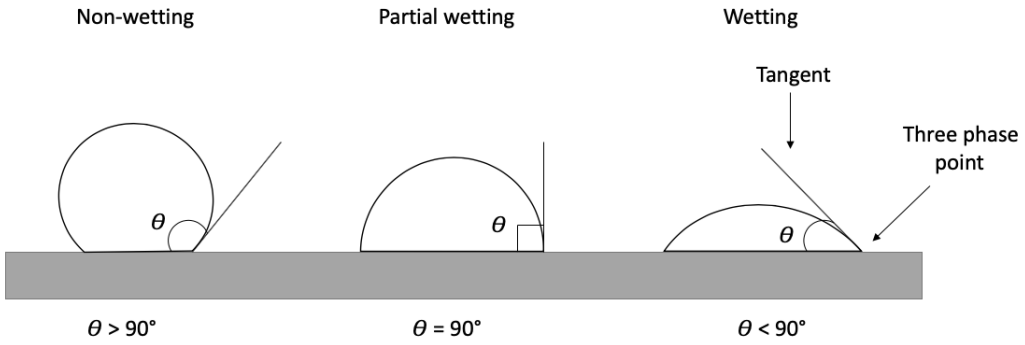

Figure 2.5: Illustration of wetting scenarios of a liquid placed on a plane solid surface.

When a system is in equilibrium, there is no change in Gibbs free energy, and Young's equation applies. The equation is given by

$$\gamma_{sg} = \gamma_{sl} + \gamma_{lg} cos\theta. \tag{2.3}$$

For the situation where there are two immiscible fluids present on a solid plane surface, the fluid with the smallest surface tension between the solid and the fluid will be the fluid wetting the solid phase [44].

The wettability of the rock in a reservoir controls the distribution, location and flow of the different fluids present. It influences both the capillary pressure and relative permeability and is therefore of high importance in oil recovery [2]. Wettability of the reservoir rocks can be defined as water-wet, oil-wet or mixed-wet [45]. Laboratory work has shown that the wettability of the reservoirs is dependent on crude oil composition. The type of rock surface will affect the

adsorption of the polar components [46]. Usually, sandstone reservoirs behave as hydrophilic surfaces, while carbonate reservoirs behave as hydrophobic surfaces in nature. However, both surfaces become more oil-wet through adsorption of polar components in the crude oil to the surfaces or through interactions between components in the crude oil and mineral surfaces. Sandstone reservoirs are negatively charged and will mainly adsorb basic polar components in the crude oil, while carbonate reservoirs are positively charged and will mainly adsorb acidic polar components in the crude oil [40]. This direct adsorption is possible when the water film between the crude oil and the surface breaks due to its instability. Sandstone reservoirs may also become more oil-wet through other mechanisms. When the asphaltenes are poorly soluble in the crude oil, it can precipitate at the surface leading it towards oil wetness. In addition, when calcium is present, bridges may form between the acidic components in the crude oil and the negatively charged surface, which leads it to an oil-wet surface [47]. The displacement of oil during water flooding in a water-wet reservoir (a) and an oil-wet reservoir (b) is shown in Figure 2.6.

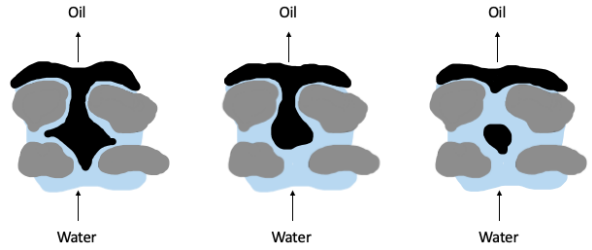

(a) Water-wet reservoir.

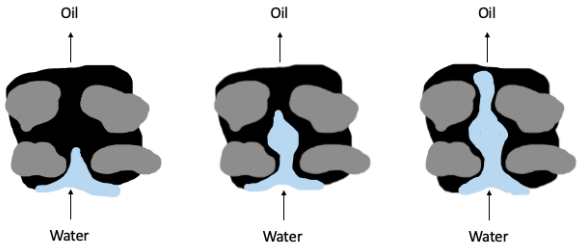

(b) Oil-wet reservoir.

Figure 2.6: Illustration of displacement of oil by injection of water in reservoir rocks with different wettability.

Altering the wettability of the rock from oil-wet to water-wet leads to a decrease of the adhesive forces between the oil and rock surface and, thus, an increase of the permeability of oil. This

leads to a higher recovery of oil in a water-wet reservoir [2].

2.3.4 The electrical double layer

When a charged surface is present in a polar medium, the distribution of adjacent ions of opposite charge (counter-ions) and ions of the same charge (co-ions) will be affected. The counter-ions will be attracted to the surface while the co-ions will be repelled from the surface. At the same time, thermal motion can lead to movements. These two effects result in the creation of the electrical double layer, consisting of an inner layer with the charged surface and a diffuse outer layer with the distribution of neutralizing excess of counter-ions. An illustration of the electrical double layer formed when a surface is charged by acid (COO-) groups is shown in Figure 2.7.

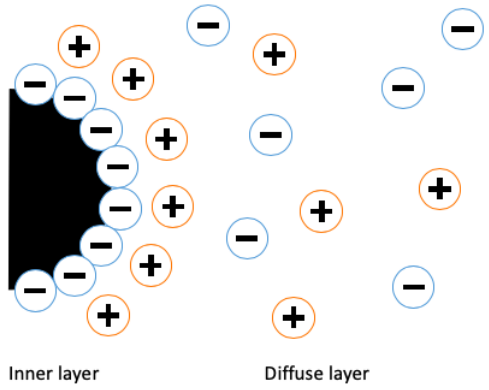

Figure 2.7: Illustration of the electrical double layer.

The effect of ion valence and concentration is expressed by the Debye-Hückel parameter, κ, given by

$$\kappa = \sqrt{\frac{2e^2 N_A C_{el} z^2}{\epsilon k_B T}} \tag{2.4}$$

where e is the elementary charge, N_A is the Avogadro number, C_{el} is the molar ion concentration in the bulk phase, z is the ion valence, ϵ is the dielectric permeability, k_B is the Boltzmann constant, and T is the temperature. The thickness of the diffuse double layer, also called Debye-length, is defined as the inverse of κ. Hence, the Debye-length decreases with increasing ion concentration and ionic charge [30].

One major problem in surfactant flooding is the loss of surfactant because of precipitation, adsorption, or phase trapping in the porous rock reservoir. Phase behaviour of surfactant depends on parameters such as ionic strength, pH, and temperature of the water phase [15]. A surface charge can arise at the interface between liquid and solid dependent on the ionic strength and pH. Anionic surfactants are attracted to surfaces with a positive charge, while cationic surfactants are attracted to surfaces with a negative charge. Normally, carbonate reservoirs are positively charged, and sandstone reservoirs are negatively charged at neutral pH. At low concentrations of surfactant, the rate of adsorption is determined by the charge of the electrical double layer. This is due to the electrostatic interactions between the charged rock surface and the head group of the surfactant. With increasing concentrations, the adsorption increases. At surfactant concentrations above CMC the adsorption keeps constant [43]. Even though anionic surfactants repel the negatively charged sandstone reservoirs, bridges may form between the anionic surfactant and the surface when calcium is present [47]. It has been shown that retention of anionic surfactants increases with an increase in ionic strength partly due to a decrease in repulsive forces between the surfactant molecules and the clay surface, and partly due to a salting-out effect [48].

2.3.5 Oil displacement mechanism

During surfactant flooding, the present surfactant molecules adsorb to the interface between the injected water and oil, which leads to a reduction in IFT. The capillary number will increase, and thereby increase the efficiency of the oil displacement [2]. The usual IFT value between crude oil and water, during waterflooding, is 10 - 30 mN/m. Addition of surfactant can reduce the value of IFT to as low as 10^{-3} mN/m [3]. Thus, the forces dominating the system will change from capillary forces to viscous forces [42]. In addition, the presence of a surfactant can lead to wettability alteration of the porous media from oil-wet to water-wet. This, in turn, increases the permeability of oil and, thus, increases the oil recovery [2]. Sandstone reservoirs are altered towards oil wetness after adsorption of basic polar components or after adsorption of acidic polar components via calcium bridges. Anionic surfactants can be used to alter the wettability due to the negatively charged surface. The negatively charged surfactant headgroups may form ion-pairs with the positively charged basic group or the calcium ions, Ca^{2+}, that bind the acid groups to the surface, due to the electrostatic interactions. The formation of ion-pairs

might cause the adsorbed layer of polar components to strip off the surface leading it towards water wetness. This mechanism is based on the study [49], where the mechanism was suggested for cationic surfactants used for carbonates. However, when divalent cations are present in the connate water, anionic surfactants may form calcium bridges between the surfactant monomers, which leads to surfactant precipitation. This, on the other hand, leads to a decrease in the oil displacement efficiency [35].

2.4 Low Salinity Water flooding

During the past decades, the injection of low salinity water (LSW) has shown to be a promising EOR technique in both carbonate and sandstone reservoirs. Compared to high salinity water (HSW) flooding, the LSW flooding has improved the oil recovery, which has drawn attention in the oil industry due to its simplicity and low expense [50].

Through several studies [4–9], it is shown that LSW flooding enhances the oil recovery. The main variables shown to affect the LSW flooding are brine composition, crude oil composition, and type of rock [10]. It is established that active ions such as calcium, Ca^{2+}, magnesium, Mg^{2+}, and sulfate, SO_4^{2-}, can alter the wettability to water wetness through interactions with carbonate reservoirs. In addition, it has been shown that amount of non-active salts, such as sodium chloride (NaCl), is an important factor for the oil recovery in carbonates [14]. However, there is no agreement between researchers on the mechanism dominating the recovery. For sandstone reservoirs, several mechanisms have been proposed for improved oil recovery due to wettability alteration of the sandstone rocks from oil-wet to water-wet, including pH effects, multicomponent ion exchange (MIE) and extension of the electrical double layer.

A study [11] proposed that a local increase in pH leads to the desorption of organic chemical compounds from the surface. However, certain conditions were needed for the injection of LSW to be efficient. Clay had to be present in the sandstone, active ions such as Ca^{2+} had to be in the formation water, and acidic and/or basic organic compounds had to be in the crude oil. The cations from the formation water and the acidic/basic compounds from the crude oil are initially adsorbed to the clay surface. During the injection of LSW, the chemical equilibrium related to the interaction between brine and rock is disrupted, which leads to desorption of cations. Thus, protons, H^+, from the water nearby the clay adsorbs to the surface, to compensate for the

cations loss. This results in a local pH increase nearby the surface. The pH increase causes acid-base proton transfer reactions between the adsorbed polar compounds. This results in partial desorption of the acidic and basic compounds, and, hence, altering the surface towards water wetness [50].

Another study [12] proposed that MIE results in the surface wettability changing towards more water-wet. Initially, the clay surface is oil-wet due to the bindings the polar organic compounds in the crude oil forms with the cations at the clay surface or the direct adsorption of polar components to the surface. During LSW flooding, multivalent or divalent ions such as Ca^{2+} and Mg^{2+} from the injected LSW adsorb to the rock surface and replaces the organic polar compounds and organo-metallic complexes, thus altering the surface towards water wetness. This mechanism is describes as MIE [27].

Another study [13] proposed that the extension of the diffuse double layer lead to the water-wet surface. Initially, electrical double layers are formed around negatively charged clay particles when they are immersed in water. The inner region of the double layer consists of the adsorbed positively charged ions (Ca^{2+} or Mg^{2+}), while the diffuse region mainly consists of the negatively charged ions. LSW contains fewer ions than HSW, which leads to an expansion of the double layer. Thus, during LSW flooding, monovalent ions such as sodium, Na^{+}, from the injected water can penetrate the diffuse layer and replace the divalent ions. This leads to an increase in the electrostatic repulsion between the oil and the clay particles. When the binding forces between oil and clay particles are exceeded by the repulsive forces, the bindings break. This results in desorption of the oil from the clay surface, and thus a more water-wet surface [50].

2.5 Low Salinity Surfactant flooding

Recently, it has been shown that injection of LSW followed by injection of surfactant solution can lead to an increase in oil recovery [51]. In addition, studies [15, 16] have shown that surfactant adsorption in the porous media is reduced under low salinity conditions. Therefore, the combination of low salinity flooding and surfactant flooding, also called low salinity surfactant (LSS) flooding, has attracted interest [17]. The objective of LSS flooding is to obtain the benefits from both of the flooding techniques. The presence of surfactant leads to a reduction in IFT, which reduces the capillary forces and, thus, more favorable conditions for oil mobilization.

In addition, it can lead to wettability alteration towards water wetness. The low salinity brine improves the surface wettability towards water wetness and leads to a reduction in retention of surfactant. In addition, the surfactant solubility is improved under low salinity conditions, which lead to less precipitation [15]. Other advantages with LSS flooding are less operational costs, fewer operational problems, and more favorable for the environment due to less consumption of surfactant. As mentioned earlier, loss of surfactant depends on the salinity, the concentration, and the type of cations present in the reservoir. Hence, these parameters need to be considered in LSS flooding. A study [18] proposed that the best option for LSS flooding is to create microemulsions of Type I, which is defined as an O/W microemulsion in equilibrium with an excess of the oil phase. This is due to less retention of surfactant, in addition to high oil recovery, although ultra-low IFT values are not achieved.

3 Methodology

In this master thesis, two crude oils displaced by different low salinity (LS) solutions, with and without surfactant, were systematically studied under both hydrophilic and hydrophobic conditions by advanced microfluidic methods.

3.1 Chemicals

3.1.1 Bis(2-ethylhexyl) sulfosuccinate sodium salt (AOT)

AOT is an anionic surfactant with a molecular weight of 444.56 g/mol. AOT consists of two relatively short but bulky hydrocarbon tails and a small ionic head group. This hydrophobic/hydrophilic imbalance leads to poor solubility of AOT in water and high solubility of AOT in non-polar solvents [52]. For alkanes with a carbon number lower than 11, the presence of AOT in the aqueous solution causes a pseudo-partial wetting between the two phases [53]. The chemical structure of AOT is shown in Figure 3.1.

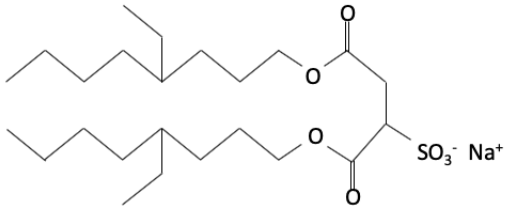

Figure 3.1: Chemical structure of bis(2-ethylhexyl) sulfosuccinate sodium salt (AOT).

AOT has a significant critical packing parameter (CPP) due to its two hydrocarbon tails. This leads to the formation of aggregates, such as lamellar phases. AOT has a strong tendency to adsorb to the interface between hydrocarbons and aqueous solutions, and therefore, reduce the IFT by orders of magnitude [54].

3.1.2 Tailoring surfaces with alkylsilanes

For decades, alkylsilanes (silanes) have been used for tailoring surfaces such as aluminates, silicates and titanetes. Amongst a wide variety of applications, hydrophobization is one of the

applications they are used for in the industry. Various complex silanes are used in industrial processes. However, monoalkylsilanes with three leaving groups are normally used in academic studies. The general formula of these is $R - SiX_3$. R represents a short- or long-chain alkane with a simple structure or an alkyl chain that contains the silane-carbon bond at one of the ends. X, usually, is an alkoxy group or a halogen.

Silanes form surface coatings by reacting with the surface. The mechanism of this reaction is not fully understood [55]. However, a commonly believed mechanism for silanization is a three-step process. First, silanes form silanols through a hydroxylation process. Further, the silanols react with the hydroxylated surface by elimination of water. Then, by a polymerization condensation process, the surface silanols react with one another through siloxane bonds [56].

Trichloro(octadecyl)silane (OTS) generates self-assembled monolayers (SAM) and is, amongst the silanes, the most used surface active reagent [57]. OTS is an amphiphilic molecule consisting of a polar headgroup and a non-polar long-chain alkyl group. The chemical structure of OTS is shown in Figure 3.2.

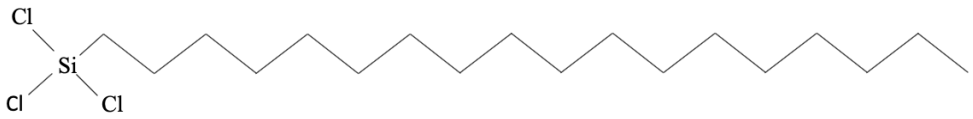

Figure 3.2: Chemical structure of trichloro(octadecyl)silane (OTS).

3.2 Apparatus theory

3.2.1 Density measurements by the oscillating U-tube method

Density meter is an instrument used to measure the density of fluid samples. Density, ρ, is defined as

$$\rho = \frac{m}{V} \tag{3.1}$$

where m is mass, and V is Volume.

The principle behind the density meter is based on the oscillating U-tube method. The sample is pumped into a U-shaped borosilicate glass tube of a known volume. The U-tube vibrates with

a characteristic frequency that varies with the sample's density. The density can be measured by a mathematical conversion and determination of the frequency. From the reference oscillator and the quotient of the period of oscillations of the U-tube, the density is calculated by,

$$\rho = A \cdot Q^2 \cdot f_1 - B \cdot f_2 \tag{3.2}$$

where A and B are specific constants of the instrument, Q is the ratio between the oscillation period of the U-tube and the oscillation period of the reference oscillator, and f_1 and f_2 are both correction factors for viscosity, temperature, and nonlinearity [58].

3.2.2 Spinning drop tensiometry

Spinning drop video tensiometer is an instrument that can be used to measure very low IFTs (< 1 μN/m) between two immiscible fluids in the absence of a gas phase. The principle is based on the analysis of the optical contour of a drop [59]. A drop is placed inside a rotating fast exchange capillary where the gravitational forces can be negligible at a sufficiently high speed. The centrifugal forces cause the denser fluid to move outwards in the capillary and the less dense fluid to move towards the rotational axis. The shape of the drop is dependent on the IFT and the rotational speed, ω. By increasing the rotational speed, the drop gets more deformed cylindrically, which leads to an increase in interfacial area [60]. An illustration of this can be seen in Figure 3.3.

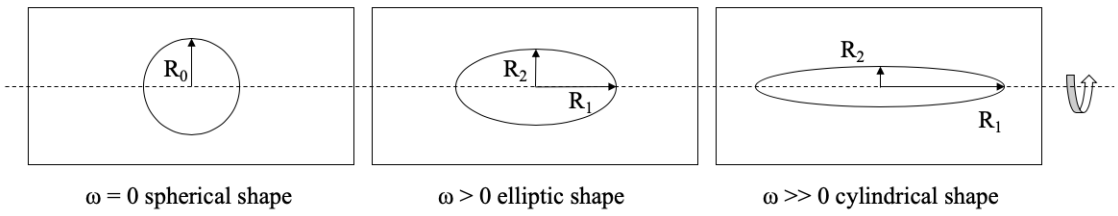

Figure 3.3: Illustration of how the shape of the fluid drop depends on the rotational speed, ω.

The IFT counteracts the increase in interfacial area and can, therefore, be found by analyzing the shape of the drop obtained at equilibrium. Different methods can be used to calculate the IFT. One method for IFT calculation is by the Vonnegut equation, where the drop shape formed with the rotational speed is approximated by a cylinder. The rotational energy of the

cylinder decreases when the radius decreases. At the same time, the interfacial energy of the cylinder is increasing when the elongation of the drop is increasing, and thus, the interface area is increasing. The total energy will reach an energy minimum in equilibrium [59]. The IFT calculation by Vonnegut is given by,

$$\gamma = \frac{\Delta\rho R_d^3 \omega^2}{4}, \tag{3.3}$$

where $\Delta\rho$ is the difference in density between the two fluids, and R_d is the radius of the cylindrical drop at its center. However, this method can only be used when the elongation of the drop is four times longer than the radius of the cylinder formed [60]. The other method used to calculate the IFT is based on the Young-Laplace equation, given in Equation 2.1, and is given by,

$$\gamma(\frac{1}{R_1} + \frac{1}{R_2}) = \frac{2\gamma}{R_0} + \Delta\rho\omega^2\lambda^2 \tag{3.4}$$

where the term on the left side represents the non-spherical conditions and the first term on the right side represents the spherical conditions. The final term represents the centrifugal forces where λ is the potential movement of the drop from the rotation axis due to the gravitational field [61].

3.2.3 Microfluidics

Microfluidics is the technology and science of fluid behavior, control and manipulation on the micro- and nanometer scale. The field is interdisciplinary, which leads to a wide variety of applications within engineering, chemistry, engineering, biotechnology, physics, material science and reservoir engineering. The development of micro-miniaturized devices has led to fast growth for the field of microfluidics over the past years [62].

In the petroleum industry, microfluidics has opened a whole new platform for research that has not been possible to carry out in core samples. Two of the main reasons for this are the controlled laminar flow obtained in the microchannels of pores and the possibility to observe the fluid flow due to the transparent micromodels. Furthermore, there are many advantages to the use of microfluidics. The small amount of volumes leads to a reduction in cost and also less waste, which makes it more environmentally favorable. It is less time consuming compared to

macroscopic processes and allows us to perform many experiments per unit time. The setup design is simple, safer to perform trial experiments and can be run by a single person. In addition, less instrument is used, which makes it easy to be serviced [63].

4 Experimental

4.1 Crude oils

Two crude oils produced at the Norwegian Continental Shelf were used in this study. The physical and chemical properties of the oils are shown in Table 4.1.

Table 4.1: Physical and chemical properties of crude oil A and C [64].

Crude oil	API [°]	η @20°C $[mPa \cdot s]$	TAN $[\frac{mgKOH}{g_{oil}}]$	TBN $[\frac{mgKOH}{g_{oil}}]$	SARA			
					S [%]	Ar [%]	R [%]	As [%]
A	19.2	354.4	2.2	2.8	50.6	31.2	15.7	2.5
C	23	74.4	2.7	1.1	64.9	26.3	8.4	0.4

4.2 Low salinity solutions

The low salinity solutions were made of calcium chloride dihydrate (Sigma-Aldrich) and sodium chloride (Merck KGaA) with the ionic strength of 20 mmol/L. The cationic composition was varied to study its influence on IFT and, thus, the displacement. The molar calcium/sodium ratio, $X_{Ca/Na}$, was set to be 0, 0.005, 0.010, 0.017, 0.022, 0.033 and 0.040. Preparation and calculations of the mass of each salt needed to prepare these solutions can be found in A.1. The pH of the LS solutions was measured to be just below 6. Exact values of these can be found in A.3

4.3 Low salinity surfactant solutions

A surfactant was added to the low salinity solutions (20 mmol/L) to make the low salinity surfactant solutions. The surfactant used was bis(2-ethylhexyl) sulfosuccinate sodium salt (AOT; Sigma-Aldrich, purity: $\geq$ 97%). The concentration of AOT in the solutions was fixed at 2.47 mmol/L. Preparation and calculation of the mass of surfactant needed to make these solutions can be found in A.2. The pH of the LS-AOT solutions was measured to be around 6. Exact values of these can be found in A.3

4.4 Density meter

The density of the low salinity solutions, with and without surfactant, were measured using the density meter, DMA-5000 M (Anton Paar GmbH). Before starting the measurement, the instrument was checked to be clean. The density shown on the apparatus was checked to be below 0.0013 g/cm^3. If the density was above this value, the cleaning procedure was performed before running the experiment. The correct solvents for the cleaning procedure were connected to the instrument. DI water was connected to "Rinse 1", and methanol was connected to "Rinse 2". The density was measured at 23°C. After the measurement, the apparatus was cleaned with the following cleaning liquids: DI water and methanol.

4.5 Spinning drop tensiometer

The spinning drop tensiometer, SVT 20N (DataPhysics Instruments GmbH) was used to measure the interfacial tension between the crude oils and the LS solutions, with and without AOT. The software, SVT20_uEye, is used to set the densities of the liquids used in the measurement, and to control the rotational speed and camera position. The temperature is controlled by a water bath. Setup of the instrument is shown in Figure 4.1.

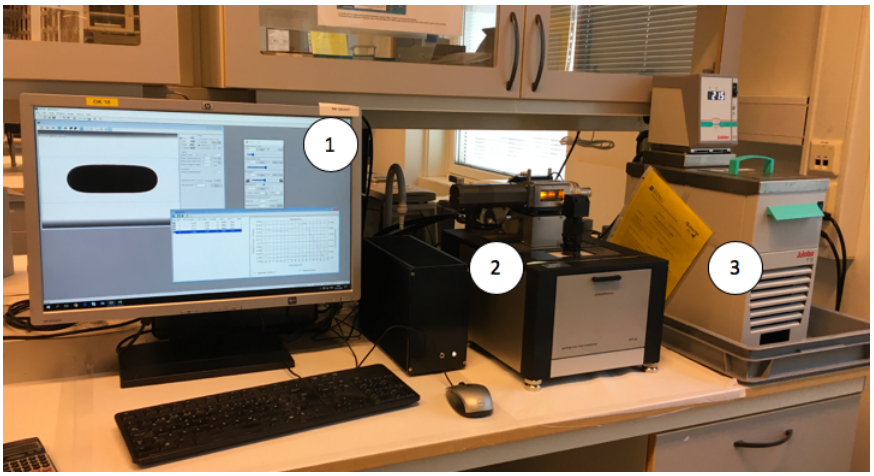

Figure 4.1: Spinning drop tensiometer. Number 1 shows the software, SVT20_uEye, number 2 shows the spinning drop video tensiometer, SVT 20N, and number 3 shows the water bath.

First, the denser solution (water phase) was injected carefully into the fast exchange capillary by a pipette. To ensure that there were no hidden air bubbles in the capillary, the capillary

was held vertical and hit with the fingers to make them escape. The lighter phase (oil phase) was loaded in a 1 mL syringe through a long needle (80 mm). The capillary was then held horizontally while one oil drop was injected into the middle of the capillary so that the drop stuck to the glass. To ensure that there were no air bubbles in the capillary, the capillary was again turned vertical, and a drop of the denser phase was loaded on top. The capillary was completely closed with a screw lid with PTFE septum. Some excess solution escaped from the holes on the side of the lid. The capillary was placed into the instrument and locked by applying the lever on the back of the motor.

In the software, the densities of both the denser and lighter phase were entered. Then, the rotor motor was turned on and speeded up until a stable elongated droplet was observed on the screen. If the droplet was unstable, the position was fixed by tilting the camera table. After the droplet reached a stable position, the zoom and focus were adjusted. Afterwards, the camera was calibrated. The calibration was performed by camera movement where the left side of the drop was detected at two positions. After the calibration, the profile of the droplet was extracted. The droplet was then fitted with a red profile. If this did not happen, the illumination was adjusted before the measurement was started. The IFT was measured at 23°C. The temperature was adjusted with the cooler. To reach equilibrium IFT, each experiment ran up to two hours. However, if the IFT appeared stable for about 30 minutes, the measurement was stopped before two hours. After the experiment, the capillary and lid were adequately cleaned by rinsing with solvents in the following order: water, acetone, toluene, acetone, water and acetone. The capillary and lid were then dried in the heating cabinet for two hours at 55 °C.

To ensure repeatability, the interfacial tension between each fluid pair was measured two times with the spinning drop tensiometer.

4.6 Universal Microfluidic Platform

The Universal Microfluidic Platform (UMP) was used to study the displacement of crude oils by various aqueous solutions in porous media.

4.6.1 Setup

The chip (Micronit Microfluidics) is placed in the chipholder (Micronit Microfluidics), which is connected to the flow control unit (Cetoni Qmix). The chipholder is placed under a high-resolution camera (DeltaPix), used to capture the displacement. The setup of the UMP is shown in Figure 4.2.

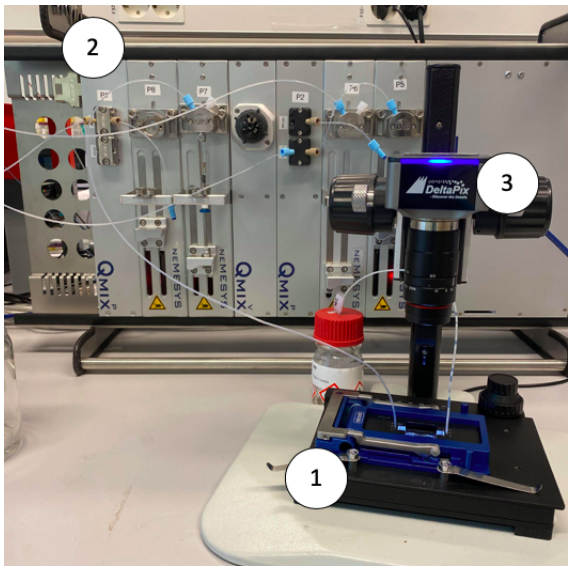

Figure 4.2: Universal Microfluidic Platform. Number 1 shows the chipholder, number 2 shows the flow control unit and number 3 shows the high-resolution camera.

Both the flow control unit and the camera are connected to the computer. The flow rate is controlled by the software, Qmix Elements, and the camera is controlled by the software, DeltaPix Insight. Pictures of the two softwares are shown in Figure 4.3.

(a) Qmix Elements.

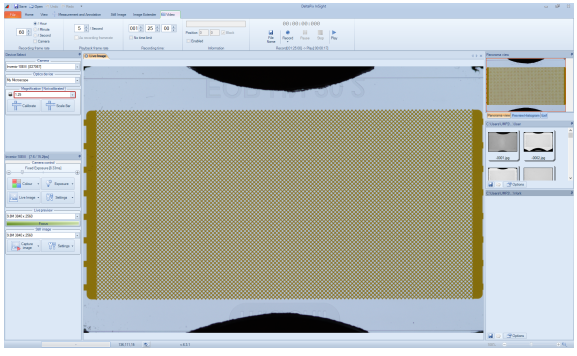

(b) DeltaPix Insight.

Figure 4.3: Softwares used to control injection rate and camera.

The chips used in this study were made of borosilicate glass and contained a uniform network of microchannels. A picture of the chip is shown in Figure 4.4. The chip has a network area with a total width, w, of 1 cm and a length, l, of 2 cm. The channels width, w_c, is 50 μm and the channels height, h_c, is 20 μm. The rock pore volume, V_p, of the uniform network is 2.1 μL and the porosity is 0.52 [65].

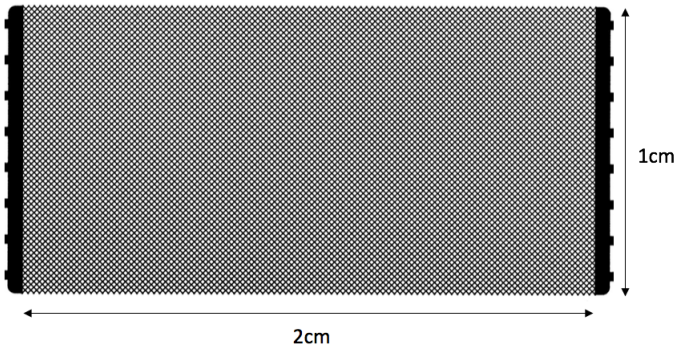

Figure 4.4: Chip with a uniform network of microchannels.

4.6.2 Preparations before the displacement experiments

First, the chip was placed in the chipholder and manually saturated with crude oil using a 1 mL syringe. The chip was then left to age for 2 hours in a suitable container where the openings of the micromodel were completely blocked. This was to prevent evaporation of the light crude oil components. A 1 mL glass syringe was filled with the aqueous flood solution, ensuring that there was no air bubbles in the syringe. Afterwards, the syringe was connected to the flow control unit. The pump was turned on, and the aqueous solution was pushed through the tubing into a waste container to ensure no air left in the tube. The chip was placed in the chipholder. The chipholder was connected to the tube and placed under the camera. The camera was then adjusted to get a clear image of the chip. To be able to process the displacement images (see 4.6.7), a picture of the calibration ruler with a 1 mm scale subdivided into 100 divisions of 0.01 mm was captured with the same focus [66].

4.6.3 One-step displacement experiments

The one-step displacement experiments describe the processes where crude oil is displaced by one of the different LS and LS-AOT solutions. The constant low volumetric injection rates used were 0.5 and 0.065 μL/min. The volume of aqueous solution injected after the flood reached the

network of channels was set to be 5 μL, which is about two and a half pore volumes (volume injected/volume of the network area). The video of the displacement for the injection rate of 0.5 μL/min was acquired with a rate of 10 frames per minute, while the video of the displacement for the injection rate of 0.065 μL/min was acquired with a rate of 60 frames per hour. To ensure repeatability, the one-step displacement experiments were performed three times for each of the fluid pairs.

4.6.4 Two-step displacement experiments

The two-step displacement experiments describe the processes where the crude oil first is displaced by a high salinity (HS) solution (0.06 M, Ca/Na = 0.017) at the improved oil recovery (IOR) stage and then displaced by the different LS and LS-AOT solutions at the EOR stage. The HS solution was injected at a constant low volumetric flow rate of 0.5 μL/min. Just before the water phase started to invade the network area, the recording of the video was started at a frame rate of 10 frames per minute. In this stage, the fixed volume for the injection of HS solution was set to 5 μL. Afterwards, the inlet tubing was disconnected and replaced with the tubing connected to the syringe with the EOR solution. The EOR solution was injected at the same flow rate and was recorded at the same frame rate as it was done with the HS injection. The fixed volume for the injection of the EOR solution was set to 10 μL. To ensure repeatability, the EOR displacement experiments were performed three times for each of the fluid pairs.

4.6.5 Cleaning procedure

After each displacement experiment, the chip was manually cleaned with the following procedure. A syringe was filled with xylene (1 mL) and injected into the chip, followed by isopropanol (1 mL), DI water (1 mL), and air (20 mL). The chips were left in the furnace overnight at a specific heating program. The program starts by increasing the temperature with a rate of 5°C/min up to 450°C, where it keeps the same temperature for 6 hours.

4.6.6 Wettability alteration of micromodels

To assess the effect of surface wettability, the micromodel was chemically altered to hydrophobic. The chips were made hydrophobic by injecting a solution of trichloro(octadecyl)silane (OTS; Sigma-Aldrich) in toluene with a concentration of 0.2 V/V%. The solution was left in the chip

for 15 minutes before air (15 mL) was injected into the chip to empty it. The hydrophobic chips were then left to dry in the fume hood for 24 hours before the displacement experiments could be performed. The preparation before the experiment, one-step displacement experiments, EOR displacement experiments, cleaning, and drying procedure were proceeded as described in the sections above.

4.6.7 Image analysis

The video of the displacement was acquired with a high-resolution camera, DeltaPix camera, connected to a computer and controlled by the software, DeltaPix InSight. After converting the video from .mP4 to .AVI, the video was processed with ImageJ. First, the image of the calibration ruler was used to set the scale. Then the video was opened as an image sequence. The series of images were processed by adjusting the colour threshold. Then the images were converted from RGB to 8-bit. Further, the percentage of the white area in the network was measured by the tool, ROI (region of interest) manager. The recovery of crude oil during the displacements was calculated by

$$R = \frac{A_{o,start} - A_o}{A_{o,start}}, \tag{4.1}$$

where $A_{o,start}$ is the percentage of the area with crude oil before the aqueous solution invades the network area, and A_o is the percentage of the area with crude oil throughout the displacement experiment.

5 Results and discussion

5.1 Density measurements

The density, ρ, of the LS and LS-AOT solutions with molar calcium/sodium ratio equal to 0, 0.010, and 0.040 was measured by the density meter at 23°C. The obtained results are shown in Table 5.1.

Table 5.1: Density of the LS and LS-AOT solutions.

Aqueous solution	Density [g/cm^3]
AOT + Ca/Na (0)	0.999
AOT + Ca/Na (0.010)	0.999
AOT + Ca/Na (0.040)	0.999
Ca/Na (0)	0.998
Ca/Na (0.010)	0.998
Ca/Na (0.040)	0.998

From Table 5.1, it can be seen that the density did not change with the molar calcium/sodium ratio. The density 0.998 g/cm^3 and 0.999 g/cm^2 was used further in the IFT measurements for the LS and LS-AOT solutions, respectively.

5.2 Interfacial tension measurements

The dynamic interfacial tension between the crude oils and the aqueous solutions was measured for up to two hours by the spinning drop tensiometer at 23°C. The dynamic interfacial tension between the crude oils and the LS solutions with varied molar calcium/sodium ratio is shown in Figure 5.1a and 5.1b, respectively.

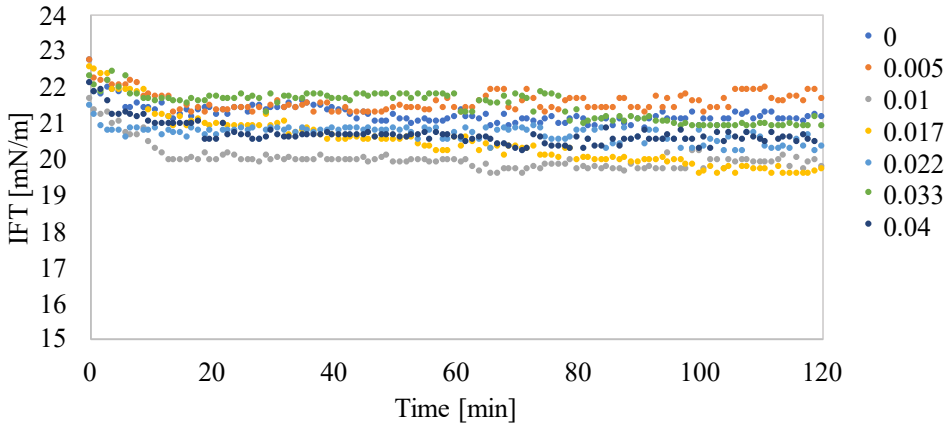

(a) Crude oil A.

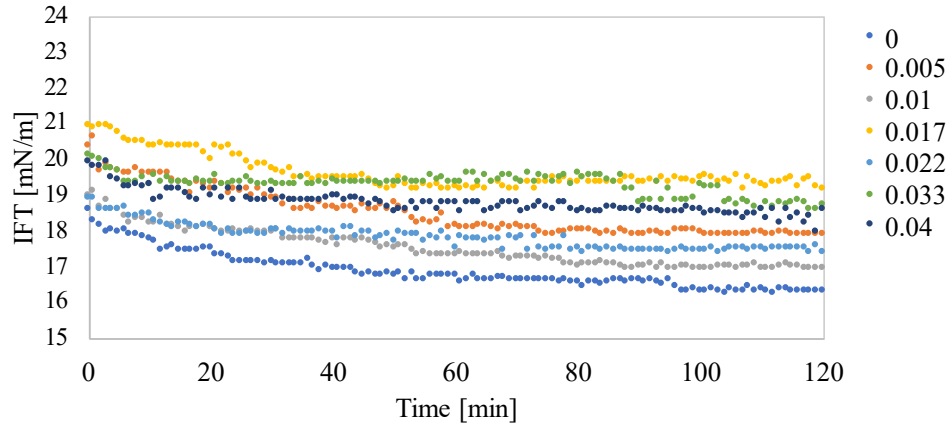

(b) Crude oil C.

Figure 5.1: Dynamic IFT between the crude oils and the LS solutions with different molar calcium/sodium ratios at 23°C.

From Figure 5.1a and 5.1b, it can be seen that the IFT, for all the molar calcium/sodium ratios, slowly decreased until it reached equilibrium. The decrease in IFT is probably because the surface active components in the crude oil adsorb to the interface and, thus, decrease the IFT. In general, it can be seen that the IFT is lower for crude oil C compared to crude oil A. According to Table 4.1, crude oil A consists of a larger amount of polar components, such as asphaltenes and resins, than crude oil C. However, crude oil C has a higher acidity than crude oil A. Hence, crude oil C might contain more naphthenic acids than crude oil A. Thus, among the surface active components in the crude oils, it seems like the naphthenic acids have the

largest effect on IFT. In addition, the naphthenic acids are smaller components compared to the asphaltenes and may, therefore, migrate to the interface faster. According to the two graphs, it can also be seen that the presence of calcium leads to a smaller decrease in IFT and, thus, the time before the IFT reaches equilibrium is shorter for the higher calcium/sodium ratios. This might be because the presence of calcium cause a reduction in the surface activity of naphthenic acids due to a salting-out effect [67, 68].

An average value of the IFT was calculated from the final 20 minutes of the measurement. These equilibrium IFT values between the crude oils and the LS solutions with different molar calcium/sodium ratios are shown in Figure 5.2. Exact values of the equilibrium IFT can be found in B.1.

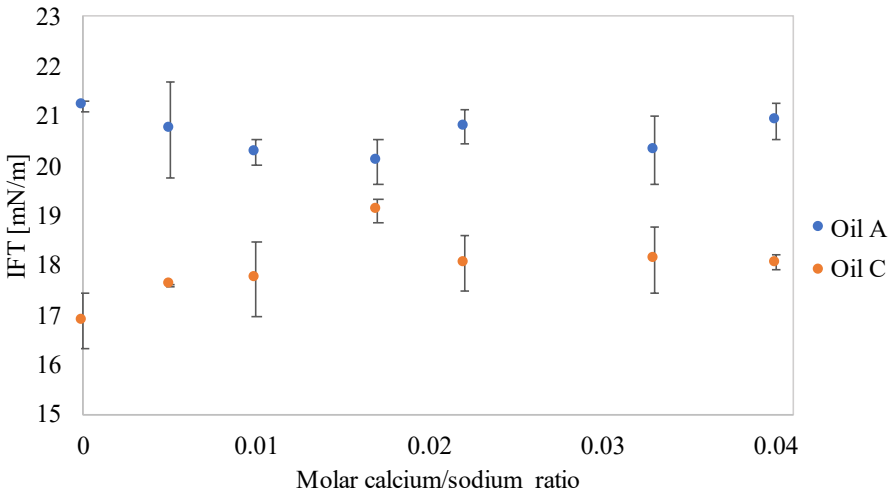

Figure 5.2: Interfacial tension (IFT) between the crude oils and the LS solutions with varying molar calcium/sodium ratio at 23°C.

According to Figure 5.2, the equilibrium IFT values measured with the different molar calcium/sodium ratios do not seem to have a specific trend for crude oil A. However, the molar calcium/sodium ratio equal to 0.017 appears to be a maximum point for crude oil C.

The dynamic interfacial tension between the crude oils and the LS-AOT solutions with varied molar calcium/sodium ratio is shown in Figure 5.3a and Figure 5.3b, respectively.

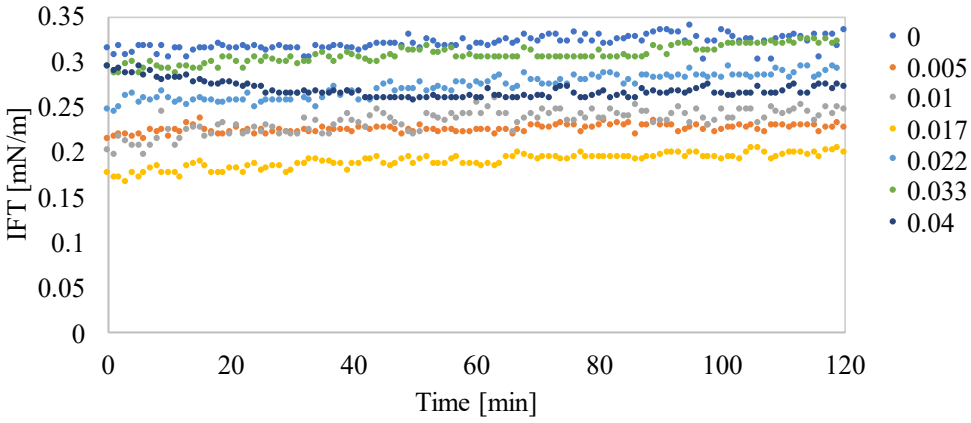

(a) Crude oil A.

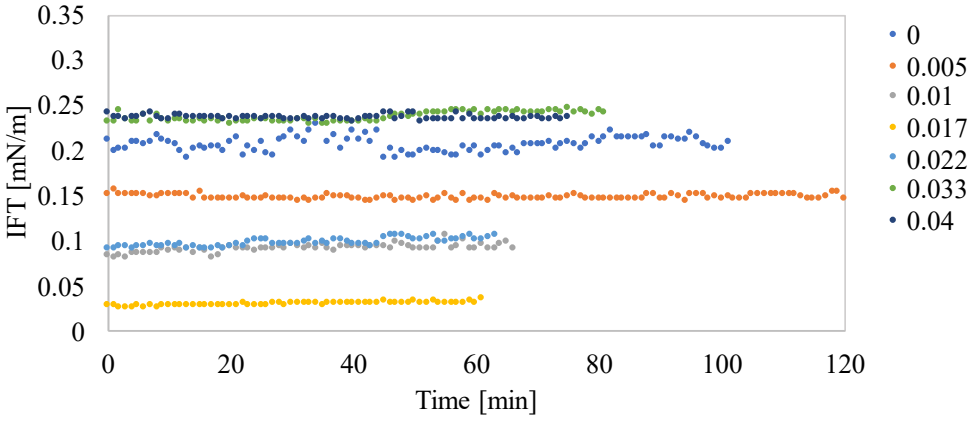

(b) Crude oil C.

Figure 5.3: Dynamic IFT between the crude oils and the LS-AOT solutions with different molar calcium/sodium ratios at 23°C.

By comparing Figure 5.1 and 5.3, it can be seen that the addition of AOT to the systems led to an IFT decrease by a couple orders of magnitude. In general, surfactants decrease the IFT more than surface active components in the crude oil and, thus, the surfactant will be the surface active component dominating the interface. From Figure 5.3a, it can be seen that the IFT is more or less stable through the entire measurements. However, it can be seen that the dynamic IFT, in some cases, mainly the middle molar calcium/sodium ratios, increased slightly with time before it stabilized. Adsorption of surface active compounds at the interface causes a reduction in IFT. Hence, an increase in IFT can indicate that processes where the interfacial excess is

reduced occur. This can include desorption of AOT to the oil phase. Calcium ions can form a bridge between two negatively charged components. If the bridge forms between two AOT molecules, the composed molecule gets hydrophobic and might, therefore, migrate to the oil phase. When equilibrium is reached, adsorption and desorption of surface active components are expected to be in steady-state. Comparison of the dynamic IFT for crude oil A and C show, in general, that the molar calcium/sodium ratio leads to a broader range in IFT for crude oil C. From Figure 5.3b, it can also be seen that the dynamic IFT values between crude oil C and the LS-AOT solutions reached steady state before two hours. The stable dynamic IFT for both crude oils might be because the surfactant molecule added to the system has a high adsorption rate. Hence, the surfactant has probably adsorbed to the interface during the start-up of the measurement.

The equilibrium IFT values between the crude oils and the LS-AOT solutions with different molar calcium/sodium ratios are shown in Figure 5.4. Exact values of the equilibrium IFT can be found in B.1.

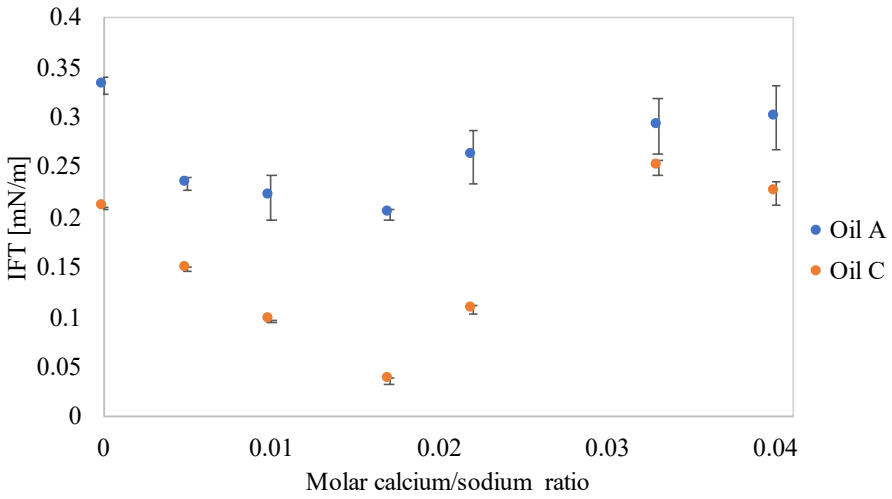

Figure 5.4: Interfacial tension (IFT) between the crude oils and LS-AOT with varying molar calcium/sodium ratio at 23°C.

From Figure 5.4, it can be seen that the IFT depends on the molar calcium/sodium ratio. The minimum IFT obtained for both crude oils is measured with the molar calcium/sodium ratio equal to 0.017, even though the minimum is less clear for crude oil A. Hence, the optimal point for recovery is expected to be with the molar calcium/sodium ratio equal to 0.017. For crude

oil C, the minimum IFT value is around one order of magnitude lower than the IFT value measured without calcium. Previous studies [67, 68] have suggested that the surface activity of AOT increases with the presence of calcium. In addition, they suggested that the presence of calcium leads to a decrease in the surface activity of naphthenic acids due to the salting-out effect. Crude oil C contains a higher number of TAN and might, therefore, lead to this larger decrease in IFT when a small amount of calcium is present. At a certain point, the increase in molar calcium/sodium ratio leads to an increase in IFT. This might be because bridges between two AOT molecules occurs which can lead to migration of AOT to the oil phase.

As a result of the equilibrium IFT values measured between the different fluid pairs, it was decided to investigate the displacement of the two crude oils by the LS-AOT solutions and LS solutions with molar calcium/sodium ratios equal to 0, 0.017 and 0.040.

5.3 Microfluidics: One-step displacement experiments

Displacement experiments were performed for the two crude oils by the LS-AOT and LS solutions with molar calcium/sodium ratios equal to 0, 0.017 and 0.040. The capillary numbers in these experiments range from $1.4 \cdot 10^{-7}$ to $6.2 \cdot 10^{-4}$.

5.3.1 Effect of molar calcium/sodium ratio

The recovery factors for crude oil A and C after injection of the LS-AOT and LS solutions, with different molar calcium/sodium ratios, at a flow rate of 0.065 μL/min are presented in Figure 5.5.

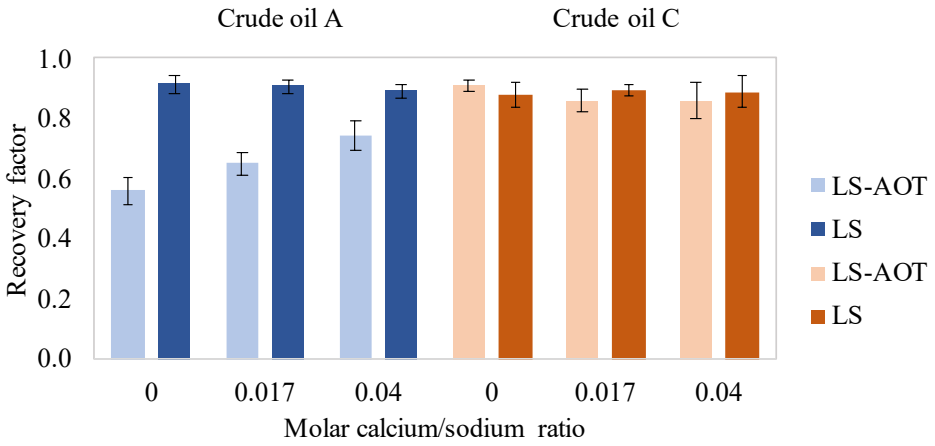

Figure 5.5: Recovery factors for crude oil A and C after injection of the LS-AOT and LS solutions, with different molar calcium/sodium ratios, in the hydrophilic micromodel at 0.065 μL/min.

From Figure 5.5, it can be seen that varying molar calcium/sodium ratio only appears to affect the recovery factor for crude oil A displaced by the LS-AOT solutions. With the increasing amount of calcium, the recovery factor gradually increased. As mentioned previously, it is suggested that presence of calcium can lead to an increase in the surface activity of AOT and a decrease in surface activity of naphthenic acids [67, 68]. However, this trend is not consistent with the IFT results, where the expected optimum point for recovery would be with molar calcium/ratio equal to 0.017. This indicates that the IFT is probably not the only factor that affect the recovery. Other factors that may affect the recovery factor are capillary and viscous forces, wettability and structure of the network. For the other fluid pairs, the recovery factors did not vary significantly when the molar calcium/sodium ratio was increased.

The displacement experiments where crude oil A was displaced by the different LS-AOT solutions at an injection rate of 0.065 μL/min, all showed unstable displacements. One of the displacement patterns where crude oil A is displaced by the LS-AOT solution with molar calcium/sodium ratio equal to 0, 0.017 and 0.040 is shown in Figure 5.6a, 5.6b and 5.6c, respectively.

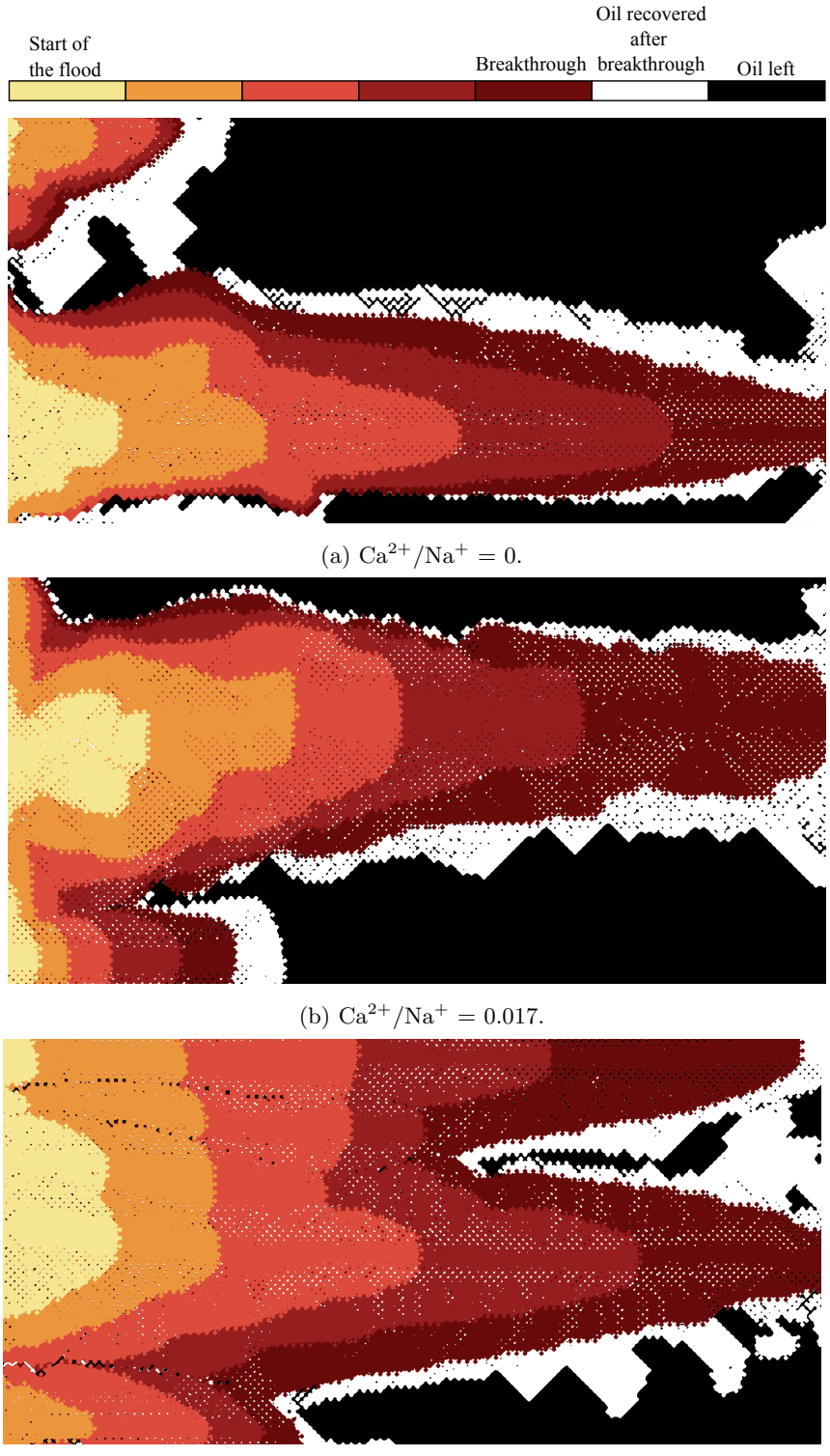

(a) $Ca^{2+}/Na^{+} = 0$.

(b) $Ca^{2+}/Na^{+} = 0.017$.

(c) $Ca^{2+}/Na^{+} = 0.040$.

Figure 5.6: Evolution of the LS-AOT solutions with various molar calcium/sodium ratio displacing crude oil A in the hydrophilic micromodel at 0.065 μL/min. The voids are coloured by the colour of the surrounding channels.

The capillary numbers in these displacement experiments range from $8.7{\cdot}10^{-6}$ to $1.4{\cdot}10^{-5}$. By observations, it seems like the displacement patterns are dominated by viscous forces. In addition, according to the figures above, it seems like the displacement stability gradually increases with increasing molar calcium/sodium ratio. There is no significant change in displacement patterns between Figures 5.6a and 5.6b. However, the finger displacing the oil in Figure 5.6b is thicker than the finger displacing the oil in Figure 5.6a which lead to a higher recovery of oil. When the molar calcium/sodium ratio was equal to 0.040, the stability increased greatly. Hence, leading to the gradual increase in sweep efficiency and, thus, recovery factor.

The displacement experiments where crude oil C was displaced by the different LS-AOT solutions at an injection rate of 0.065 μL/min, all showed an initial stable front that evolved to an unstable front throughout the displacements. As an example, one of the displacement patterns where crude oil C is displaced by the LS-AOT solution with molar calcium/sodium ratio equal to 0.017 is shown in Figure 5.7.

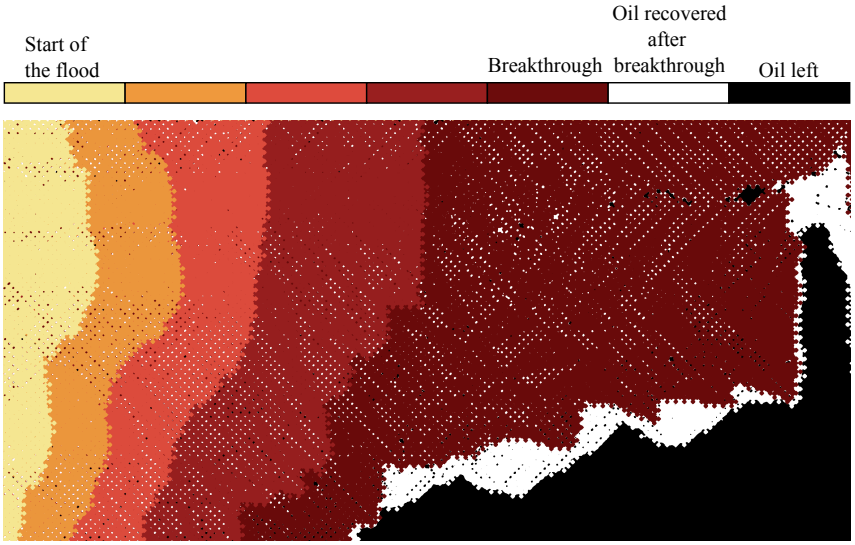

Figure 5.7: Evolution of the LS-AOT solution with molar calcium/sodium ratio equal to 0.017 displacing crude oil C in the hydrophilic micromodel at 0.065 μL/min. The voids are coloured by the colour of the surrounding channels.

The capillary numbers for the displacement of crude oil C by LS-AOT solutions at 0.065 μL/min range from $1.1{\cdot}10^{-5}$ to $8.1{\cdot}10^{-5}$. From Figure 5.7, it can be seen that there is still some oil left in the network, due to the evolved viscous displacement front.

The white spots observed in the displacement patterns shown in Figure 5.6 and 5.7, indicate that the trapped oil in the pores was released as oil droplets by moving with the injection flow after breakthrough. Thus, the surfactant solution not only extracts oil by moving the interface between oil and water, but also releases the oil that may be trapped during the flooding. This leads to continued oil recovery of oil even after breakthrough.

The displacement experiments where both crude oil A and crude oil C were displaced by the different LS solutions at an injection rate of 0.065 μL/min, all showed stable displacements. As an example, one of the displacement patterns where the LS solution with molar calcium/sodium ratio equal to 0.017 displaced crude oil A is shown in Figure 5.8.

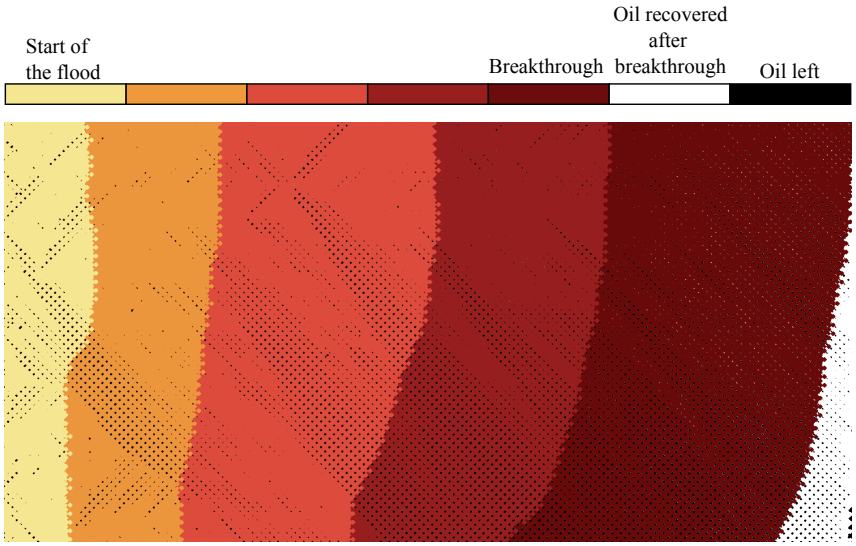

Figure 5.8: Evolution of the LS solution with molar calcium/sodium ratio equal to 0.017 displacing crude oil A in the hydrophilic micromodel at 0.065 μL/min. The voids are coloured by the colour of the surrounding channels.

The capillary numbers for the displacement of either crude oil A or crude oil C by the LS solutions at 0.065 μL/min range from $1.4{\cdot}10^{-7}$ to $1.7{\cdot}10^{-7}$. From Figure 5.8, it can be seen that the stable displacement lead to a complete sweep of the network. Thus, high recovery factors for both crude oils were obtained in these experiments. However, black spots are observed in the displacement pattern, which indicates that oil is still trapped in the pores.

To increase the capillary numbers in the displacement experiments, the injection rate was increased to 0.5 μL/min. The recovery factors for crude oil A and C after injection of the LS-AOT

and LS solutions, with different molar calcium/sodium ratio, at a flow rate of 0.5 μL/min are presented in Figure 5.9.

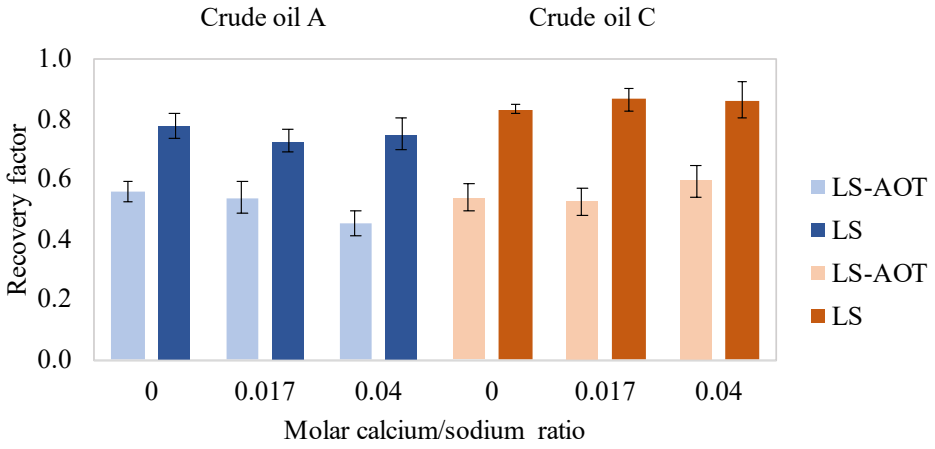

Figure 5.9: Recovery factors for crude oil A and C after injection of the LS-AOT and LS solutions, with different molar calcium/sodium ratio, in the hydrophilic micromodel at 0.5 μL/min.

From Figure 5.9, it can be seen that varying molar calcium/sodium ratio does not seem to have a significant effect on the recovery factors when flooding with the LS solutions. However, the recovery factors for the crude oils displaced by the LS-AOT solutions seem to be affected by the calcium ions. The recovery factor is approximately equal when the molar calcium/sodium ratio is equal to 0 and 0.017 for both crude oils. However, for the molar calcium/sodium ratio equal to 0.040, the recovery factor decreased for crude oil A and increased for crude oil C. Again, this is not consistent with the IFT results where the expected optimum point for recovery would be with molar calcium/ratio equal to 0.017. In addition, comparing between Figure 5.5 and 5.9, show that the trend for crude oil A displaced by the LS-AOT solutions is different. The only parameter changed is the injection rate. By increasing the injection rate, the capillary number increases. Hence, the capillary forces acting on the fluid meniscus contact line between the fluid and the pore wall decreased while the viscous forces present increased. Thus, the capillary number might be the factor leading to the two different trends.

Crude oil C contains a larger amount of naphthenic acids than crude oil A. As mentioned previously, the presence of calcium has shown to decrease the surface activity of naphthenic acids, in addition to increase the surface activity of AOT [67, 68]. Thus, the surface might

be altered towards more water wetness with a high amount of calcium, thus, leading to higher recovery. Crude oil A contains a larger amount of polar components. Thus, the decrease in recovery factor might indicate that the calcium bridges that may form with the asphaltenes in the crude oil are stronger than the calcium bridges that may form with the naphthenic acids, at this injection rate. However, further investigations need to be performed to know the exact reason for this.

The displacement experiments where crude oil A was displaced by the different LS-AOT solutions at an injection rate of 0.5 μL/min, all showed unstable displacements. When the molar calcium/sodium ratio was equal to 0 and 0.017, the water phase displaced the crude oil with a high branching level. Increasing the ratio to 0.040 led to a pattern with fewer branches and, thus, a lower sweep efficiency. One of the displacement patterns where crude oil A is displaced by the LS-AOT solutions with molar calcium/sodium ratio equal to 0.017 and 0.040 is shown in Figure 5.10a and 5.10b, respectively.

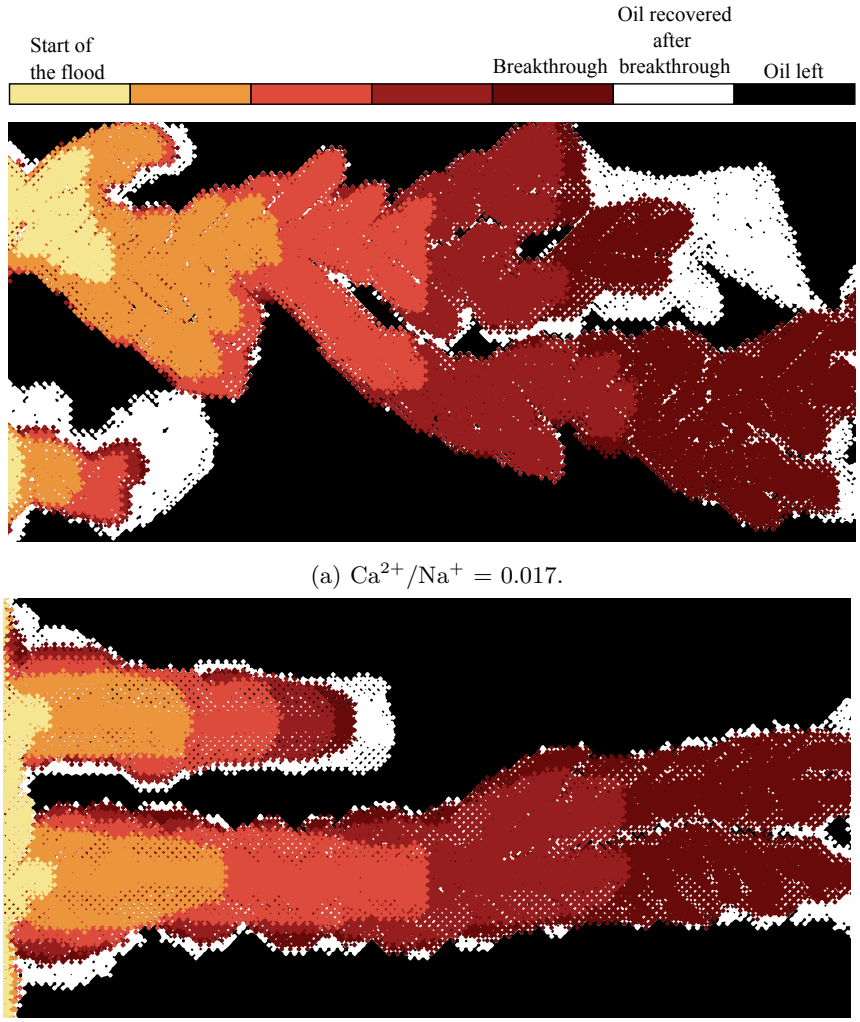

(a) $Ca^{2+}/Na^{+} = 0.017$.

(b) $Ca^{2+}/Na^{+} = 0.040$.

Figure 5.10: Evolution of the LS-AOT solutions with different molar calcium/sodium ratio displacing crude oil A in the hydrophilic micromodel at 0.5 μL/min. The voids are coloured by the colour of the surrounding channels.

The capillary numbers for the displacement of crude oil A by the LS-AOT solutions at 0.5 μL/min range from $6.7{\cdot}10^{-5}$ to $0.1{\cdot}10^{-4}$. From Figure 5.10, it appears that viscous forces dominate the unstable displacements leading to viscous fingering. There was no significant effect on the patterns when the molar calcium/sodium ratio was increased from 0 to 0.017. However, comparing between Figure 5.10a and 5.10b, show that when the molar calcium/sodium ratio was increased from 0.017 to 0.040, a decrease in branching level occurred. Hence, the decrease in oil recovery factor.

The displacement experiments where crude oil C was displaced by the different LS-AOT solutions at an injection rate of 0.5 μL/min, all showed unstable displacement patterns with the growth of a single finger. As an example, one of the displacement patterns where the LS-AOT solution with molar calcium/sodium ratio equal to 0.017 displaced crude oil C is shown in Figure 5.11.

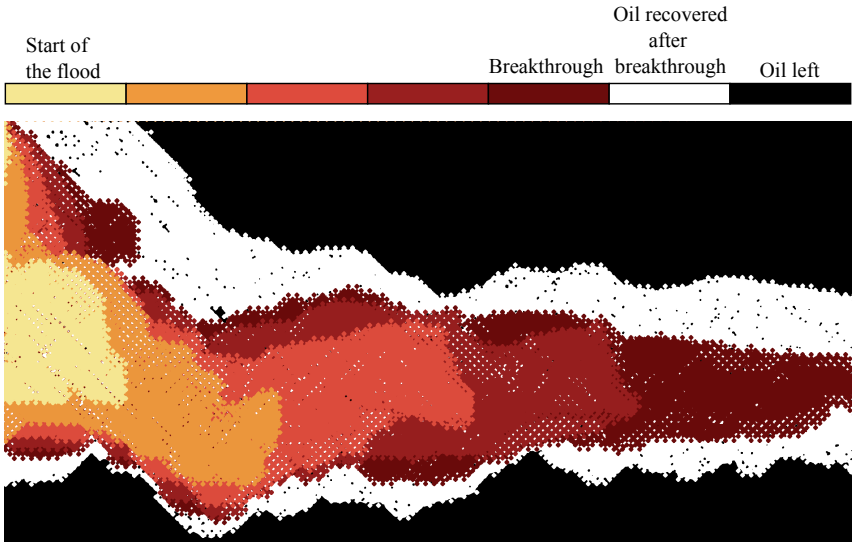

Figure 5.11: Evolution of the LS-AOT solution with molar calcium/sodium ratio equal to 0.017 displacing crude oil C in the hydrophilic micromodel at 0.5 μL/min. The voids are coloured by the colour of the surrounding channels.

The capillary numbers for the displacement of crude oil C by the LS-AOT solutions at 0.5 μL/min range from $9.8{\cdot}10^{-5}$ to $0.6{\cdot}10^{-4}$. From Figure 5.11, the displacement patterns showed dominance by viscous forces leading to viscous fingering. The single finger displacing the oil lead to bypassed oil.

The displacement experiments where crude oil A was displaced by the different LS solutions at an injection rate of 0.5 μL/min, all showed unstable displacement. As an example, one of the displacement patterns where the LS solution with molar calcium/sodium ratio equal to 0.017 displaced crude oil A is shown in Figure 5.12.

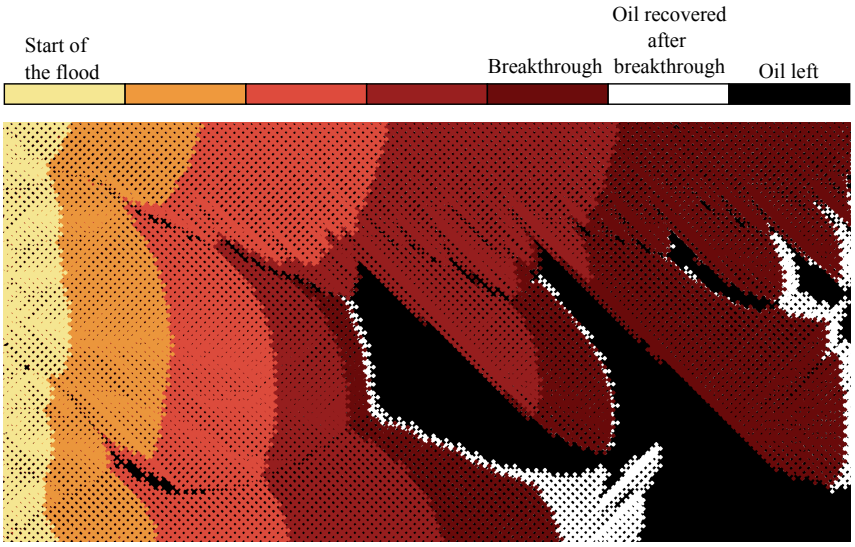

Figure 5.12: Evolution of the LS solution with molar calcium/sodium ratio equal to 0.017 displacing crude oil A in the hydrophilic micromodel at 0.5 μL/min. The voids are coloured by the colour of the surrounding channels.

The capillary numbers for the displacement of crude oil A by the LS solutions at 0.5 μL/min range from $1.0 \cdot 10^{-6}$ to $1.1 \cdot 10^{-6}$. From Figure 5.12, it can be seen that the displacement patterns appear to be dominated by viscous forces. The effect of calcium ions does not seem to affect the displacement pattern under these conditions.

The displacement experiments where crude oil C was displaced by the different LS solutions at an injection rate of 0.5 μL/min, all showed an initial unstable front evolving to a stable front throughout the displacement. As an example, one of the displacement patterns where the LS solution with molar calcium/sodium ratio equal to 0.017 displaced crude oil C is shown in Figure 5.13.

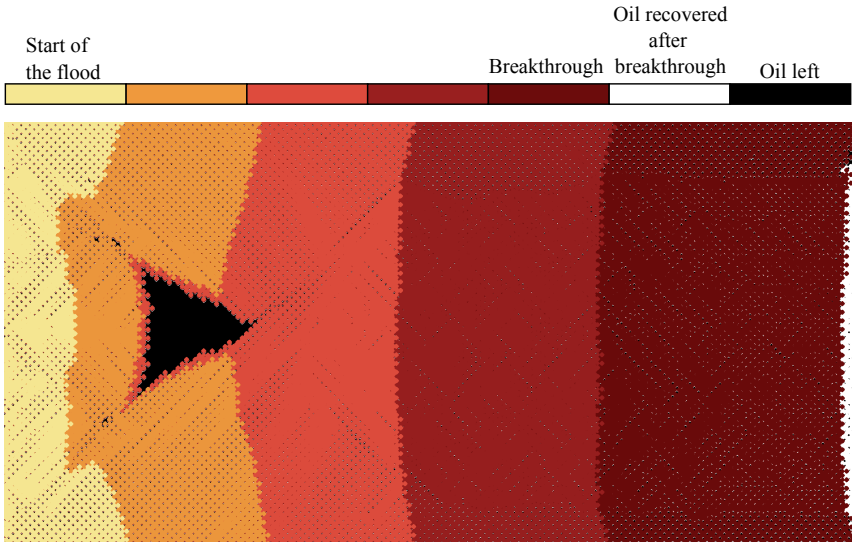

Figure 5.13: Evolution of the LS solution with molar calcium/sodium ratio equal to 0.017 displacing crude oil C in the hydrophilic micromodel at 0.5 μL/min. The voids are coloured by the colour of the surrounding channels.

The capillary numbers for the displacement of crude oil C by the LS solutions at 0.5 μL/min range from $1.2{\cdot}10^{-6}$ to $1.3{\cdot}10^{-6}$.

In general, it can be seen that increasing the injection rate from 0.065 to 0.5 μL/min lead to a decrease in the stability of the displacement. As expected, the dominance of viscous forces seems to increase when the injection rate is increased. Hence, leading to a lower sweep efficiency in these experiments.

5.3.2 Effect of surfactant

By the addition of AOT to the LS solutions, the patterns changed and, hence, affected the recovery factors. In general, it seems like the addition of surfactant leads to a more unstable displacement, which causes a lower recovery of oil in the one-step displacement experiments. However, it is clearly shown that the surfactant reduces the IFT and alters the wettability of the reservoir, and ,therefore, recovers trapped oil during the displacement. As an example, the final picture of the experiments where crude oil A is displaced by the LS-AOT and LS solution with molar calcium/sodium ratio equal to 0.017 at the injection rate of 0.5 μL/min is shown in Figure 5.14.

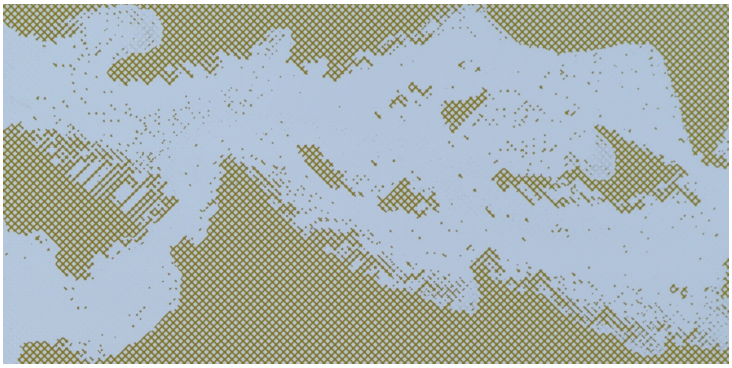

(a) LS-AOT solution.

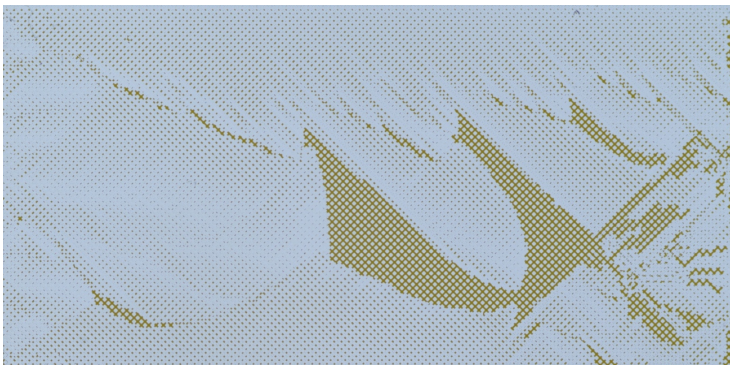

(b) LS solution.

Figure 5.14: Final picture of crude oil A displaced by the LS-AOT and LS solution with molar calcium/sodium ratio equal to 0.017 at 0.5 μL/min.

A comparison between Figure 5.14a and 5.14b, show that the LS solution with AOT almost completely washed away the oil droplets on its path while the LS solution left a lot of trapped oil in the pore throats. When the injection rate is 0.065 μL/min, the process of releasing trapped oil droplets were slower. This can be seen in the dynamic recovery graphs. As an example, the dynamic recovery of crude oil A displaced by the LS-AOT solution with molar calcium/sodium ratio equal to 0.017 at an injection rate of 0.065 μL/min is shown in Figure 5.15.

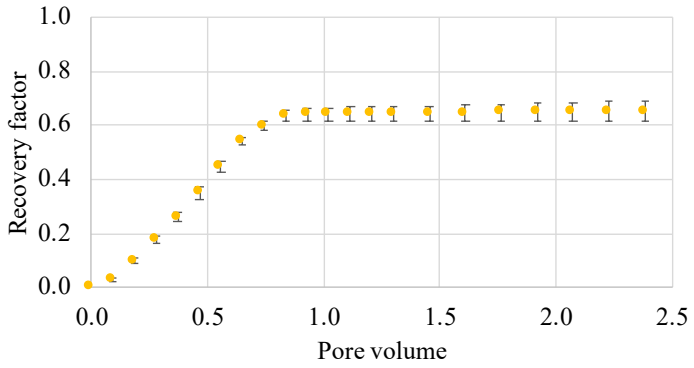

Figure 5.15: Dynamic recovery of crude oil A displaced by the LS-AOT solution, with molar calcium/sodium ratio equal to 0.017, in the hydrophilic micromodel at 0.065 μL/min.

According to Figure 5.15, the recovery increased significantly until breakthrough and then it flattened out. However, the recovery factor does not reach equilibrium. Even though the recovery increased slowly after breakthrough, it will eventually lead to a complete sweep of the network. This is because the surfactant solution keeps releasing oil droplets from the pores. A picture of the displacement after injecting 32 pore volumes is shown in Figure 5.16.

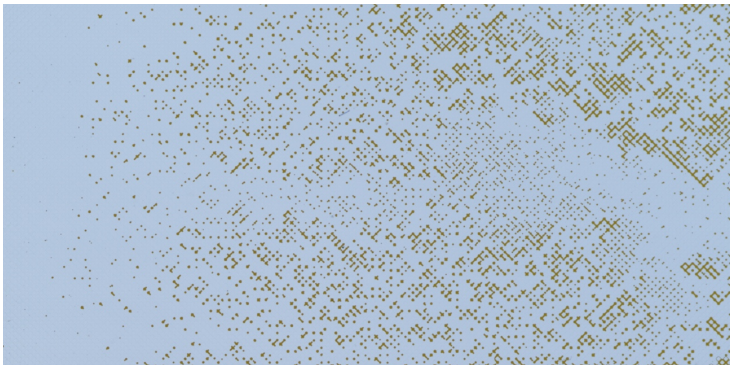

Figure 5.16: Picture of crude oil A displaced by the LS-AOT solution with molar calcium/sodium ratio equal to 0.017 at 0.065 μL after flooding 32 pore volumes.

Even though the displacement has not reached a complete sweep of the network yet, this will eventually occur. Since the process of releasing droplets occurs more rapidly when the injection rate is 0.5 μL/min, a complete sweep of the network would be obtained earlier with this injection rate.

In general, the LS solutions do not seem to release oil droplets that are trapped during the

displacement. Thus, the oil recovery for these displacements reaches equilibrium at some point. As an example, this can be seen in Figure 5.17 where the dynamic recovery of crude oil A displaced by the LS solution with molar calcium/sodium ratio equal to 0.017 at an injection rate of 0.065 μL/min is shown.

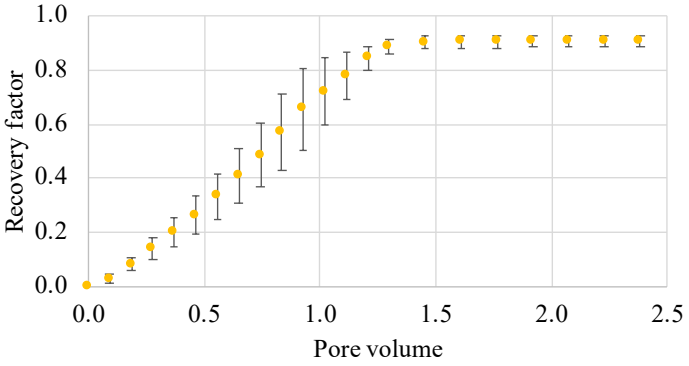

Figure 5.17: Dynamic recovery of crude oil A displaced by LS solution, with molar calcium/sodium ratio equal to 0.017, in the hydrophilic micromodel at 0.065 μL/min.

By comparing Figure 5.15 and 5.17, it can be seen that the flooding of LS-AOT solution reaches breakthrough before the LS solution. This might be due to the sufficiently lower IFT obtained for the LS-AOT solutions. Hence, a lower pressure is needed for the water phase to invade the network. However, part of this difference is also because the recovery factor of oil A is higher in Figure 5.17 by 25% compared to Figure 5.15. The recovery graphs for the other fluid pairs displaced with an injection rate of 0.065 and 0.5 μL/min in the one-step displacement experiments can be found in C.1.

5.3.3 Effect of crude oil

In general, a comparison between the displacement patterns of crude oil A and C displaced by the various LS-AOT and LS solutions show that the flooding of crude oil C is more stable. Since most of the flooding experiments appeared to be either stable or dominated by viscous forces, the viscosity ratio plays an important part in these experiments. Crude oil A has a higher viscosity than crude oil C and, thus, a lower mobility ratio. Hence, this might be the reason for the lower stability observed in the displacements of crude oil A.

In addition, surface wettability might be affected by the amount of adsorbed surface active

components in the crude oil onto the surface. Both crude oil A and C are acidic crude oils, but crude oil C contains a larger amount of acidic components. Crude oil A contains a larger total amount of resins and asphaltenes. Thus, it may imply that the adsorption of asphaltenes lead to more oil wetness compared to the adsorption of naphthenic acids.

The more stable displacement patterns obtained for crude oil C leads to higher recovery factors. When the injection rate was 0.065 μL/min, the largest difference in recovery factors for the crude oils appeared with the flooding of LS-AOT solutions. This can be seen in Figure 5.5. When the injection rate was 0.5 μL/min, the largest difference in recovery factors for the crude oils appeared with the flooding of LS solutions. This can be seen in Figure 5.9.

The time before the flooding reaches breakthrough when injection rate is 0.5 μL/min seems to depend on the crude oil. As an example, the dynamic recovery of crude oil A and C displaced by the LS-AOT solution with molar calcium/sodium ratio equal to 0.017 at an injection rate of 0.5 μL/min can be seen in Figure 5.18.

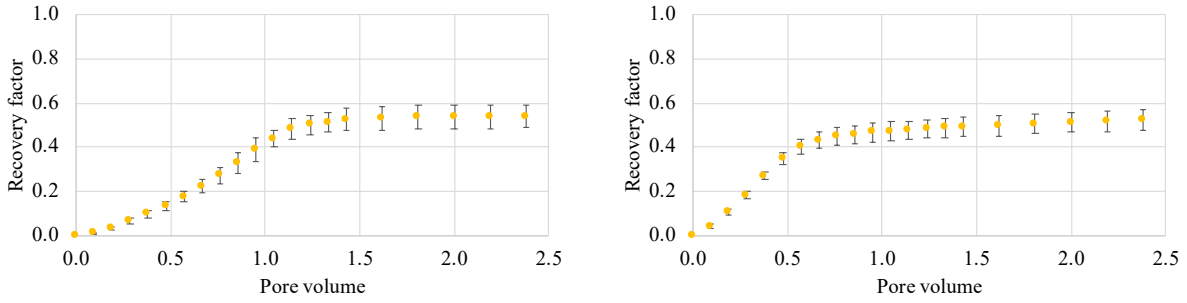

(a) Crude oil A.

(b) Crude oil C.

Figure 5.18: Dynamic recovery of both crude oil A and C during the displacement of LS-AOT solution, with molar calcium/sodium ratio equal to 0.017, in the hydrophilic micromodel at 0.5 μL/min.

According to Figure 5.18, the displacement of crude oil C reaches breakthrough before crude oil A. This might be because crude oil C has a higher mobility ratio or because the surface might be less oil-wet or a combination of both. In addition, by comparing the recovery slopes after breakthrough shows that the recovery of crude oil C after breakthrough is at a higher pace compared to crude oil A.

5.3.4 Effect of aging

To assess the effect of aging, a chip was filled with crude oil C and left to age for seven weeks. In this experiment, crude oil C was displaced by the LS-AOT solution with molar calcium/sodium ratio equal to 0 at a constant flow rate of 0.5 μL/min. The effect of aging was studied by comparing the displacement patterns and the recovery factors from the displacement experiments with the same fluid pairs displaced after two hours of aging. The displacement pattern of crude oil C displaced by the LS-AOT solution with molar calcium/sodium ratio equal to 0 after seven weeks of aging can be seen in Figure 5.19.

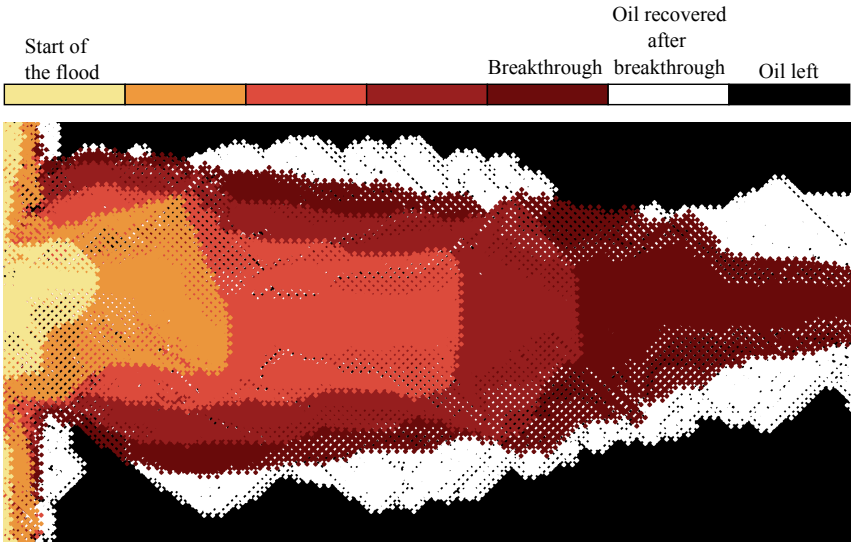

Figure 5.19: Evolution of the LS-AOT solution with molar calcium/sodium ratio equal to 0 displacing crude oil C after seven weeks of aging at 0.5 μL/min. The voids are coloured by the colour of the surrounding channels.

From the displacement pattern shown in Figure 5.19, it can be seen that the displacement front is unstable dominated by viscous forces. Compared to the displacement after two hours of aging, shown in Figure 5.11, both displaced the crude oil with one finger. However, the finger observed displacing the oil after seven weeks of aging is thicker and therefore recovering more oil. However, it can be seen that after breakthrough similar amount of oil is recovered because of the presence of surfactant. The recovery factors for crude oil C displaced by the LS-AOT solution with molar calcium/sodium ratio equal to 0 after two hours of aging and seven weeks of aging are presented in Figure 5.20.

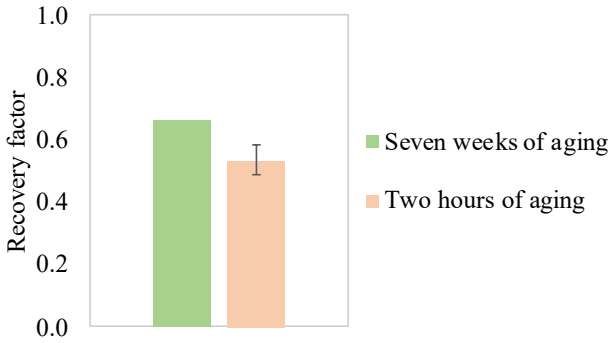

Figure 5.20: Recovery factors for crude oil C displaced by the LS-AOT solution with molar calcium/sodium ratio equal to 0 at 0.5 μL/min after seven weeks and two hours of aging.

From Figure 5.20, it can be seen that the recovery factor for crude oil C was higher after seven weeks of aging. However, this experiment was only performed one time, and the corresponding deviation could, therefore, fall into the range of the recovery factor after two hours of aging. The increase in recovery might be because the volume injected before reaching breakthrough was higher for this experiment. Due to the alike displacement patterns obtained for both cases it seems like crude oil C does not depend on if the aging time is two hours or more. This may indicate that the surface active components in the crude oil have already adsorbed to the surface before two hours.

5.3.5 Effect of wettability

To assess the effect of surface wettability, the two crude oils were displaced by the LS-AOT solutions with molar calcium/sodium ratio equal to 0 and 0.017 in the hydrophobic micromodel at a constant flow rate of 0.065 and 0.5 μL/min. The effect of surface wettability was studied by comparing the displacement patterns and the recovery factors from the displacement experiments with the same fluid pairs performed in the hydrophilic micromodel.

The displacement experiments where the LS-AOT solutions displaced crude oil A at an injection rate of 0.065 μL/min, all showed unstable displacements that seem to be dominated by viscous forces. One of the displacement patterns where crude oil A is displaced by the LS-AOT solution with molar calcium/sodium ratio equal to 0.017 under hydrophobic conditions at a constant injection rate of 0.065 μL/min is shown in Figure 5.21.

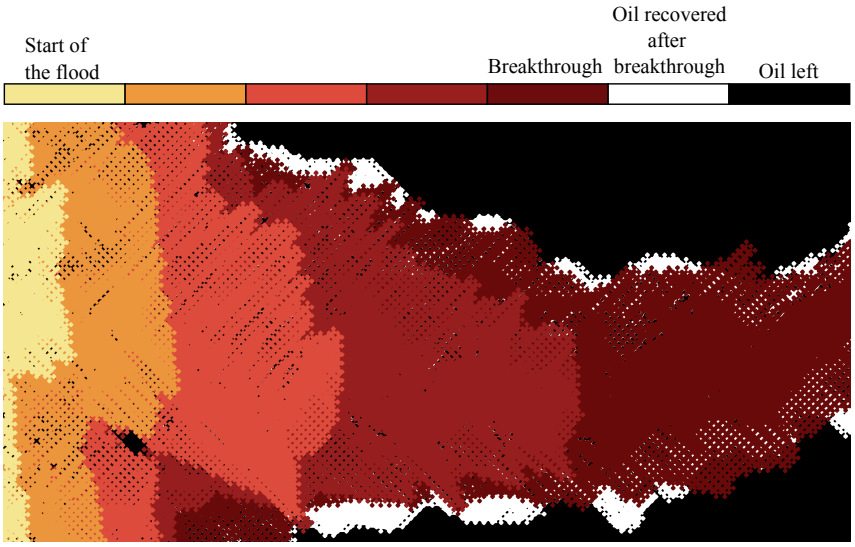

Figure 5.21: Evolution of the LS-AOT solution with molar calcium/sodium ratio equal to 0.017 displacing crude oil A in the hydrophobic micromodel at 0.065 μL/min. The voids are coloured by the colour of the surrounding channels.

From Figure 5.21, it can be seen that the LS-AOT solution displaced the oil with a stable front before a single finger displaced the oil further. Compared to the displacement pattern obtained for the same fluid pair displaced in the hydrophilic micromodel, shown in Figure 5.6b, the finger breaks out later in the hydrophobic system. In addition, it can be observed that the front line is less stable under hydrophobic conditions.

The displacement experiments where the LS-AOT solutions displaced crude oil C at an injection rate of 0.065 μL/min, all showed stable displacement. One of the displacement patterns where crude oil C is displaced by the LS-AOT solution with molar calcium/sodium ratio equal to 0.017 under hydrophobic conditions at a constant injection rate of 0.065 μL/min is shown in in Figure 5.22.

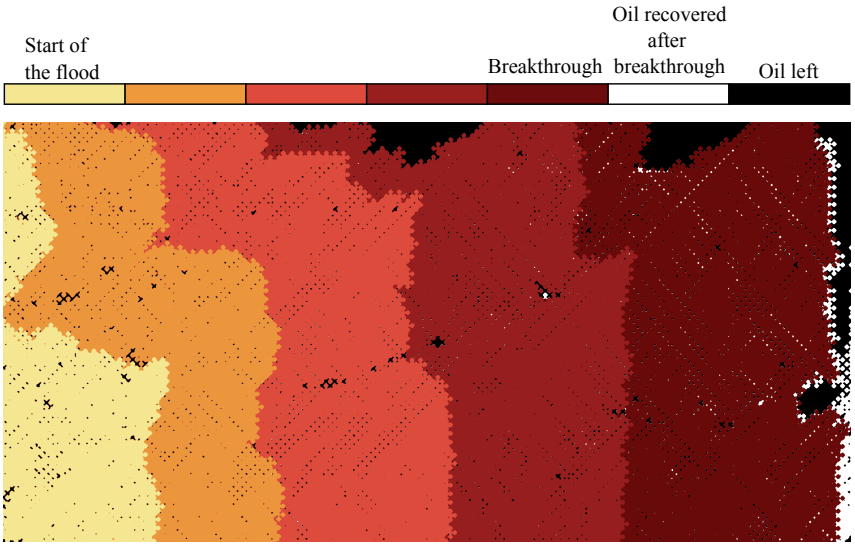

Figure 5.22: Evolution of the LS-AOT solution with molar calcium/sodium ratio equal to 0.017 displacing crude oil C in the hydrophobic micromodel at 0.065 μL/min. The voids are coloured by the colour of the surrounding channels.

From Figure 5.22, it can be seen that the stability of the displacement is similar to the one obtained in the hydrophilic system, shown in Figure 5.7. The stable displacement leads to an almost complete sweep of the network. Compared to the displacement of crude oil A, shown in Figure 5.21, the stability has increased. This might be because crude oil A is more viscous than crude oil C, leading to a less favorable mobility ratio. In general, for both crude oil A and C, it can be seen that changing the micromodel from hydrophilic to hydrophobic leads to more trapped oil during the displacement by the LS-AOT solutions at 0.065 μL/min. Hence, the black spots observed in the displacement patterns shown in Figure 5.21 and 5.22. The trapped oil in the pores might imply that there are some loss of surfactant due to hydrophobic tail adsorption on the hydrophobic surface.

The recovery factors for crude oil A and C displaced by the various LS-AOT solutions at a constant flow rate of 0.065 μL/min in both the hydrophilic and hydrophobic systems are presented in Figure 5.23.

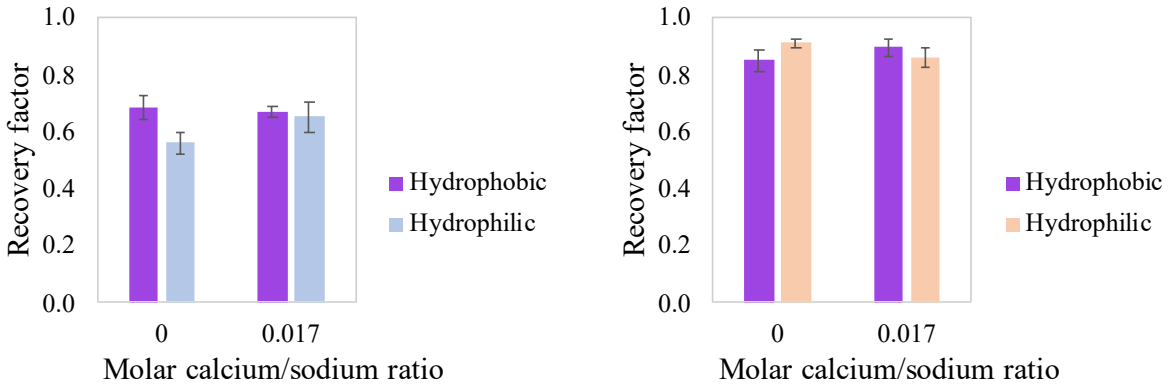

(a) Crude oil A.

(b) Crude oil C.

Figure 5.23: Recovery factors for crude oil A and C displaced by the LS-AOT solutions with molar calcium/sodium ratio equal to 0 and 0.017 at a constant flow rate of 0.065 μL/min under both hydrophilic and hydrophobic conditions.

According to Figure 5.23a, the recovery factor for crude oil A was higher after displacement by the LS-AOT solution with molar calcium/sodium ratio equal to 0 under hydrophobic conditions compared to the same fluid displacement under hydrophilic conditions. This is probably due to the more stable pattern obtained at the beginning of the flooding under hydrophobic conditions, shown in Figure 5.21, compared to the pattern obtained under hydrophilic conditions, shown in Figure 5.6a. The recovery factor for crude oil A displaced by the LS-AOT solution with molar calcium/sodium ratio equal to 0.017 did not seem to be affected by the surface wettability. According to Figure 5.23b, the recovery factor for crude oil C was lower after displacement by the LS-AOT solutions with molar calcium/sodium ratio equal to 0 under hydrophobic conditions compared to the same fluid displacement under hydrophilic conditions. This might be due to the larger amount of trapped oil during the displacement under hydrophobic conditions. The recovery factor for crude oil C displaced by the LS-AOT solution with molar calcium/sodium ratio equal to 0.017 did not seem to be significantly affected by changing the surface from hydrophilic to hydrophobic. For crude oil A, the presence of calcium ions did not seem to have an effect in recovery factor under hydrophobic conditions. For crude oil C, the presence of calcium seemed to slightly increase the recovery factor. This might be due to the significant lower IFT measured for this molar calcium/sodium ratio. However, this increase might be insignificant due to the small overlap in deviations.

The displacement experiments where the LS-AOT solutions displaced crude oil A at an injection rate of 0.5 μL/min, all showed unstable displacement with the growth of a single finger or a single finger evolving to two fingers. As an example, one of the displacement patterns where crude oil A is displaced by the LS-AOT solution with molar calcium/sodium ratio equal to 0.017 under hydrophobic conditions at 0.5 μL/min is shown in Figure 5.24.

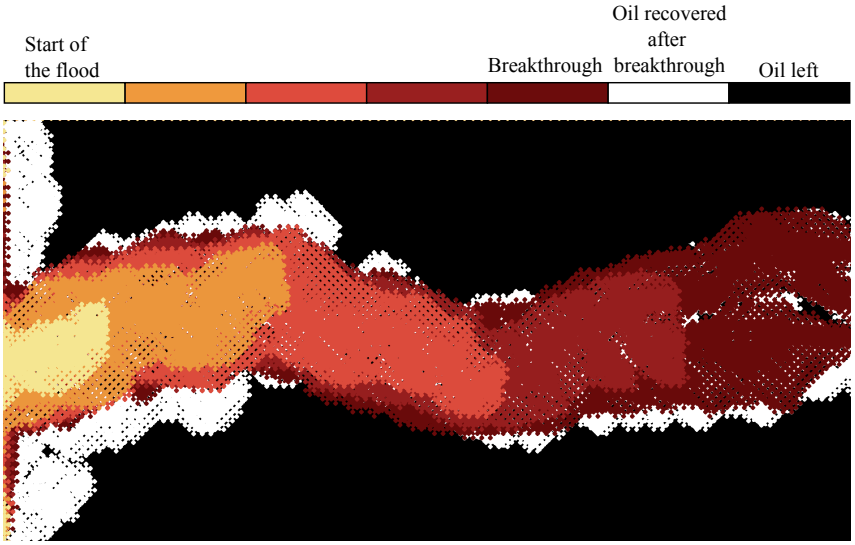

Figure 5.24: Evolution of the LS-AOT solution with molar calcium/sodium ratio equal to 0.017 displacing crude oil A in the hydrophobic micromodel at 0.5 μL/min. The voids are coloured by the colour of the surrounding channels.

A comparison between the displacement pattern of crude oil A displaced by the LS-AOT solution with molar calcium/sodium ratio equal to 0.017 at a constant flow rate of 0.5 μL/min in the hydrophilic micromodel, shown in Figure 5.10a and the hydrophobic micromodel, shown in Figure 5.24, shows that the branching level has decreased under hydrophobic conditions.

The displacement experiments where the LS-AOT solutions displaced crude oil C at an injection rate of 0.5 μL/min, all showed unstable displacement. One of the displacement patterns where crude oil C is displaced by the LS-AOT solution with molar calcium/sodium ratio equal to 0.017 under hydrophobic conditions at a constant injection rate of 0.5 μL/min is shown in in Figure 5.25.

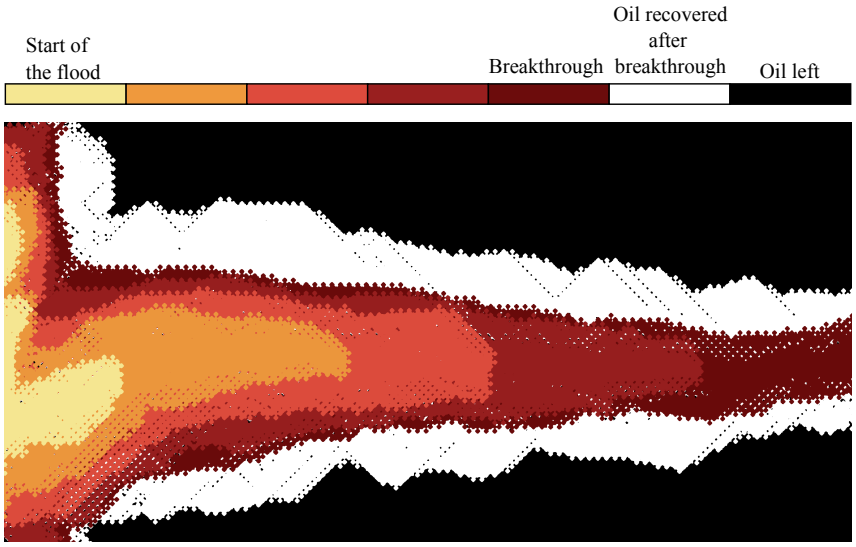

Figure 5.25: Evolution of the LS-AOT solution with molar calcium/sodium ratio equal to 0.017 displacing crude oil C in the hydrophobic micromodel at 0.5 μL/min. The voids are coloured by the colour of the surrounding channels.

From Figure 5.25, it can be seen that the displacement pattern is similar to the obtained displacement pattern in the hydrophilic micromodel, shown in Figure 5.11. Comparing Figure 5.24 and 5.25 clearly show that crude oil C is easier recovered after breakthrough compared to crude oil A, when they are displaced by the LS-AOT solutions at 0.5 μL/min under hydrophobic conditions.

The recovery factors for the two crude oils displaced by the various LS-AOT solutions at a constant flow rate of 0.5 μL/min in both the hydrophilic and hydrophobic systems are presented in Figure 5.26.

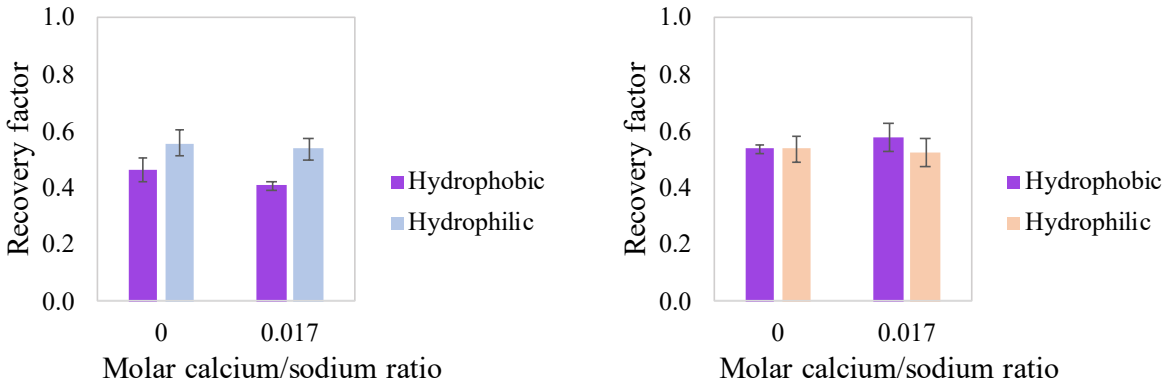

(a) Crude oil A.

(b) Crude oil C.

Figure 5.26: Recovery factors for crude oil A and C displaced by the LS-AOT solutions with molar calcium/sodium ratio equal to 0 and 0.017 at a constant flow rate of 0.5 μL/min under both hydrophilic and hydrophobic conditions.

According to Figure 5.26a, the recovery factor for crude oil A was, in general, lower after displacement by the LS-AOT solutions under hydrophobic conditions compared to the same fluid displacement under hydrophilic conditions. This might be because of loss of surfactant due to hydrophobic tail adsorption to the surface. According to Figure 5.26b, the recovery factor for crude oil C after displacement by the LS-AOT solution with molar calcium/sodium ratio equal to 0 in the hydrophilic and hydrophobic system was approximately equal. Presence of calcium ions in the LS-AOT solutions decreased the recovery factor for crude oil A and increased the recovery factor for crude oil C under hydrophobic conditions. The surface might not be homogeneously hydrophobic after the alteration which can lead to some hydrophilic areas. Since crude oil A contains a larger amount of polar components, the calcium bridges that may form with asphaltenes might be stronger than the calcium bridges that may form with the naphthenic acids. The increase in recovery factor for crude oil C when the molar calcium/sodium ratio was increased to 0.017 can also be due to the lower IFT measured between the oil and LS-AOT solution with this ratio.

5.4 Microfluidics: Two-step displacement experiments

The two-step displacement experiments were performed with the two crude oils displaced by the HS solution at the IOR step followed by the LS solutions, with and without AOT, with

molar calcium/sodium ratio equal to 0 and 0.017 at the EOR step, under both hydrophilic and hydrophobic conditions.

5.4.1 Hydrophilic conditions

The recovery factors for the two crude oils after injection of HS solution at 0.5 μL/min followed by the LS-AOT/LS solutions at 0.5 μL/min under hydrophilic conditions are presented in Figure 5.27.

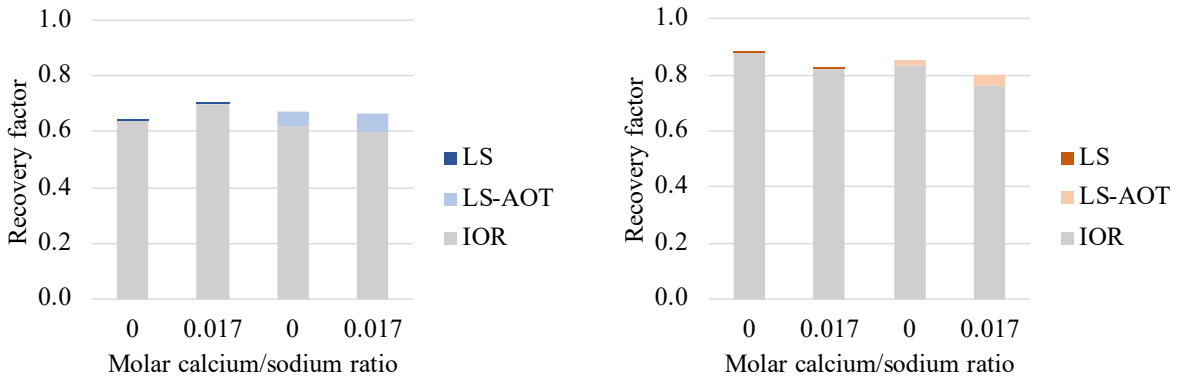

(a) Crude oil A.

(b) Crude oil C.

Figure 5.27: Average recovery factors for crude oil A and crude oil C after injection of the HS solution (IOR stage) and further injection of the EOR solutions in the hydrophilic micromodel.

According to Figure 5.27, it can be seen that the LS-AOT solutions have a larger effect on recovery compared to the LS solutions when it is injected at the EOR step. Exact values of the recovery factors for crude oil A and C after the HS flooding and EOR flooding under hydrophilic conditions, are shown in Table 5.2 and 5.3, respectively.

Table 5.2: Recovery factors (RF) for crude oil A after HS flooding (IOR stage) and EOR flooding under hydrophilic conditions.

EOR solution	IOR RF [%]	EOR RF [%]	Total RF [%]
LS (0)	64.00 ± 6.47	0.09	64.09 ± 6.71
LS (0.017)	69.50 ± 7.31	0.43	69.94 ± 7.13
LS-AOT (0)	61.92 ± 6.12	5.38	67.30 ± 4.21
LS-AOT (0.017)	60.22 ± 1.58	6.41	66.63 ± 1.99

Table 5.3: Recovery factors (RF) for crude oil C after HS flooding (IOR stage) and EOR flooding under hydrophilic conditions.

EOR solution	IOR RF [%]	EOR RF [%]	Total RF [%]
LS (0)	87.89 ± 2.82	0.02	87.91 ± 2.70
LS (0.017)	81.70 ± 6.30	0.04	81.74 ± 6.04
LS-AOT (0)	83.52 ± 4.69	1.40	85.01 ± 4.11
LS-AOT (0.017)	76.09 ± 2.67	4.14	80.23 ± 4.13

According to the tables above, the recovery of oil A increased by approximately 5 and 6% after injection of the LS-AOT solutions. For oil C, the recovery increased by approximately 1 and 4% after injection of the LS-AOT solutions. For both crude oils, the molar calcium/sodium ratio equal to 0.017 led to the highest increase in recovery. This might be due to the lower IFT obtained with the molar calcium/sodium ratio equal to 0.017. However, to be able to know if the minimum IFT gives the higher recovery or if the recovery increases with increasing amount of calcium, these experiments should be performed with the molar calcium/sodium ratio equal to 0.040. Thus, a decrease might indicate that the minimum IFT gives the optimum recovery and an increase might indicate that there are other factors affecting the recovery too. When the LS solutions are used at the EOR stage, the recovery increased by less than 1%. Thus, it seems like the low salinity solutions do not further increase the recovery after the IOR stage in the hydrophilic micromodel. Hence, it seems like the presence of calcium in the LS solutions does not promote wettability alteration towards water wetness. The small increase can be due

to deviations from the image analysis.

The dynamic recovery of crude oil A after injection of the HS solution followed by the LS-AOT and the LS solutions with molar calcium/sodium ratio equal to 0.017 under hydrophilic conditions are shown in Figure 5.28a and 5.28b, respectively.

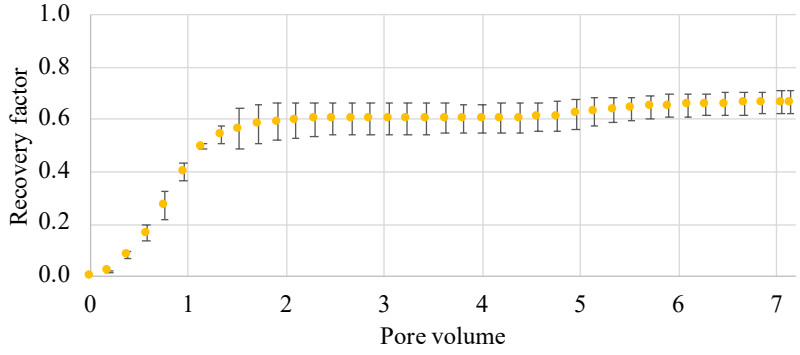

(a) LS-AOT.

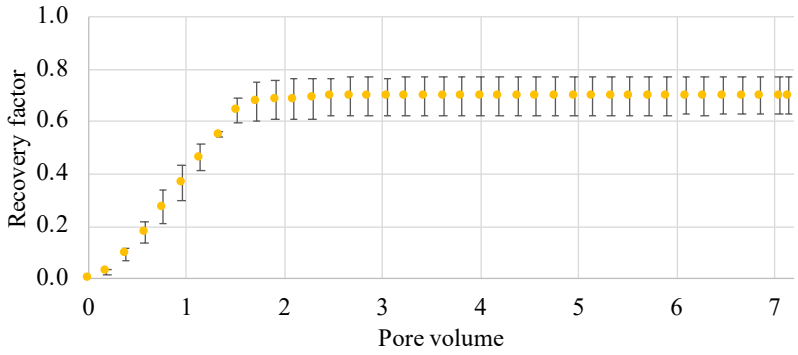

(b) LS.

Figure 5.28: Dynamic recovery of crude oil A during the displacement by the HS solution followed by the LS solution, with and without surfactant, with molar calcium/sodium ratio equal to 0.017 in the hydrophilic micromodel.

From Figure 5.28a, it can be seen that the injection of HS solution lead to an oil recovery of about 0.6. By further injection of the LS-AOT solution, it can be seen that the recovery starts to increase again when the total pore volume injected is around 4, which is where the EOR flood is introduced to the system. Hence, the surfactant starts to reduce the capillary forces and to alter the wettability towards water wetness, which leads to the release of trapped oil droplets. The oil droplets flow through the pores to the outlet leading to the small increase in recovery. From

Figure 5.28b, it can be seen that the further injection of LS solution did not seem to enhance the recovery. Thus, equilibrium seems to be reached after the flooding of the HS solution.

5.4.2 Hydrophobic conditions

Exact values of the recovery factors for crude oil A and C after the HS flooding and EOR flooding under hydrophobic conditions are shown in Table 5.4 and 5.5.

Table 5.4: Recovery factors (RF) for crude oil A after HS flooding (IOR stage) and EOR flooding under hydrophobic conditions.

EOR solution	IOR RF [%]	EOR RF [%]	Total RF [%]
LS (0)	68.69 ± 2.18	0.47	69.16 ± 1.87
LS (0.017)	69.99 ± 1.40	1.53	68.53 ± 2.14
LS-AOT (0)	66.92 ± 3.34	-0.44	66.47 ± 4.34
LS-AOT (0.017)	61.53 ± 4.01	-0.85	60.68 ± 3.90

Table 5.5: Recovery factors (RF) for crude oil C after HS flooding (IOR stage) and EOR flooding under hydrophobic conditions. * Experiment performed twice.

EOR solution	IOR RF [%]	EOR RF [%]	Total RF [%]
LS (0) *	83.91 ± 3.52	-1.46	82.45 ± 4.97
LS (0.017) *	86.95 ± 2.03	-0.85	86.10 ± 1.11
LS-AOT (0)	82.73 ± 2.32	-0.86	81.87 ± 1.40
LS-AOT (0.017)	77.40 ± 2.11	-2.51	74.89 ± 3.79

According to the tables above, the recovery only increased when the LS solutions displaced oil A at the EOR stage. However, the increase seems to be because the HS flooding did not reach steady-state before the EOR flooding was started. For the other fluid pairs displaced, the recovery seemed to decrease. A decrease in recovery is not possible to obtain in reality. However, in this case, the image analysis is based on the recovery of OOIP in the network area of the chip. Before the oil reaches the network of channels, it flows through inlet channels. In

these channels, there is usually some oil left after the IOR stage. When the EOR flooding was started, it released some of the oil left in the inlet channels and carried it to the network area. A higher amount of oil entered the network compared to the amount that was recovered, leading to the decrease in recovery.

6 Further work

Microfluidic methods show good potential as a technique to study the displacement of crude oils by low salinity solutions, with and without surfactant, at constant ionic strength when the molar calcium/sodium ratio is varied. However, more work has to be proceeded to know the effect and mechanisms that may occur under hydrophilic and hydrophobic conditions.

To be able to dictate the wettability of the hydrophilic micromodel after the aging of crude oil A and C, the adsorbed amount of surface active components in the crude oil can be measured by the quartz crystal microbalance. In addition, the contact angles could be measured in the different systems. Further, the zeta potentials of the oil-water and water-solid interfaces could be measured. The value and sign of the zeta potentials can provide a better understanding of the mechanism that takes place during the different displacements.

To provide a better view for the effect of calcium ions at the EOR stage under hydrophobic conditions, the two-step displacement experiments proceeded under hydrophobic conditions could be performed for a longer time. It is also possible to develop a method to measure the distribution of oil entering and leaving the network. Additionally to the displacement experiments performed, displacement experiments of complete EOR tests could be performed. Complete EOR tests describe an additional step to the two-step experiments where the micromodel is initially saturated with brine before the injection of crude oil. The complete EOR tests could give a better understanding of the displacements in a more realistic reservoir. In addition, displacement experiments could be performed where the initial flooding step is HS solution followed by the LS solution and further the LS-AOT solutions. This could give a better picture of the differences in using HS flooding and LS flooding before the surfactant solutions. In general, it can also be an idea to use micromodels with more realistic surfaces.

7 Conclusion

One-step and two-step displacement experiments were proceeded with the UMP to study the displacement of crude oils by low salinity solutions, with and without surfactant, at constant ionic strength when the molar calcium/sodium ratio was varied. Two crude oils and LS solutions, with and without AOT, with seven molar calcium/sodium ratios varying from 0 to 0.040, were studied.

The IFT measurements showed that the IFT between the LS-AOT solutions and the crude oils depends on the molar calcium/sodium ratio when the ionic strength is constant. For both crude oils, the minimum IFT, and thus, the optimum point for recovery, was found to be when the molar calcium/sodium ratio is equal to 0.017. The IFT measurements between the crude oils and the LS solutions showed no significant trend when the molar calcium/sodium ratio was varied. The IFT results also showed that the IFT, in general, was lower for crude oil C compared to crude oil A. Thus, the naphthenic acids seemed to have a larger effect on IFT compared to the other surface active components in the crude oil.

The one-step displacement experiments in the hydrophilic micromodel were performed for the two crude oils displaced by the LS-AOT and LS solutions with molar calcium/sodium ratios equal to 0, 0.017 and 0.040. In general, stable displacement was observed with capillary numbers less than 10^{-6}, and unstable displacement dominated by viscous forces was observed with capillary numbers above 10^{-6}. When the injection rate was fixed at 0.065 μL/min, the recovery of crude oil A gradually increased with an increasing amount of calcium in the LS-AOT solution. The other fluid pairs displaced showed no significant effect on the recovery factor when the molar calcium/sodium ratio was increased. When the injection rate was fixed at 0.5 μL/min, the recovery factor for crude oil A decreased while the recovery factor for crude oil C increased when the molar calcium/sodium ratio was increased to 0.040 in the LS-AOT solutions. When crude oil A and C were displaced by the LS-solutions, the increase in molar calcium/sodium ratio showed no significant effect. In general, the displacements by the LS solutions left a lot of trapped oil in the pore throats. On the contrary, the LS-AOT solutions showed to wash away the oil droplets on its path. Besides, most of the displacements of crude oil A showed to be less stable than the displacements of crude oil C, and thus, leading to a lower recovery factor.

The one-step displacement experiments in the hydrophobic micromodel were performed for the two crude oils displaced by the LS-AOT solutions with molar calcium/sodium ratio equal to 0 and 0.017 at a constant flow rate of 0.065 and 0.5 μL/min to assess the effect of surface wettability. The recovery factors for crude oil A and C after the displacements at 0.065 μL/min showed no significant effect of increasing the molar calcium/sodium ratio from 0 to 0.017. The effect of hydrophobicity showed to increase the recovery factor for crude oil A in the absence of calcium due to a more stable displacement. For the other fluid pairs displaced, there was no significant effect in recovery factors when the micromodel was altered to hydrophobic. However, the displacement patterns showed that more oil was trapped in the pores during the displacements. When the injection rate was fixed at 0.5 μL/min, the recovery factor for crude oil A increased while the recovery factor for crude oil C increased when the molar calcium/sodium ratio was increased from 0 to 0.017.

The two-step displacement experiments performed in the hydrophilic micromodel showed that the LS solutions did not increase the recovery factor for crude oil A or C significantly after the HS flooding. However, the LS-AOT solutions showed to increase the recovery factors. For crude oil A, the recovery increased by approximately 5 and 6% after injection of the LS-AOT solutions. For oil C, the recovery increased by approximately 1 and 4% after injection of the LS-AOT solutions. For both crude oils, the molar calcium/sodium ratio equal to 0.017 led to the highest increase in recovery. Thus, the minimum IFT might be the optimum point for recovery when the LS-AOT solutions are used at the EOR stage. However, further investigation needs to be performed.

References

1. Belhaj, A. F. *et al.* The effect of surfactant concentration, salinity, temperature, and pH on surfactant adsorption for chemical enhanced oil recovery: a review. *Journal of Petroleum Exploration and Production Technology* **10,** 125–137 (Jan. 2020).
2. Gbadamosi, A. O., Junin, R., Manan, M. A., Agi, A. & Yusuff, A. S. An overview of chemical enhanced oil recovery: recent advances and prospects. *International Nano Letters* **9,** 171–202 (Sept. 2019).
3. Ahmed, S. & Elraies, K. A. Microemulsion in Enhanced Oil Recovery. *Science and Technology Behind Nanoemulsions* (Aug. 2018).
4. Mahani, H. *et al. Analysis of field responses to low-salinity waterflooding in secondary and tertiary mode in Syria* in (Society of Petroleum Engineers, Jan. 2011).
5. Xie, Q., Saeedi, A., Pooryousefy, E. & Liu, Y. Extended DLVO-based estimates of surface force in low salinity water flooding. *Journal of Molecular Liquids* **221,** 658–665 (Sept. 2016).
6. Alshakhs, M. J. & Kovscek, A. R. Understanding the role of brine ionic composition on oil recovery by assessment of wettability from colloidal forces. *Advances in Colloid and Interface Science. Clayton Radke Festschrift* **233,** 126–138 (July 2016).
7. Pooryousefy, E., Xie, Q., Chen, Y., Sari, A. & Saeedi, A. Drivers of low salinity effect in sandstone reservoirs. *Journal of Molecular Liquids* **250,** 396–403 (Jan. 2018).
8. Erke, S. I. *et al. Low Salinity Flooding Trial at West Salym Field* in (Society of Petroleum Engineers, Apr. 2016).
9. Abdulla, F. *et al. First EOR Trial using Low Salinity Water Injection in the Greater Burgan Field, Kuwait* in (Society of Petroleum Engineers, Mar. 2013).
10. Chávez-Miyauch, T. E., Lu, Y. & Firoozabadi, A. Low salinity water injection in Berea sandstone: Effect of wettability, interface elasticity, and acid and base functionalities. *Fuel* **263,** 116572 (Mar. 2020).
11. Austad, T., Rezaeidoust, A. & Puntervold, T. *Chemical Mechanism of Low Salinity Water Flooding in Sandstone Reservoirs* in (Society of Petroleum Engineers, Jan. 2010).
12. Lager, A., Webb, K. J., Black, C. J. J., Singleton, M. & Sorbie, K. S. Low Salinity Oil Recovery - An Experimental Investigation1. *Petrophysics* **49** (Feb. 2008).

13. Ligthelm, D. J. *et al. Novel Waterflooding Strategy By Manipulation Of Injection Brine Composition.* in (Society of Petroleum Engineers, Jan. 2009).
14. Fathi, S. J., Austad, T. & Strand, S. "Smart Water" as a Wettability Modifier in Chalk: The Effect of Salinity and Ionic Composition. *Energy & Fuels* **24,** 2514–2519 (Apr. 2010).
15. Alagic, E. & Skauge, A. Combined Low Salinity Brine Injection and Surfactant Flooding in MixedWet Sandstone Cores. *Energy & Fuels* **24,** 3551–3559 (June 2010).
16. Glover, C. J., Puerto, M. C., Maerker, J. M. & Sandvik, E. L. Surfactant Phase Behavior and Retention in Porous Media. *Society of Petroleum Engineers Journal* **19,** 183–193 (June 1979).
17. Pourafshary, P. & Moradpour, N. Hybrid EOR Methods Utilizing Low-Salinity Water. *Enhanced Oil Recovery Processes - New Technologies* (July 2019).
18. Spildo, K., Sun, L., Djurhuus, K. & Skauge, A. A strategy for low cost, effective surfactant injection. *Journal of Petroleum Science and Engineering* **117,** 8–14 (May 2014).
19. Alagic, E., Spildo, K., Skauge, A. & Solbakken, J. Effect of crude oil ageing on low salinity and low salinity surfactant flooding. *Journal of Petroleum Science and Engineering* **78,** 220–227 (Aug. 2011).
20. Viswanathan, B. in *Energy Sources* 29–57 (Elsevier, Amsterdam, Jan. 2017).
21. Akmaz, S., Iscan, O., Gürkaynak, M. & Yasar, M. The Structural Characterization of Saturate, Aromatic, Resin, and Asphaltene Fractions of Batiraman Crude Oil. *Petroleum Science and Technology - PET SCI TECHNOL* **29,** 160–171 (Jan. 2011).
22. Fan, T., Wang, J. & Buckley, J. S. *Evaluating Crude Oils by SARA Analysis* in (Society of Petroleum Engineers, Jan. 2002).
23. Rana, B. S., Cho, D.-W., Cho, K. & Kim, J.-N. Total Acid Number (TAN) reduction of high acidic crude oil by catalytic esterification of naphthenic acids in fixed-bed continuous flow reactor. *Fuel* **231,** 271–280 (Nov. 2018).
24. Mullins, O. C., Sheu, E. Y., Hammami, A. & Marshall, A. G. *Asphaltenes, Heavy Oils, and Petroleomics* (Springer, Nov. 2007).
25. Wolak, A. TBN performance study on a test fleet in real-world driving conditions using present-day engine oils. *Measurement* **114,** 322–331 (Jan. 2018).
26. Zhang, P. & Austad, T. *The Relative Effects of Acid Number and Temperature on Chalk Wettability* in (Society of Petroleum Engineers, Jan. 2005).

27. J.Sheng, J. *Modern Chemical Enhanced Oil Recovery: Theory and Practice* (Gulf Professional Publishing, Nov. 2010).

28. *primary recovery - Schlumberger Oilfield Glossary* `https://www.glossary.oilfield.slb.com/en/Terms/p/primary_recovery.aspx` (2020).

29. *secondary recovery - Schlumberger Oilfield Glossary* `https://www.glossary.oilfield.slb.com/Terms/s/secondary_recovery.aspx` (2020).

30. Mørk, P. C. *Overflate og kolloidkjemi - Grunnleggende prinsipper og teorier* 8th ed. (Institutt for kjemisk prosessteknologi).

31. Ursin, J.-R. Fluid flow in gas condensate reservoirs: the interplay of forces and their relative strengths. *Journal of Petroleum Science and Engineering* **41,** 253–267 (Feb. 2004).

32. Lifton, V. A. Microfluidics: an enabling screening technology for enhanced oil recovery (EOR). *Lab on a chip* **16,** 1777–1796 (2016).

33. Zhang, C., Oostrom, M., Wietsma, T. W., Grate, J. W. & Warner, M. G. Influence of Viscous and Capillary Forces on Immiscible Fluid Displacement: Pore-Scale Experimental Study in a Water-Wet Micromodel Demonstrating Viscous and Capillary Fingering. *Energy & Fuels* **25,** 3493–3505 (Aug. 2011).

34. Tiab, D. & Donaldson, E. C. en. in *Petrophysics (Third Edition)* (eds Tiab, D. & Donaldson, E. C.) 327–370 (Gulf Professional Publishing, Boston, Jan. 2012). `http://www.sciencedirect.com/science/article/pii/B9780123838483000050` (2020).

35. Erle C. Donaldson, George V. Chilingarian & Teh Fu Yen. *Enhanced Oil Recovery, II, Volume 17B* 1st ed. (Elsevier Science).

36. Vladimir Alvarado & Eduardo Manrique. *Enhanced Oil Recovery: Field Planning and Development Strategies* 1st ed. (Gulf Professional Publishing, Oxford).

37. Nazar, M. F., Shah, S. S. & Khosa, M. A. Microemulsions in Enhanced Oil Recovery: A Review. *Petroleum Science and Technology* **29,** 1353–1365 (May 2011).

38. Manshad, A. K., Rezaei, M., Moradi, S., Nowrouzi, I. & Mohammadi, A. H. Wettability alteration and interfacial tension (IFT) reduction in enhanced oil recovery (EOR) process by ionic liquid flooding. *Journal of Molecular Liquids* **248,** 153–162 (Dec. 2017).

39. Nelson, R. C. in *Surface Phenomena in Enhanced Oil Recovery* (ed Shah, D. O.) 73–104 (Springer US, Boston, MA, 1981).

40. Benner, F. C. & Bartel, F. E. *The Effect Of Polar Impurities Upon Capillary And Surface Phenomena In Petroleum Production* in (American Petroleum Institute, Jan. 1941).
41. Bera, A. & Mandal, A. Microemulsions: a novel approach to enhanced oil recovery: a review. *Journal of Petroleum Exploration and Production Technology* **5,** 255–268 (Sept. 2015).
42. GmbH, K. Ultralow interfacial tension in enhanced oil recovery (EOR), 4.
43. Kamal, M. S., Hussein, I. A. & Sultan, A. S. Review on Surfactant Flooding: Phase Behavior, Retention, IFT, and Field Applications. *Energy & Fuels* **31,** 7701–7720 (Aug. 2017).
44. Reynolds, P. in *Colloid Science* 159–179 (John Wiley & Sons, Ltd, 2009).
45. Kułynycz, V. The influence of wettability on oil recovery. *AGH Drilling, Oil, Gas* **32,** 493 (Jan. 2015).
46. Sayyouh, M. H., Hemeida, A. M., Al-Blehed, M. S. & Desouky, S. M. Role of polar compounds in crude oils on rock wettability. *Journal of Petroleum Science and Engineering* **6,** 225–233 (Nov. 1991).
47. Buckley, J. S., Liu, Y. & Monsterleet, S. Mechanisms of Wetting Alteration by Crude Oils. *SPE Journal* **3,** 54–61 (Mar. 1998).
48. Baviere, M., Ruaux, E. & Defives, D. Sulfonate Retention by Kaolinite at High pH - Effect of Inorganic Anions. *SPE Reservoir Engineering* **8,** 123–127 (May 1993).
49. Salehi, M., Johnson, S. J. & Liang, J.-T. Mechanistic Study of Wettability Alteration Using Surfactants with Applications in Naturally Fractured Reservoirs. *Langmuir* **24,** 14099–14107 (Dec. 2008).
50. Katende, A. & Sagala, F. A critical review of low salinity water flooding: Mechanism, laboratory and field application. *Journal of Molecular Liquids* **278,** 627–649 (Mar. 2019).
51. Alameri, W., Teklu, T. W., Graves, R., Kazemi, H. & Alsumaiti, A. *Low-salinity Water-alternate-surfactant in Low-permeability Carbonate Reservoirs* in (Apr. 2015).
52. Sheu, E. Y., Chen, S. H. & Huang, J. S. Structure and growth of bis(2-ethylhexyl) sulfosuccinate micelles in aqueous solutions. *The Journal of Physical Chemistry* **91,** 3306–3310 (June 1987).
53. Wilkinson, K. M., Bain, C. D., Matsubara, H. & Aratono, M. Wetting of Surfactant Solutions by Alkanes. *ChemPhysChem* **6,** 547–555 (2005).
54. Rosen, M. J., Wang, H., Shen, P. & Zhu, Y. Ultralow Interfacial Tension for Enhanced Oil Recovery at Very Low Surfactant Concentrations. *Langmuir* **21,** 3749–3756 (Apr. 2005).

55. Naik, V. V., Crobu, M., Venkataraman, N. V. & Spencer, N. D. Multiple Transmission-Reflection IR Spectroscopy Shows that Surface Hydroxyls Play Only a Minor Role in Alkylsilane Monolayer Formation on Silica. *The Journal of Physical Chemistry Letters* **4,** 2745–2751 (Aug. 2013).

56. Sagiv, J. Organized monolayers by adsorption. 1. Formation and structure of oleophobic mixed monolayers on solid surfaces. *Journal of the American Chemical Society* **102,** 92–98 (Jan. 1980).

57. McGovern, M. E., Kallury, K. M. R. & Thompson, M. Role of Solvent on the Silanization of Glass with Octadecyltrichlorosilane. *Langmuir* **10,** 3607–3614 (Oct. 1994).

58. *Instruction Manual DMA 4100 M DMA 4500 M DMA 5000 M* Feb. 2012.

59. *SVT Spinning drop video tensiometer - DataPhysics Instruments* `https://www.dataphysics-instruments.com/products/svt/` (2019).

60. Tichelkamp, T. *Procedure - Spinning Drop Tensiometer* Oct. 2012.

61. Viades-Trejo, J. & Gracia-Fadrique, J. Spinning drop method: From Young–Laplace to Vonnegut. *Colloids and Surfaces A: Physicochemical and Engineering Aspects* **302,** 549–552. (2020) (July 2007).

62. Jiang, L. & Korivi, N. S. in *Nanolithography* (ed Feldman, M.) 424–443 (Woodhead Publishing, Jan. 2014).

63. Gogoi, S. & Gogoi, S. B. Review on microfluidic studies for EOR application. *Journal of Petroleum Exploration and Production Technology* **9,** 2263–2277 (Sept. 2019).

64. Dudek, M., Bertheussen, A., Dumaire, T. & Øye, G. Microfluidic tools for studying coalescence of crude oil droplets in produced water. *Chemical Engineering Science* **191,** 448–458 (Dec. 2018).

65. *Enhanced Oil Recovery chips with physical rock network structure* `https://store.micronit.com/microfluidic-chips/enhanced-oil-recovery-chips/3-pack-eor-chips-physical-rock-network-446` (2020).

66. *S48 Stage Micrometer 1mm/0.01mm without Coverglass — Graticules Optics Limited* `https://www.graticulesoptics.com/products/stage-micrometers-calibration-scales-grids/stage-micrometers-s-series/s48-stage-micrometer-1mm001mm-without-coverglass` (2019).

67. Eftekhardadkhah, M. & Øye, G. Correlations between Crude Oil Composition and Produced Water Quality: A Multivariate Analysis Approach. *Industrial & Engineering Chemistry Research* **52,** 17315–17321 (Dec. 2013).

68. Jönsson, B., Lindman, B., Holmberg, K. & Kronberg, B. *Surfactants and Polymers in Aqueous Solution* 1 edition (Wiley, Chichester ; New York, May 1998).

Appendices

A Aqueous solutions

The surfactant and the salt solutions were prepared to a double concentration of the desired value.

A.1 Salt solution

The salt solutions with different molar ratios between calcium chloride (M_m: 147.01 g/mol) and sodium chloride (M_m: 58.44 g/mol) where all prepared with an ionic strength of 40 mmol/L. The mass of each salt needed to make the different solutions where calculated as following. First, concentration of sodium was calculated by the equation for ionic strength, I, given by

$$I = \frac{1}{2}\sum_{i=1}^{n} c_i z_i^2, \tag{A.1}$$

where c_i and z_i is the concentration and valency of ion, i. Further, the value of ionic strength was inserted and the summation sign was solved by inserting the ions present in the solution.

$$40 \text{ mmol/L} = \frac{1}{2}[c_{Ca^{2+}} \cdot (+2)^2 + 2 \cdot c_{Cl^-} \cdot (-1)^2 + c_{Na^+} \cdot (+1)^2 + c_{Cl^-} \cdot (-1)^2], \tag{A.2}$$

where $c_{Ca^{2+}}$, c_{Cl^-} and c_{Na^+} is concentration of respectively calcium, chloride and sodium. The molar ratio between chloride and sodium, X_{Cl^-/Na^+}, is equal to 1, while the molar ratio between calcium and sodium, X_{Ca^{2+}/Na^+}, varied between 0 and 0.040. Equation A.2, was then solved for the concentration of sodium ions. Afterward, the relationship between the ions were used to calculate the concentration of sodium. The two molar concentrations were then multiplied with the molecular weight to find the mass concentrations needed in each solution. An overview of the mass concentrations of calcium and sodium ions needed in each solution for the different molar ratios between the two ions are shown in Table A.

Table A.1: Calculated values for both molar and mass concentrations of calcium and sodium ions needed in each solution for different molar ratio between the two ions, $X_{Ca^{2+}/Na^{+}}$.

$X_{Ca^{2+}/Na^{+}}$ [-]	$c_{Na^{+}}$ [mol/L]	$c_{Ca^{2+}}$ [mol/L]	$c_{Na^{+}}$ [g/L]	$c_{Ca^{2+}}$ [g/L]
0	0.0400	0.0000	2.3376	0.0000
0.005	0.0394	0.0002	2.3031	0.0230
0.01	0.0388	0.0004	2.2695	0.0571
0.017	0.0381	0.0006	2.2242	0.0951
0.022	0.0375	0.0008	2.1929	0.1214
0.033	0.0364	0.0012	2.1270	0.1766
0.04	0.0357	0.0014	2.0871	0.2100

To obtain LS solutions with the ionic strength of 20 mmol/L, the salt solutions were mixed 1:1 with DI water.

In the EOR displacement experiments, a high salinity solution with a molar calcium/sodium ratio equal to 0.017 was used as the IOR step. The HS solution, was prepared with an ionic strength of 60 mmol/L. The mass concentration of each salt needed was calculated with the same calculation procedure above. The concentration of calcium was calculated to be 0.1427 g/L, and the concentration of sodium was calculated to be 3.3363 g/L.

A.2 Surfactant solution

The stock solution (1 L) with the AOT was made with a concentration of 4.94 mmol/L. Amount of moles, n, is given by

$$n = c \cdot V, \tag{A.3}$$

where c is concentration and V is volume. In addition, the amount of moles is given by

$$n = \frac{m}{M_m}, \tag{A.4}$$

where m is mass and M_m is molecular weight. By rearranging Equation A.3 and A.4 mass can be calculated by

$$m = c \cdot M_m \cdot V. \tag{A.5}$$

Inserting values of the desired concentration of AOT, the molecular weight of AOT, and the volume of the stock solution wanted to prepare, gives

$$m = 4.94 \ \frac{\text{mmol}}{\text{L}} \cdot 444.56 \ \frac{\text{mg}}{\text{mmol}} \cdot 1 \text{ L} = 2.196 \text{ g}. \tag{A.6}$$

The surfactant solution was mixed 1:1 with the different salt solutions with the ionic strength of 40 mmol/L to obtain LS-AOT solutions of 2.47 mmol/L AOT and 20 mmol/L of salt.

A.3 pH

The pH of the LS solutions, with and without AOT, was measured with a pH-meter. To ensure repeatability, the pH was measured two times. The results obtained for the LS solutions and the LS-AOT solutions are shown in Table A.2 and A.3, respectively.

Table A.2: The pH of the LS solutions.

$X_{Ca^{2+}/Na^{+}}$ [-]	pH
0	5.735 ± 0.105
0.005	5.745 ± 0.015
0.01	5.745 ± 0.105
0.017	5.825 ± 0.085
0.022	5.705 ± 0.105
0.033	5.875 ± 0.005
0.04	5.665 ± 0.075

Table A.3: The pH of the LS-AOT solutions.

$X_{Ca^{2+}/Na^{+}}$ [-]	pH
0	6.080 ± 0.050
0.005	6.120 ± 0.060
0.01	6.120 ± 0.070
0.017	6.185 ± 0.065
0.022	5.990 ± 0.010
0.033	6.280 ± 0.100
0.04	5.955 ± 0.005

B IFT measurements

B.1 Equilibrium IFT

Exact values of the equilibrium interfacial tension between the two crude oils and the different LS solutions, with different calcium/sodium molar ratios, are shown in Table B.1, B.2, B.3 and B.4.

Table B.1: Equilibrium interfacial tension, γ, between crude oil A and the LS-AOT solutions with different molar calcium/sodium ratios, $X_{Ca^{2+}/Na^{+}}$, at 23°C, with corresponding standard deviation, σ.

$X_{Ca^{2+}/Na^{+}}$ [mol/mol]	γ [mN/m]	σ [mN/m]
0	0.331	0.009
0.005	0.234	0.006
0.01	0.220	0.023
0.017	0.203	0.005
0.022	0.261	0.027
0.033	0.292	0.028
0.04	0.230	0.033

Table B.2: Equilibrium interfacial tension, γ, between crude oil A and the LS solutions with different molar calcium/sodium ratios, $X_{Ca^{2+}/Na^{+}}$, at 23°C, with corresponding standard deviation, σ.

$X_{Ca^{2+}/Na^{+}}$ [mol/mol]	γ [mN/m]	σ [mN/m]
0	21.212	0.104
0.005	20.731	0.969
0.01	20.291	0.267
0.017	20.091	0.434
0.022	20.802	0.343
0.033	20.320	0.681
0.04	20.905	0.380

Table B.3: Equilibrium interfacial tension, γ, between crude oil C and the LS-AOT solutions with different molar calcium/sodium ratios, $X_{Ca^{2+}/Na^{+}}$, at 23°C, with corresponding standard deviation, σ.

$X_{Ca^{2+}/Na^{+}}$ [mol/mol]	γ [mN/m]	σ [mN/m]
0	0.210	0.000
0.005	0.147	0.002
0.01	0.096	0.001
0.017	0.036	0.004
0.022	0.106	0.004
0.033	0.250	0.007
0.04	0.224	0.011

Table B.4: Equilibrium interfacial tension, γ, between crude oil C and the LS solutions with different molar calcium/sodium ratios, $X_{Ca^{2+}/Na^{+}}$, at 23°C, with corresponding standard deviation, σ.

$X_{Ca^{2+}/Na^{+}}$ [mol/mol]	γ [mN/m]	σ [mN/m]
0	16.896	0.548
0.005	17.626	0.004
0.01	17.736	0.742
0.017	19.119	0.237
0.022	18.056	0.549
0.033	18.124	0.651
0.04	18.069	0.136

C Oil recovery

C.1 One step displacement experiments under hydrophilic conditions

C.1.1 Crude oil A

The dynamic recovery of crude oil A displaced by the LS-AOT solutions with various molar calcium/sodium ratio at 0.065 μL/min are shown in Figure C.1.

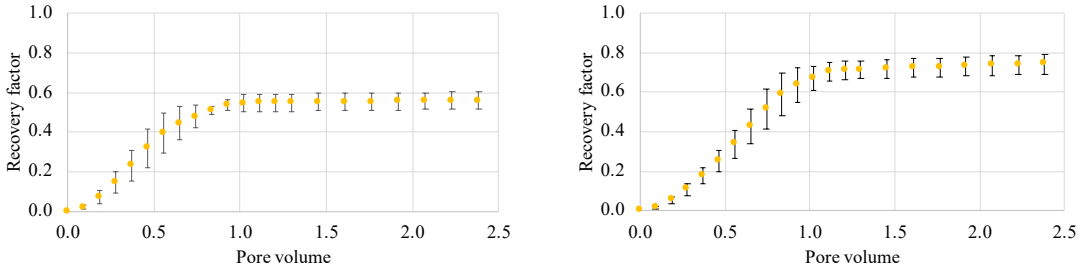

(a) AOT + $Ca^{2+}/Na^{+} = 0$.

(b) AOT + $Ca^{2+}/Na^{+} = 0.040$.

Figure C.1: Dynamic recovery of crude oil A displaced by the LS-AOT solutions with various calcium/sodium ratios at 0.065 μL/min.

The dynamic recovery of crude oil A displaced by the LS solutions with various molar calcium/sodium ratio at 0.065 μL/min are shown in Figure C.2.

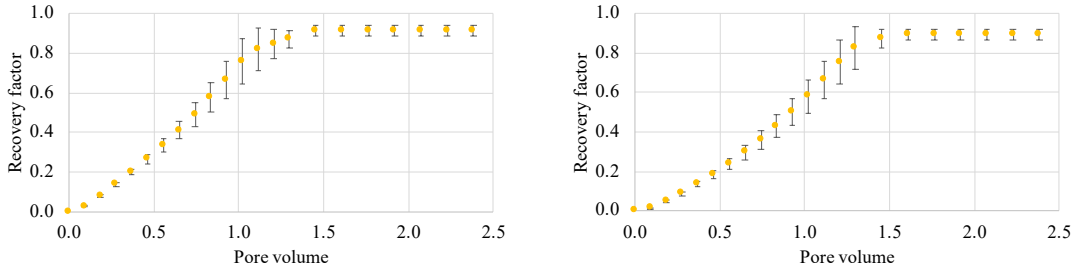

(a) $Ca^{2+}/Na^{+} = 0$. (b) $Ca^{2+}/Na^{+} = 0.040$.

Figure C.2: Dynamic recovery of crude oil A displaced by the LS solutions with various calcium/sodium ratios at 0.065 μL/min.

The dynamic recovery of crude oil A displaced by the LS-AOT solutions with various molar calcium/sodium ratio at 0.5 μL/min are shown in Figure C.3.

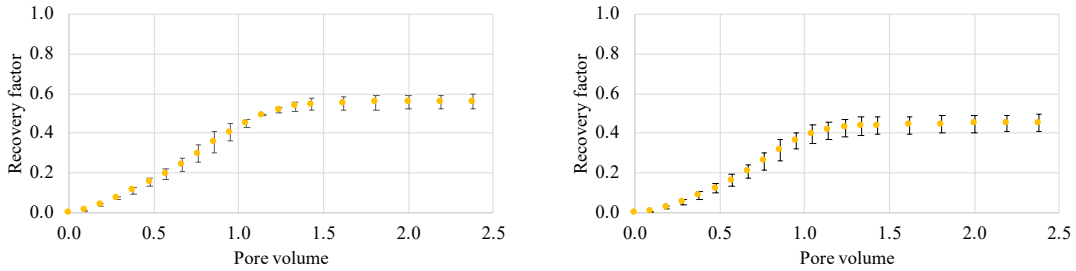

(a) AOT + $Ca^{2+}/Na^{+} = 0$. (b) AOT + $Ca^{2+}/Na^{+} = 0.040$.

Figure C.3: Dynamic recovery of crude oil A displaced by the LS-AOT solutions with various calcium/sodium ratios at 0.5 μL/min.

The dynamic recovery of crude oil A displaced by the LS solutions with various molar calcium/sodium ratio at 0.5 μL/min are shown in Figure C.4.

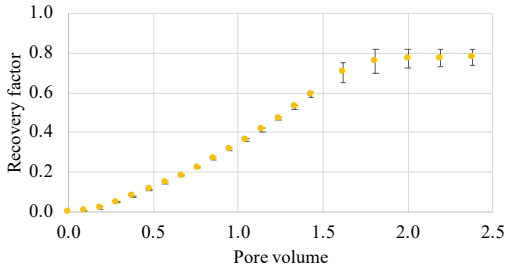

(a) $Ca^{2+}/Na^{+} = 0$.

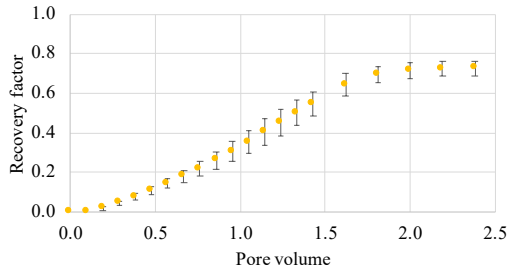

(b) $Ca^{2+}/Na^{+} = 0.017$.

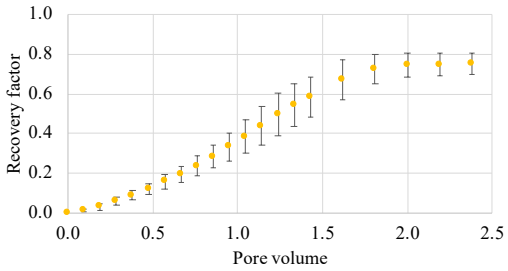

(c) $Ca^{2+}/Na^{+} = 0.040$.

Figure C.4: Dynamic recovery of crude oil A displaced by the LS solutions with various calcium/sodium ratios at 0.5 μL/min.

C.1.2 Crude oil C

The dynamic recovery of crude oil C displaced by the LS-AOT solutions with various molar calcium/sodium ratio at 0.065 μL/min are shown in Figure C.5.

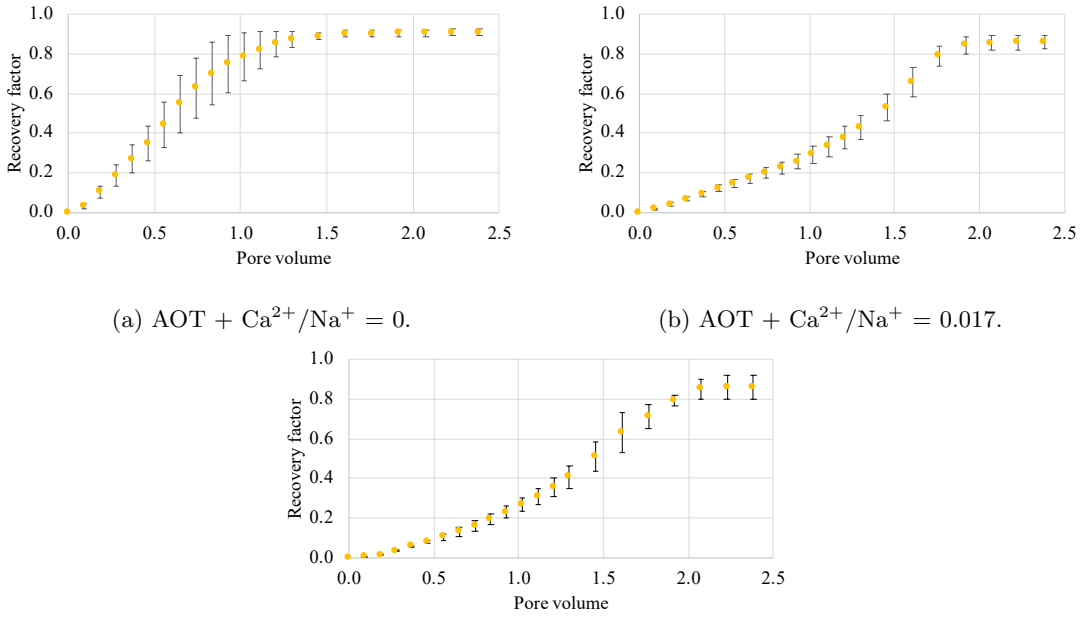

(a) AOT + $Ca^{2+}/Na^{+} = 0$.

(b) AOT + $Ca^{2+}/Na^{+} = 0.017$.

(c) AOT + $Ca^{2+}/Na^{+} = 0.040$.

Figure C.5: Dynamic recovery of crude oil C displaced by the LS-AOT solution with various molar calcium/sodium ratio at 0.065 μL/min are shown in the figures below

The dynamic recovery of crude oil C displaced by the LS solutions with various molar calcium/sodium ratio at 0.065 μL/min are shown in the Figure C.6.

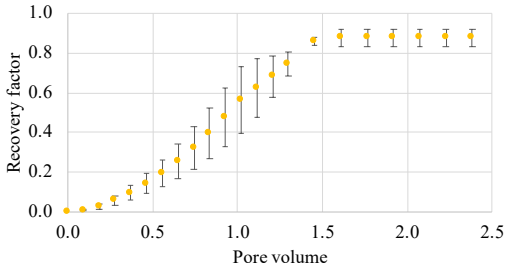

(a) $Ca^{2+}/Na^{+} = 0$.

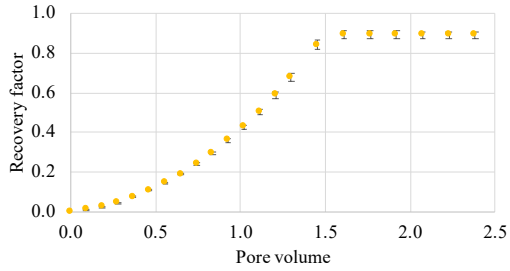

(b) $Ca^{2+}/Na^{+} = 0.017$.

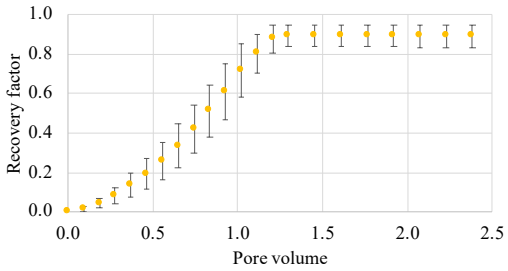

(c) $Ca^{2+}/Na^{+} = 0.040$.

Figure C.6: Dynamic recovery of crude oil C displaced by the LS solutions with various calcium/sodium ratios at 0.065 μL/min.

The dynamic recovery of crude oil C displaced by the LS-AOT solutions with various molar calcium/sodium ratio at 0.5 μL/min are shown in Figure C.7.

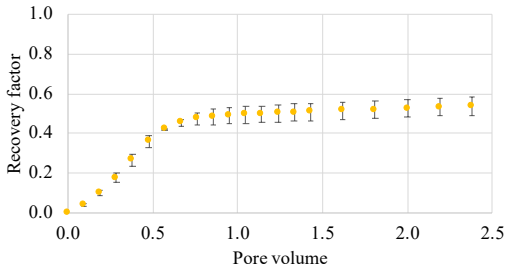

(a) AOT + $Ca^{2+}/Na^{+} = 0$.

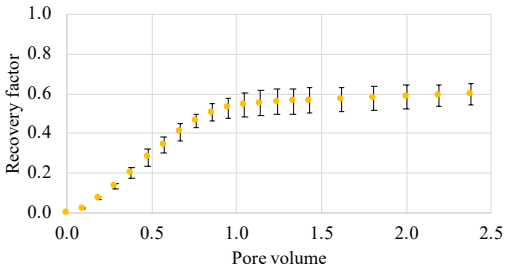

(b) AOT + $Ca^{2+}/Na^{+} = 0.040$.

Figure C.7: Dynamic recovery of crude oil C displaced by the LS-AOT solutions with various molar calcium/sodium ratio at 0.5 μL/min are shown in the figures below.

The dynamic recovery of crude oil C displaced by the LS solutions with various molar calcium/sodium ratio at 0.5 μL/min are shown in Figure C.8.

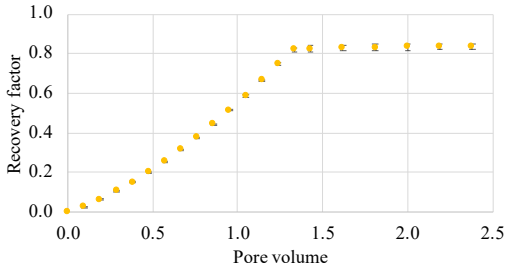

(a) $Ca^{2+}/Na^{+} = 0$.

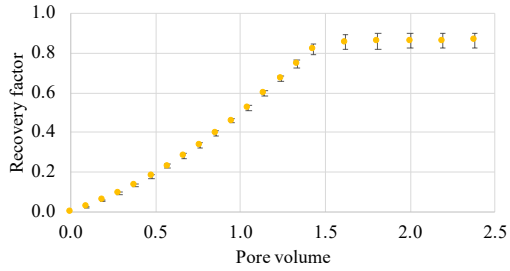

(b) $Ca^{2+}/Na^{+} = 0.017$.

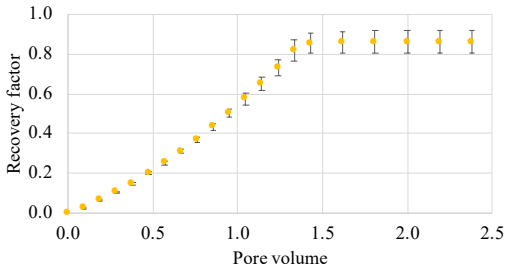

(c) $Ca^{2+}/Na^{+} = 0.040$.

Figure C.8: Dynamic recovery of crude oil C displaced by the LS solutions with various calcium/sodium ratios at 0.5 μL/min.

C.2 One step displacement experiments under hydrophobic conditions

C.2.1 Crude oil A

The dynamic recovery of crude oil A displaced by the LS-AOT solutions with various molar calcium/sodium ratio under hydrophobic conditions at 0.065 μL/min are shown in Figure C.9.

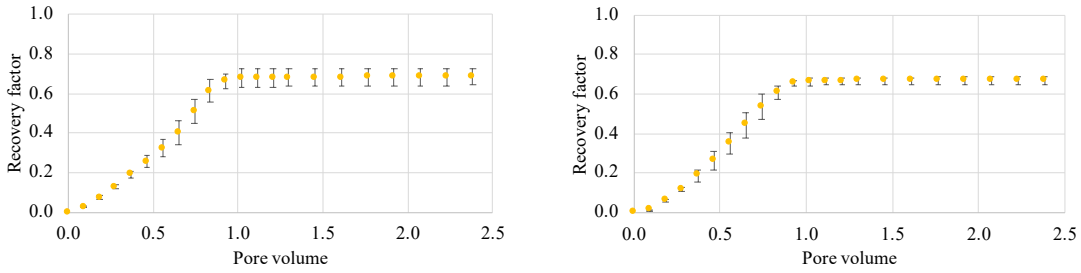

(a) AOT + Ca^{2+}/Na^{+} = 0. (b) AOT + Ca^{2+}/Na^{+} = 0.017.

Figure C.9: Dynamic recovery of crude oil A displaced by the LS-AOT solutions with different calcium/sodium ratio, in the hydrophobic micromodel at 0.065 μL.

The dynamic recovery of crude oil A displaced by the LS-AOT solutions with various molar calcium/sodium ratio under hydrophobic conditions at 0.5 μL/min are shown in Figure C.10.

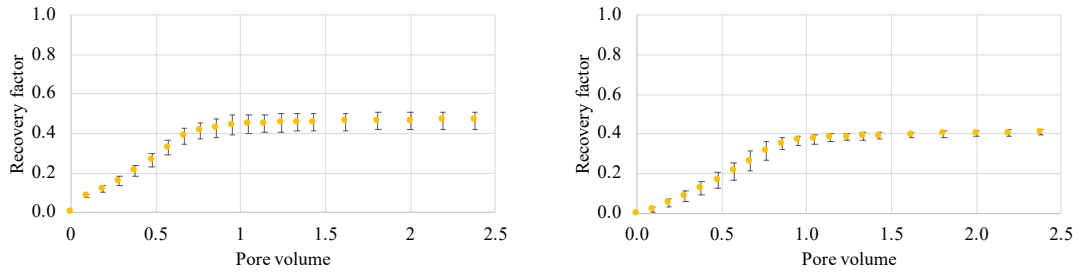

(a) AOT + Ca^{2+}/Na^{+} = 0. (b) AOT + Ca^{2+}/Na^{+} = 0.017.

Figure C.10: Dynamic recovery of crude oil A displaced by the LS-AOT solutions with different calcium/sodium ratio, in the hydrophobic micromodel at 0.5 μL.

C.2.2 Crude oil C

The dynamic recovery of crude oil C displaced by the LS-AOT solutions with various molar calcium/sodium ratio under hydrophobic conditions at 0.065 μL/min are shown in Figure C.11.

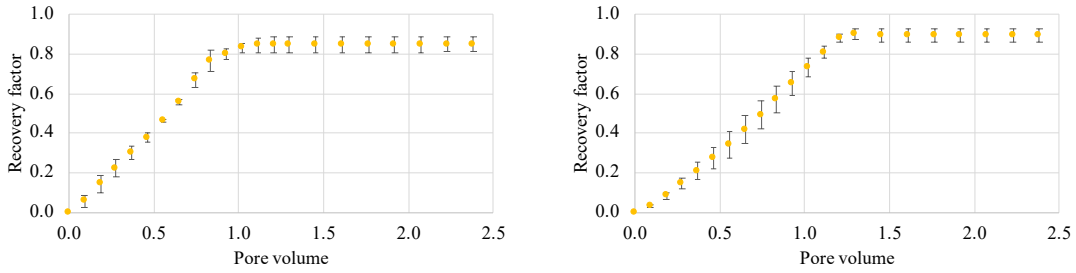

(a) AOT + $Ca^{2+}/Na^{+} = 0$. (b) AOT + $Ca^{2+}/Na^{+} = 0.017$.

Figure C.11: Dynamic recovery of crude oil C displaced by the LS-AOT solutions with different calcium/sodium ratio, in the hydrophobic micromodel at 0.065 μL.

The dynamic recovery of crude oil C displaced by the LS-AOT solutions with various molar calcium/sodium ratio under hydrophobic conditions at 0.5 μL/min are shown in Figure C.12.

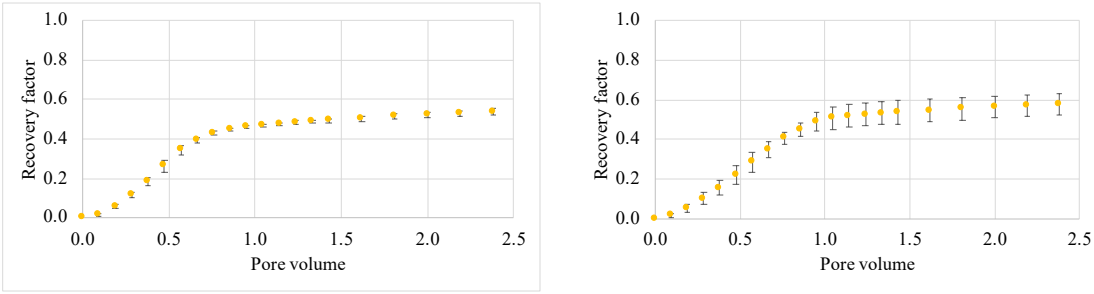

(a) AOT + $Ca^{2+}/Na^{+} = 0$. (b) AOT + $Ca^{2+}/Na^{+} = 0.017$.

Figure C.12: Dynamic recovery of crude oil C displaced by the LS-AOT solutions with different calcium/sodium ratio, in the hydrophobic micromodel at 0.5 μL.

C.3 EOR displacement experiments under hydrophilic conditions

C.3.1 Crude oil A

The dynamic recovery factors of crude oil A during injection of the HS solution followed by the LS-AOT or the LS solution with molar calcium/sodium ratio equal to 0 under hydrophilic conditions are shown in Figure C.13.

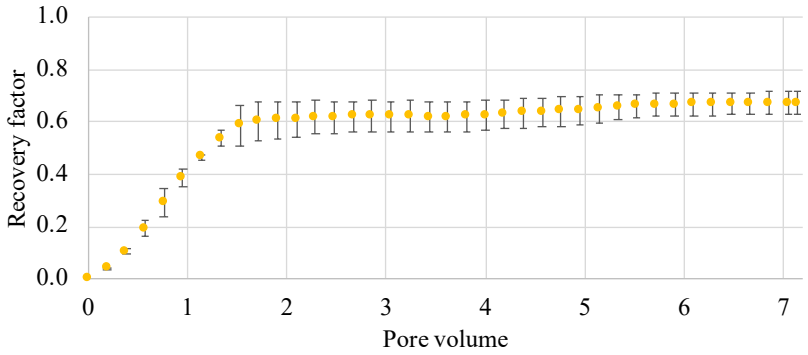

(a) LS-AOT.

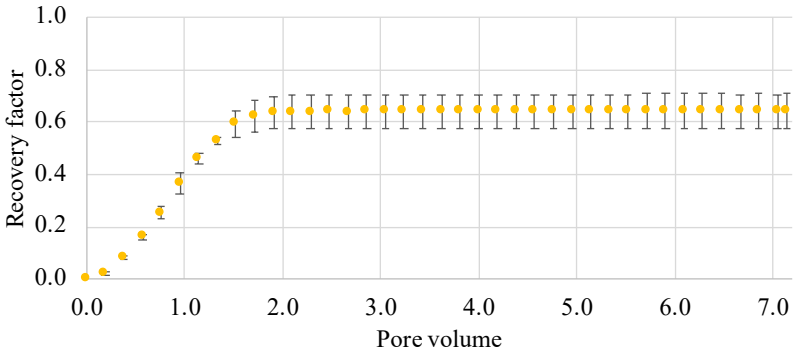

(b) LS.

Figure C.13: Dynamic recovery of crude oil A during the displacement by the HS solution followed by the LS solutions, with and without surfactant, with molar calcium/sodium ratio equal to 0 in the hydrophilic micromodel.

C.3.2 Crude oil C

The dynamic recovery factors of crude oil C during injection of the HS solution followed by the LS-AOT solutions with various calcium/sodium ratio under hydrophilic conditions are shown in Figure C.14.

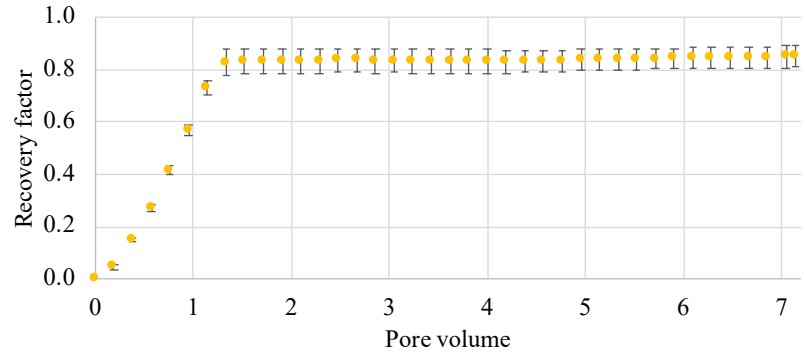

(a) AOT + $Ca^{2+}/Na^{+} = 0$.

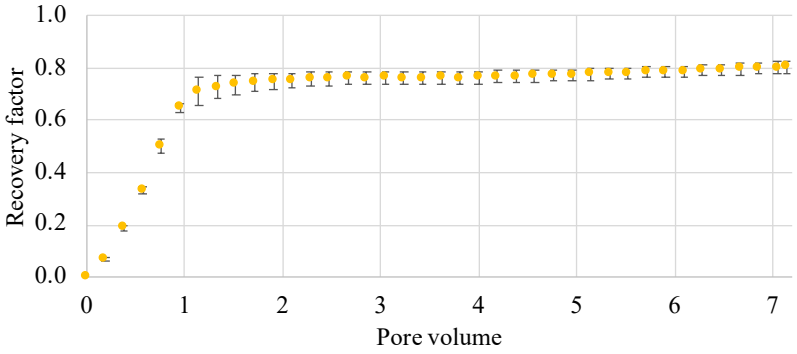

(b) AOT + $Ca^{2+}/Na^{+} = 0.017$.

Figure C.14: Dynamic recovery of crude oil C during the displacement by the HS solution followed by the LS-AOT solutions with various molar calcium/sodium ratio in the hydrophilic micromodel.

The dynamic recovery factors of crude oil C during injection of the HS solution followed by the LS solutions with various calcium/sodium ratio under hydrophilic conditions are shown in Figure C.15.

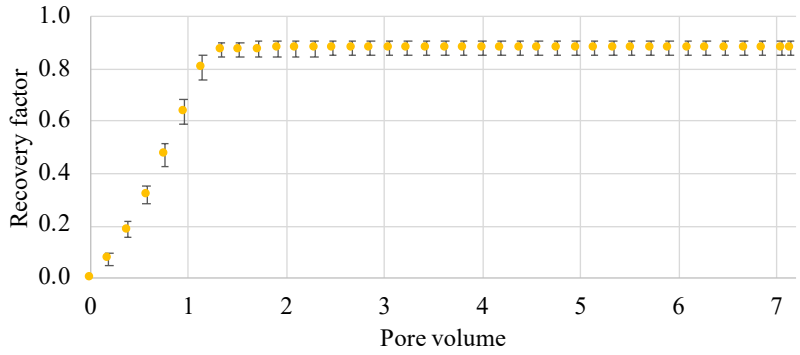

(a) $Ca^{2+}/Na^{+} = 0$.

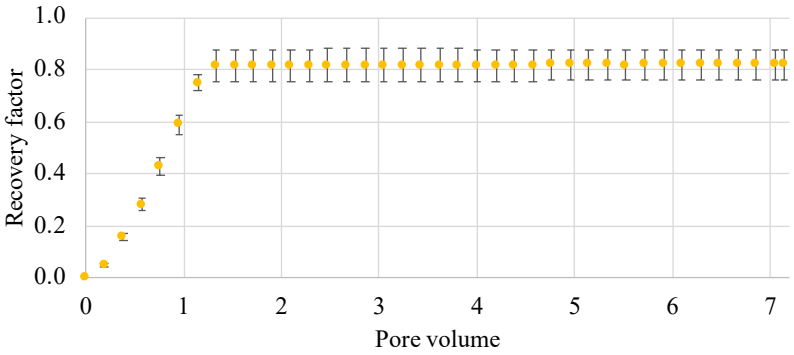

(b) $Ca^{2+}/Na^{+} = 0.017$.

Figure C.15: Dynamic recovery of crude oil C during the displacement by the HS solution followed by the LS solutions with various molar calcium/sodium ratio in the hydrophilic micromodel.

C.4 EOR displacement experiments under hydrophobic conditions

C.4.1 Crude oil A

The dynamic recovery factors of crude oil A during injection of the HS solution followed by the LS-AOT solutions under hydrophobic conditions are shown in Figure C.16.

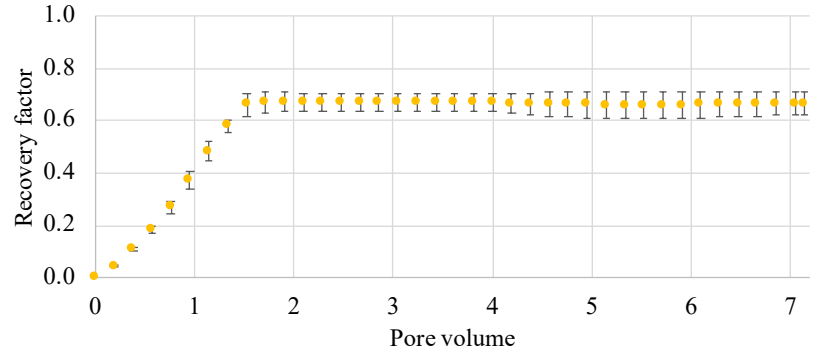

(a) AOT + $Ca^{2+}/Na^{+} = 0$.

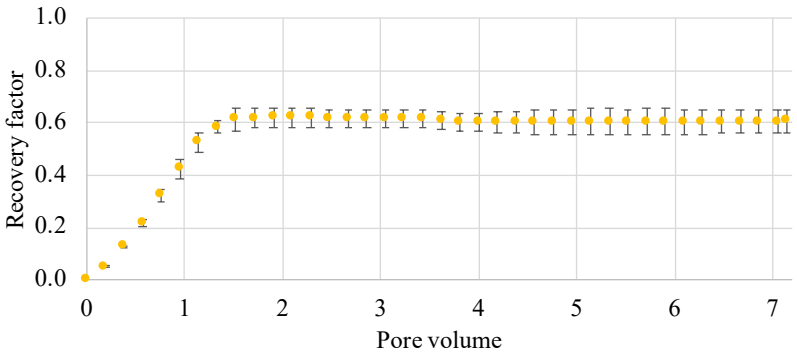

(b) AOT + $Ca^{2+}/Na^{+} = 0.017$.

Figure C.16: Dynamic recovery of crude oil A during the displacement by the HS solution followed by the LS-AOT solutions with various molar calcium/sodium ratio in the hydrophobic micromodel.

The dynamic recovery factors of crude oil A during injection of the HS solution followed by the LS solutions under hydrophobic conditions are shown in Figure C.17.

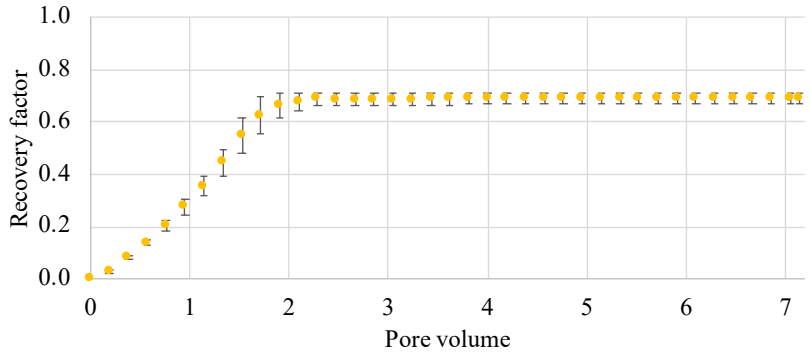

(a) $Ca^{2+}/Na^{+} = 0$.

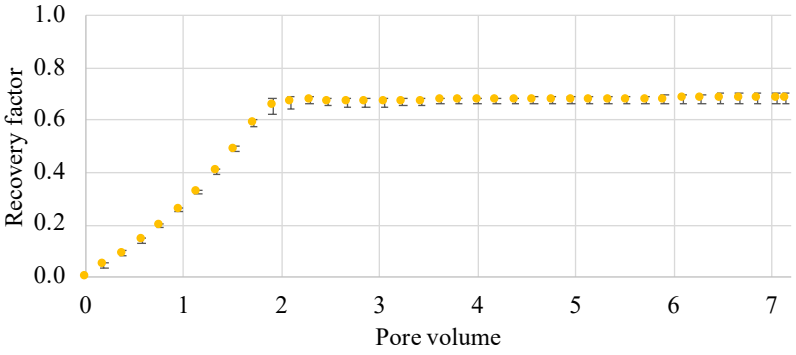

(b) $Ca^{2+}/Na^{+} = 0.017$.

Figure C.17: Dynamic recovery of crude oil A during the displacement by the HS solution followed by the LS solutions with various molar calcium/sodium ratio in the hydrophobic micromodel.

C.4.2 Crude oil C

The dynamic recovery factors of crude oil C during injection of the HS solution followed by the LS-AOT solutions under hydrophobic conditions are shown in Figure C.18.

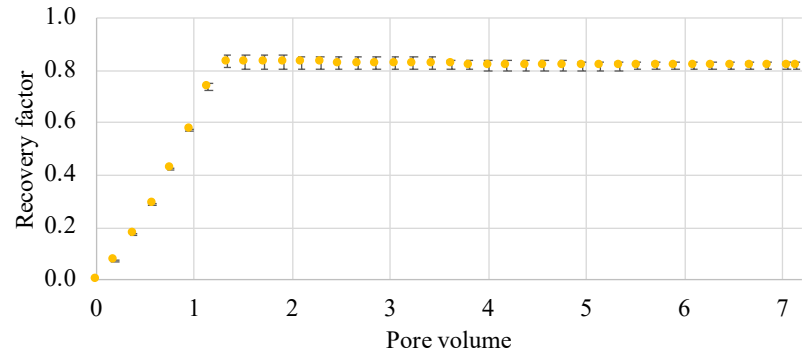

(a) AOT + $Ca^{2+}/Na^{+} = 0$.

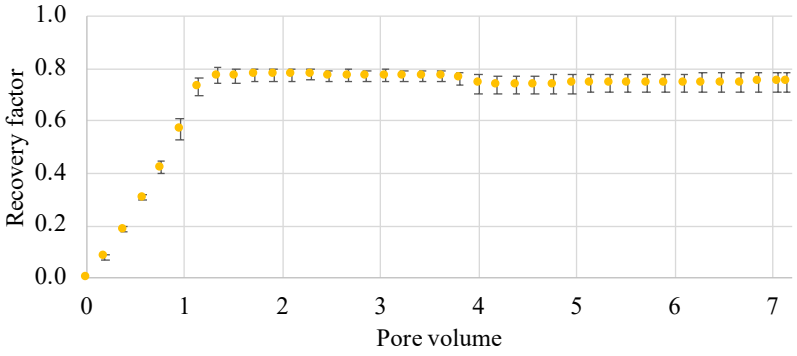

(b) AOT + $Ca^{2+}/Na^{+} = 0.017$.

Figure C.18: Dynamic recovery of crude oil C during the displacement by the HS solution followed by the LS-AOT solutions with various molar calcium/sodium ratio in the hydrophobic micromodel.

The dynamic recovery factors of crude oil C during injection of the HS solution followed by the LS solutions under hydrophobic conditions are shown in Figure C.19.

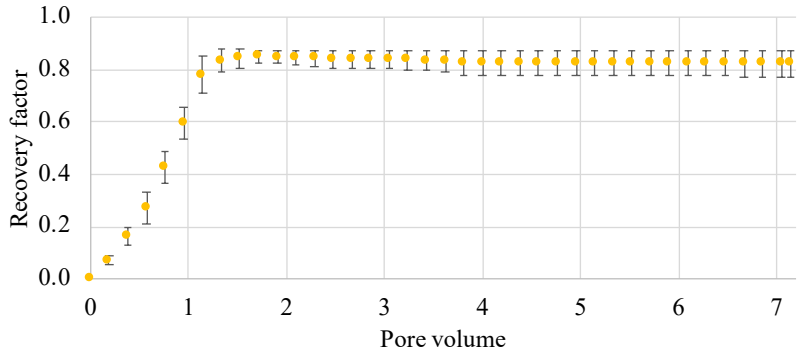

(a) $Ca^{2+}/Na^{+} = 0$.

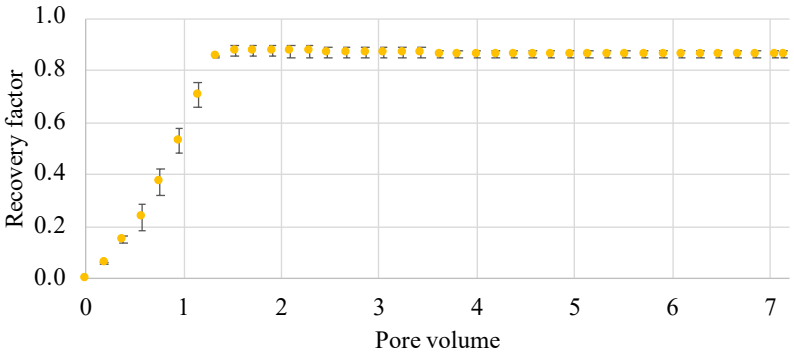

(b) $Ca^{2+}/Na^{+} = 0.017$.

Figure C.19: Dynamic recovery of crude oil C during the displacement by the HS solution followed by the LS solutions with various molar calcium/sodium ratio in the hydrophobic micromodel.

Nora Birgitte Vikse

NTNU
Norwegian University of
Science and Technology